NAVAL POSTGRADUATE SCHOOL

MONTEREY, CALIFORNIA

THESIS

PERFORMANCE AND RELIABILITY OF EXHAUST GAS WASTE HEAT RECOVERY UNITS

by

Chuan Heng Erik Koh

September 2014

Thesis Advisor: Sanjeev B. Sathe
Co-Advisor: Knox T. Millsaps

THIS PAGE INTENTIONALLY LEFT BLANK

REPORT DOCUMENTATION PAGE

Form Approved OMB No. 0704–0188

1. AGENCY USE ONLY *(Leave blank)*	**2. REPORT DATE** September 2014	**3. REPORT TYPE AND DATES COVERED** Master's Thesis

4. TITLE AND SUBTITLE
PERFORMANCE AND RELIABILITY OF EXHAUST GAS WASTE HEAT RECOVERY UNITS

5. FUNDING NUMBERS

6. AUTHOR(S) Chuan Heng Erik Koh

7. PERFORMING ORGANIZATION NAME(S) AND ADDRESS(ES)
Naval Postgraduate School
Monterey, CA 93943-5000

8. PERFORMING ORGANIZATION REPORT NUMBER

9. SPONSORING /MONITORING AGENCY NAME(S) AND ADDRESS(ES)
N/A

10. SPONSORING/MONITORING AGENCY REPORT NUMBER

11. SUPPLEMENTARY NOTES The views expressed in this thesis are those of the author and do not reflect the official policy or position of the Department of Defense or the U.S. Government. IRB Protocol number ____N/A____.

12a. DISTRIBUTION / AVAILABILITY STATEMENT
Approved for public release; distribution is unlimited

12b. DISTRIBUTION CODE

13. ABSTRACT (maximum 200 words)

This thesis presents the effect of exhaust tube length-to-diameter (L/d) ratio, jacket-to-tube diameter (D/d) ratio, coolant inlet and outlet placements, exhaust gas swirling conditions, and tube materials (steel, copper, Inconel, and ceramic) on heat recovery performance, exhaust side pressure drop, and temperature profile in the exhaust gas Waste Heat Recovery Unit (WHRU). Non-dimensional parametric studies of a selected counter-flow "Water Jacket" WHRU was conducted using analytical and Computational Fluid Dynamic (CFD) models. Exhaust gas Reynolds numbers between 20,000 and 400,000, representative of exhaust gas flow in the exhaust stacks of U.S. Marine Corps' MEP803A diesel generators and the U.S. Navy's 501-K17 gas turbine generators, were used.

Results indicate heat recovery increases with higher L/d, D/d, and swirling exhaust gases conditions but with a severe pressure drop penalty. Addition of a solid heat spreader at the exhaust gas inlet and the use of suitable tube materials were also found to influence temperature profiles in the WHRU and mitigate adverse temperature gradients to some extent without any additional pressure drop penalty. Optimal laterally shifted placement of coolant inlet and outlet was found to improve heat recovery by up to 19% and was very effective at mitigating adverse temperature profiles, which improves the reliability of exhaust gas WHRU.

14. SUBJECT TERMS waste heat recovery, heat recovery performance, swirling flow, pressure drop penalty, temperature profiles, thermal stresses			**15. NUMBER OF PAGES** 161
			16. PRICE CODE
17. SECURITY CLASSIFICATION OF REPORT Unclassified	**18. SECURITY CLASSIFICATION OF THIS PAGE** Unclassified	**19. SECURITY CLASSIFICATION OF ABSTRACT** Unclassified	**20. LIMITATION OF ABSTRACT** UU

NSN 7540–01-280-5500

Standard Form 298 (Rev. 2–89)
Prescribed by ANSI Std. 239–18

THIS PAGE INTENTIONALLY LEFT BLANK

Approved for public release; distribution is unlimited

PERFORMANCE AND RELIABILITY OF EXHAUST GAS WASTE HEAT RECOVERY UNITS

Chuan Heng Erik Koh
Military Expert 5, Republic of Singapore Navy
M. Eng., Newcastle University, 2008

Submitted in partial fulfillment of the
requirements for the degree of

MASTER OF SCIENCE IN MECHANICAL ENGINEERING

from the

NAVAL POSTGRADUATE SCHOOL
September 2014

Author: Chuan Heng Erik Koh

Approved by: Sanjeev B. Sathe
Thesis Advisor

Knox T. Millsaps
Co-Advisor

Garth V. Hobson
Chairman, Department of Mechanical and Aerospace Engineering

THIS PAGE INTENTIONALLY LEFT BLANK

ABSTRACT

This thesis presents the effect of exhaust tube length-to-diameter (L/d) ratio, jacket-to-tube diameter (D/d) ratio, coolant inlet and outlet placements, exhaust gas swirling conditions, and tube materials (steel, copper, Inconel, and ceramic) on heat recovery performance, exhaust side pressure drop, and temperature profile in the exhaust gas Waste Heat Recovery Unit (WHRU). Non-dimensional parametric studies of a selected counter-flow "Water Jacket" WHRU was conducted using analytical and Computational Fluid Dynamic (CFD) models. Exhaust gas Reynolds numbers between 20,000 and 400,000, representative of exhaust gas flow in the exhaust stacks of U.S. Marine Corps' MEP803A diesel generators and the U.S. Navy's 501-K17 gas turbine generators, were used.

Results indicate heat recovery increases with higher L/d, D/d, and swirling exhaust gases conditions but with a severe pressure drop penalty. Addition of a solid heat spreader at the exhaust gas inlet and the use of suitable tube materials were also found to influence temperature profiles in the WHRU and mitigate adverse temperature gradients to some extent without any additional pressure drop penalty. Optimal laterally shifted placement of coolant inlet and outlet was found to improve heat recovery by up to 19% and was very effective at mitigating adverse temperature profiles, which improves the reliability of exhaust gas WHRU.

THIS PAGE INTENTIONALLY LEFT BLANK

TABLE OF CONTENTS

LIST OF FIGURES

THIS PAGE INTENTIONALLY LEFT BLANK

LIST OF TABLES

THIS PAGE INTENTIONALLY LEFT BLANK

LIST OF ACRONYMS AND ABBREVIATIONS

A	Heat transfer area [m^2]
A_{csa}	Cross sectional area [m^2]
C_p	Constant pressure specific heat capacity [J/kg-K]
C_r	Ratio of minimum heat capacity to maximum heat capacity [1]
CFD	Computational Fluid Dynamics
d	Inner diameter of exhaust tube [m]
$d^* = \frac{D}{d}$	Jacket diameter-to-tube diameter ratio [1]
d_{water}	Inner diameter of water inlet and outlet pipe [m]
D	Inner diameter of water jacket [m]
D_{eff}	Effective diameter [m]
DG	Diesel Generator
ε	Heat transfer effectiveness [1]
f	Fanning friction factor [1]
g	Acceleration due to gravity [m/s^2]
h	Enthalpy [J/kg], Heat transfer coefficient [W/m^2K]
k	Thermal conductivity [W/m-K]
$k^* = \frac{k}{k_{air}}$	Non-dimensional thermal conductivity [1]
K	Kelvin
L	Length [m]
$L^* = \frac{L}{d}$	Length-to-tube diameter ratio [1]
$\dot{m}$	Mass flow rate [kg/s]
$Nu = \frac{h_c D_{eff}}{k_c}$	Nusselt number [1]
NTU	Number of Transfer Unit
P	Pressure [Pa]

$\mathrm{Pr} = \frac{\mu C_p}{K} = \frac{\upsilon}{\alpha}$	Prandtl number [1]
$\Delta P^* = \frac{\Delta P}{\rho \bar{U}^2}$	Non-dimensional pressure drop [1]
$\Delta P^{**} = \frac{\Delta P D_{eff}}{\mu \bar{U}}$	Non-dimensional pressure drop [1]
q	Amount of heat recovered [W]
$q^* = \frac{q_{exh}}{\dot{m}_{exh} C_{p,exh} (T_{exh,in} - T_{water,in})}$	Non-dimensional heat recovery as a fraction of maximum recoverable heat) [1]
Q	Volumetric flow rate [m^3/s]
$\mathrm{Re} = \frac{\rho \bar{U} D_{eff}}{\mu} = \frac{4\dot{m}}{\pi \mu D_{eff}}$	Reynolds number [1]
Re_{exh}	Reynolds number of exhaust gas flow [1]
Re_{water}	Reynolds number of water flow [1]
S_E	Energy source
S_M	Momentum source
SSGTG	Ship Service Gas Turbine Generator
t	Thickness [m]
t*	Non-dimensional thickness
T	Temperature [K]
$T^* = \frac{T - T_{water,in}}{T_{exh,in} - T_{water,in}}$	Non-dimensional temperature as fraction of the maximum temperature range [1]
ΔT	Temperature difference / change [K]
ΔT^*	Non-dimensional temperature difference [1]
u	Velocity in x-axis [m/s]
u_{axial}	Velocity in the axial axis [m/s]
u_θ	Angular velocity [radians /s]
u_r	Radial velocity [m/s]
$\bar{U}$	Average velocity [m/s]

$\vec{U}$	Velocity matrix
$\tilde{U}_{overall}$	Overall heat transfer coefficient [J/kg]
USN	United States Navy
USMC	United States Marine Corp
v	Velocity in y-axis [m/s]
w	Velocity in z-axis [m/s]
WHR	Waste Heat Recovery
WHRS	Waste Heat Recovery System
WHRU	Waste Heat Recovery Unit
x	Displacement in the x-axis [m]
$x^* = \frac{x}{R}$	Non-dimensional x displacement [1]
y	Displacement in the y-axis [m]
$y^* = \frac{y}{L}$	Non-dimensional y displacement [1]
z	Displacement in the z-axis [m]
$z^* = \frac{z}{R}$	Non-dimensional z displacement [1]
α	Thermal diffusivity [m^2/s]
μ	Dynamic viscosity [Pa-s]
ρ	Density [kg/m^3]
υ	Momentum diffusivity [m^2/s]
ϕ	Arbitrary function

Subscripts

eff	Effective
exh	Exhaust gas
water	Water
in	Inlet conditions
out	Outlet conditions

THIS PAGE INTENTIONALLY LEFT BLANK

ACKNOWLEDGMENTS

First, praise and thanks be with God for His daily providence and opportunity to do good work. I also thank the Singapore Navy for allowing me to pursue my preferred course of studies at NPS.

I would also like to express my gratitude towards my thesis advisor, Professor Sathe, for being a wonderful mentor and coach. In addition to his deep engineering knowledge, his wisdom and ability to resolve and simplify complex issues with clarity is an attribute that I will constantly try to emulate. Thank you, sir.

I also thank my thesis group team mates, Chris, Ryan, and Bob, for their valuable inputs during my thesis preparation.

Last but not least, my most wonderful wife, Rosita, for being my unwavering pillar of support and love during our time in Monterey.

THIS PAGE INTENTIONALLY LEFT BLANK

I. INTRODUCTION AND BACKGROUND

Heat engines that run on fossil fuel, such as diesel engines and gas turbines, are widely employed for propulsion and power generation. Despite technological advances, approximately 60% of the chemical energy released during fuel combustion is lost to the atmosphere as waste heat. A typical energy balance of a modern diesel engine shown in Figure 1 shows that almost 40% of the fuel energy is lost in exhaust gases (Woodyard, 2004).

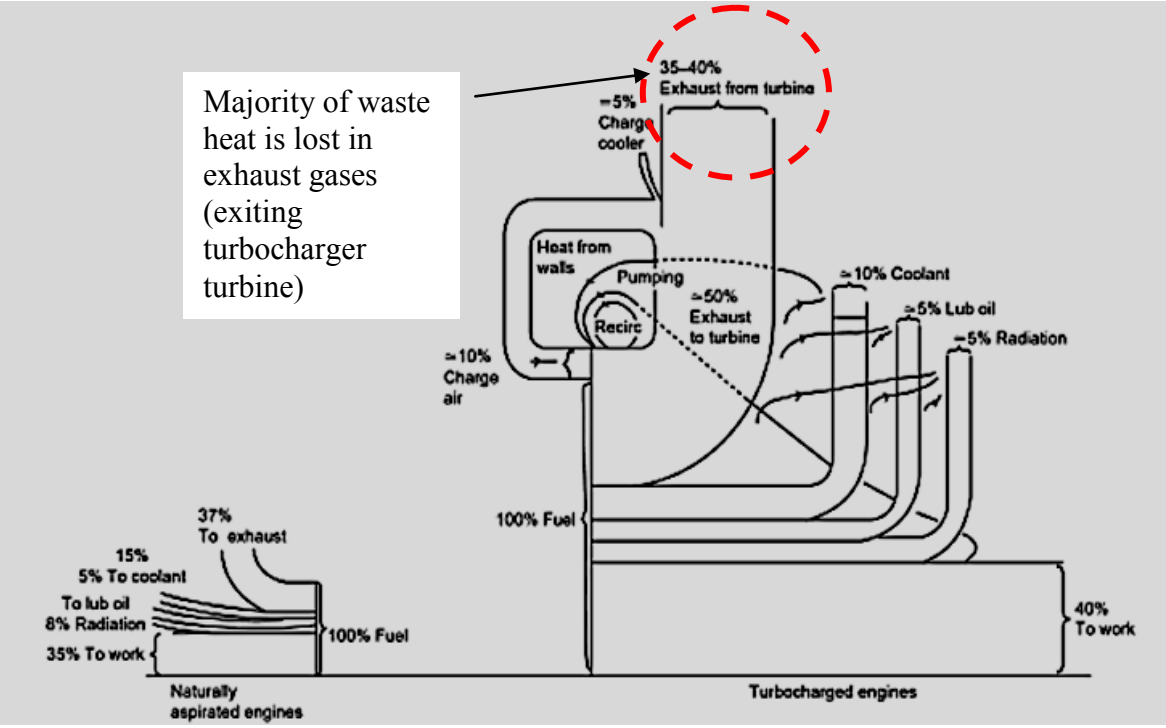

Figure 1. Energy balance of a typical modern turbocharged intercooled diesel engine (from Woodyard, 2004).

Exhaust gas Waste Heat Recovery (WHR) is the recovery of energy from waste heat in the exhaust gases for useful purposes such as heating, refrigeration, power generation, propulsion, etc. Benefits of WHR include reduced fuel consumption, reduced operating costs, and lower emissions (BCS, 2008). WHR can be achieved through bottoming, topping, and combined cycles as described by Paanu, Niemi, and Rantanen,

(2012). The waste heat recovered from exhaust gases is commonly used for heating purposes or alternatively used to generate steam which is then passed through a turbine generator in a Rankine cycle to produce electricity. A typical layout of the Combined Heat and Power (CHP) Waste Heat Recovery System (WHRS) is shown in Figure 2.

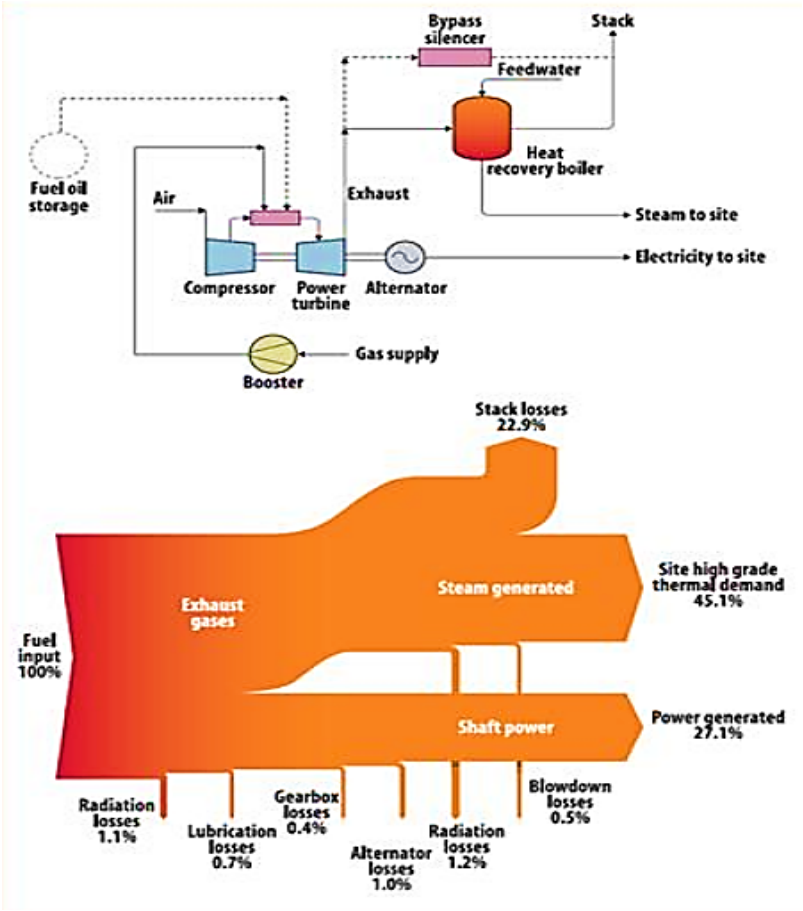

Figure 2. Layout of an typical exhaust gas WHRS used for combined heat and power (from CHP Focus, 2014)

A WHR report commissioned by U.S. Department of Energy's Industrial Technologies Program identified WHR as a proven and effective technology with the potential to improve energy efficiency by 10% to 50% (BCS, 2008). Exhaust gas WHR have also been increasingly utilized by merchant ships to improve the overall efficiency

of their propulsion and shipboard power plants so as to reduce emissions and fuel consumption (www.greenship.org, 2014).

A paper by Bailey (1985) compared exhaust gas WHR using three alternative bottoming power cycles on heavy duty truck diesel engines to supplement power generation. The systems were found to improve the specific fuel consumption of the power plants significantly. A maximum improvement of 12% was achieved by using a Rankine cycle heat-recovery system in series with turbo-compounding. A 9% improvement in specific fuel consumption was achieved when no turbo-compounding was used. Modern gas turbines equipped with optimized WHRS have been reported by Carapellucci and Giordano (2012) to achieve overall combined-cycle thermal efficiencies of up to 55%.

WHR can be used to support the U.S. Navy's (USN) energy program to increase its energy security and pursue energy independence through the increased use of alternative energy, energy conservation, higher energy efficient technologies, and energy supply management innovations (Deputy Assistant Secretary of the Navy (DASN) Energy Office, 2010). With the large number of diesel engines and gas turbines in operation, in both onshore installations and onboard ships, the USN and U.S. Marine Corps (USMC) recognize the potential of WHR applications and are putting in significant effort to develop WHR technology.

One area of development is to improve the performance and reliability of the exhaust gas waste heat recovery units (WHRUs). A WHRU is essentially a gas-to-gas or gas-to-liquid heat exchanger where energy from the hot exhaust gases is transferred into a cooler working fluid (liquid or gas) through heat exchanger surfaces such as tubes or plates. The WHRU is one of the most crucial, and the most vulnerable, components in any exhaust gas WHRS as it is subjected to harsh operating conditions such as adverse temperature gradients, fouling, and corrosive gases. Dooley, Paterson, and Pearson (2005) stated adverse temperature gradients to be one of the most common causes of WHRU tube failures. Adverse temperature results in differential expansions and thermal stresses within and between components in the WHRU. The induced thermal stresses can

also contribute towards stress corrosion cracking and fatigue, which cause premature failures of WHRUs.

The USN had limited success during the implementation of exhaust gas waste heat recovery on the DD-963s in the 1970s; availability of the WHRS was low due to issues such as poor WHRU reliability and reduction of gas turbine performance due to exhaust gas back pressure. The WHRS were subsequently removed from operation (Mastronarde, 1982).

In order to ensure a successful implementation of the next generation of WHRUs onto USN and USMC power plants, WHRU performance and reliability are crucial and are related to the temperature profiles within a WHRU. In view of this requirement, this thesis investigated how WHRU reliability and performance are affected by WHRU geometry, exhaust gas flow streams, and WHRU design features such as tube material and profile, and location of water inlet/outlet placements. Findings from this study can be applied directly to improve the performance and reliability of future WHRU designs.

II. LITERATURE REVIEW

A literature review was performed to understand the challenges faced by WHR programs in areas related to performance and reliability. The review looked at how heat recovery and exhaust side pressure drop performance as well as reliability of exhaust gas WHRUs are affected by various features related to design, construction and operations.

A. PAST EXPERIENCE WITH SHIPBOARD WHRS

In the 1970s, the USN employed WHR to produce steam for heating and auxiliary demands of the DD-963 (SPRUANCE) class destroyers. Each of the three Ship Service Gas Turbine Generators (SSGTGs) was equipped with a WHRU.

Although the WHRS was able to fulfill the steam production requirements, Rains, et al. (1976) and Mastronarde (1982) highlighted numerous problems with the first generation of WHRS. These include excessive exhaust gas side pressure drop which resulted in degradation of engine performance. The WHRUs also suffered from frequent exhaust gas leakages due to differential expansion and contraction at the casings and connecting points. As the SSGTGs and the WHRUs which have limited capability to operate in dry conditions) are interlinked, a defect on the WHRU could curtail the availability of the entire SSGTG system.

The lesson learned was the importance for power plants to be able to operate independent of their WHRU. Alternatively, WHRUs must be designed with the ability to run in dry conditions when no coolant is supplied into the WHRU. The WHRU must be able to withstand the high exhaust gas temperature during this condition. Dry operations may be required to prevent ingress of coolant from a leaking WHRU, placed within the exhaust tube from flowing into the power plant to cause damage. This capability thus became an important design criterion for subsequent generations of WHRS.

Similar issues were also faced by the Canadian Navy's WHRS which were installed on the DDH 280 class destroyers (Breaux & Davies, 1978). High spot temperatures and cracking of the heat exchanger diaphragm were experienced during operation. In addition, the WHRUs were not designed with access for maintenance in

mind. Due to improper design, fin corrosion and soot accumulation were also major problems that plagued the program. In order to address these issues, significant redesign incorporating changes in material, layout, heat exchanger tubes and fins and exhaust gas system had to be made.

B. EFFECT OF DESIGN FEATURES ON WHRU PERFORMANCE AND RELIABILITY

Heat recovery enhancement can be achieved by passive, active, or a combination of both enhancement techniques (Akpinar, 2006). Active enhancement techniques are achieved through the provision of additional flow energy to the fluid, by increasing the mass flow rate or increasing the temperature of heat source. Passive enhancements are achieved without additional input of energy but through the enhancement features, such as optimized geometries, configuration, shapes or devices such fins, materials to increase the overall heat transfer coefficients.

1. Cascading Waste Heat Recovery

In order to maximize recovery, WHRS can be made up of numerous sections of WHRUs which have been optimized to recover heat energy at specific temperature and flow profiles. Heat Recovery Steam Generators (HRSGs) are an example of such WHRUs. They have been specifically designed to generate a large quantity of steam which is subsequently used for heating or power generation via a Rankine cycle. Macdonald (2014) highlighted that typical combined-cycle HRSGs use 15 to 20 different heat-transfer sections, namely super-heaters, re-heaters, evaporators, and economizers to produce steam in three pressure levels. These sections are placed in series at different locations along the exhaust-gas path so as to recover waste heat over a wide range of temperatures. Similarly a cascading system of optimized WHRUs can be applied to maximize the performance of WHR from the exhaust tubes of power plants both on board ships and ashore.

2. Heat Recovery Enhancement Techniques

Passive heat enhancement techniques using extended surfaces such as placing fins inside the exhaust gas flow are well-established and researched. Correlations and relations of extended surfaces with heat transfers can be found in heat transfer textbooks, design handbooks, journals articles, and proceedings. The main issues with the use of extended surfaces are increased capital cost and more important the high pressure drops.

Heat transfer was found to increase when internal fins were added to a tube undergoing laminar flow (Masliyah & Nandakumar, 1976). Agrawal and Sengupta (1993) numerically studied the heat transfer and pressure drop in the annulus of a double pipe heat exchanger with fins and found that both heat transfer and pressure drop increase as compared a similar heat exchanger without fins under the same flow conditions. Pressure drop increase was due to increased friction factor as well as blockage effect from the extended surfaces. An interesting heat transfer enhancement is the use of helical inserts to induce swirling flow where an increased heat transfer coefficient is desired. Experiments were performed by Akpinar (2006) to investigate heat transfer and pressure drop performance in both parallel and counter current flow configurations with Reynolds numbers ranging from 6,500 to 13,000. A 2.64 times increase in heat transfer rate was achieved when the helical inserts were used. However, the use of these devices also increased the friction factor considerable by up to 2.74 times as compared to a tube without the insert. Pardhi and Baredar (2012) reported a 61% to 78% increase in heat coefficient over a smooth tube without inserts. However, pressure drop increased by a greater amount. Patel, Parmar, and Soni (2014) reviewed the works of various researchers and reported similar findings of higher pressure losses compared to heat transfer gains whenever helical inserts were used to induce swirling flow as a passive heat enhancement technique. It is thus apparent that the use of extended surfaces and placement of intrusive devices such as helical inserts introduce blockages and the increased pressure losses across heat transfer tubes. In order to mitigate this, Khalil, Zohir, and Farid (2010) investigated heat transfer related to swirling and non-swirling flows through sudden pipe expansions at constant pumping power. They highlighted that the use of swirling flow

coupled with sudden expansion allowed heat transfer increase to be greater than pressure losses when compared to an equivalent sudden expanded pipe without helical inserts.

Alternatively, Durmus (2002) used a snail entrance to generate swirl in air flow in a tube for a concentric double-pipe heat exchanger. The use of a snail entrance feature increased the Nusselt number in the heat exchanger from 85% to 200% with a pressure drop increase of 110%. Albadr, Tayal, and Alasadi (2013) conducted experiments to study turbulent counter flow heat transfer and flow characteristics using a coolant that is made up of water and Al_2O_3 nanofluid of concentrations of between 0.3–2% in shell and tube heat exchanger. They found heat transfer to increase with higher concentration of Al_2O_3 nanofluid. However, friction factor also increased due to the increased viscosity due to the nanofluid.

Overall, heat transfer enhancement features such as fins and helical inserts increase pressure losses which could offset the gain achieved in heat transfer. In the context of exhaust gas WHRUs, these increased pressure drop caused by the heat enhancement features induces back pressure into the exhaust system of the diesel engine or gas turbine upstream. This adversely affects their performance. A system level approach is required during new designs or the retrofitting of existing power plants with WHR so as to achieve a net improvement in thermal efficiency and specific fuel consumption.

3. Effect of WHRU Exhaust Gas Back Pressure on Power Plants

As discussed earlier, pressure drop increase adversely affects the fuel efficiency of the power plant up stream. The placement of a WHRU in the exhaust tube creates back pressure and increases specific fuel consumption. Careful design and arrangement of WHRUs must be made in order to minimize excessive back pressure to achieve an actual increase in thermal efficiency and improve specific fuel consumption. Boyce (2012) highlighted in a typical gas turbine exhaust gas WHRS that every 25 mm of water (245 Pascal) increase in turbine back pressure reduces the power output and heat rate by 0.25% and 0.08%, respectively. Hield (2011) concluded that exhaust back pressure in diesel engines resulted in increased specific fuel consumption, fluctuation in engine

speed, and higher exhaust temperatures. These induce thermal cycling which causes increased wear, overheating, and thermal failures of engine components, severely affecting WHRU reliability.

4. Effect of Differential Temperature on Reliability of Exhaust Gas WHRUs

Dooley, Paterson, and Pearson (2005) highlighted that more than 80% of pressure parts (i.e., tubes) failures in WHRUs are caused by damaging thermal effects or poor cycle chemistry. The root causes of thermal induced failures are primarily caused by adverse temperature differences within the WHRU during startup, operation, and shutdown. Adverse differential temperatures were commonly found in WHRU components such as heat exchange tubes, tube to header joints, welds, and tube bends (Daniels, 2014; Zamanzadeh, Larkin, Bayer, & Linhart, 2007). Differential temperatures result in differential expansion of these components. Expansion of these components is influenced by their geometry and dimension, the materials' thermal conductivity and thermal expansion coefficient, and the surrounding flow field. Differential expansions cause thermal-mechanical stresses both globally and locally, and contribute significantly to thermal fatigue as well as chemical fatigue factors such as stress corrosion cracking (SCC). Although startup and shutdown operating procedures could be established to mitigate thermal-mechanical damage (EPRI, 2009), the best prevention is to understand and incorporate features into the WHRU design to prevent or minimize such adverse differential temperature profiles. As discussed earlier in Breaux and Davies (1978) and Mastronarde (1982), failure to resolve the reliability problem was one of primary reasons for the limited success in the WHR programs.

THIS PAGE INTENTIONALLY LEFT BLANK

III. OBJECTIVES AND APPROACH

This study aimed to investigate and gain insight into how heat recovery performance, exhaust side pressure drop, and temperature profile of WHRUs are impacted by features related to WHRU design and construction, as well as and WHR operation. This thesis study was part of the USN, Naval Postgraduate School (NPS) WHR capability roadmap (see Figure 3), which aims to build up WHR subject matter expertise and provide solutions for issues relating to WHRS reliability and performance in support of the strategic goals of the USN Energy Program.

Specifically, the effect of WHRU geometry (tube length-to-tube diameter ratio and shell diameter-to-tube diameter ratio), water inlet and outlet placements, exhaust gas swirl, tube materials of different thermal conductivity (steel, copper, Inconel 625, and "Pyroceram" ceramic), and the use of heat spreader features were investigated and contribute toward in the buildup of WHR knowledge. In particular, knowledge on exhaust side pressure drop, heat recovery performance, and adverse temperature profiles were sought.

The study was achieved using analytical and Computational Fluid Dynamic (CFD) models based on a counter flow Water Jacket WHRU. Exhaust gas parameters for the study were based on USN's Rolls Royce 501K SSGTG and USMC's MEP803A Diesel Engine Generator (DG) at steady state operating conditions. The rationale for the choice of the Water Jacket WHRU configuration, as well as the model setup is discussed later in this chapter.

In order to cover the wide range of exhaust parameters found in both power plants, non-dimensional parameters and analysis were used in both analytic and CFD models. Definition and derivation of non-dimensional parameters, governing equations and analytical correlations used are covered in Chapter IV.

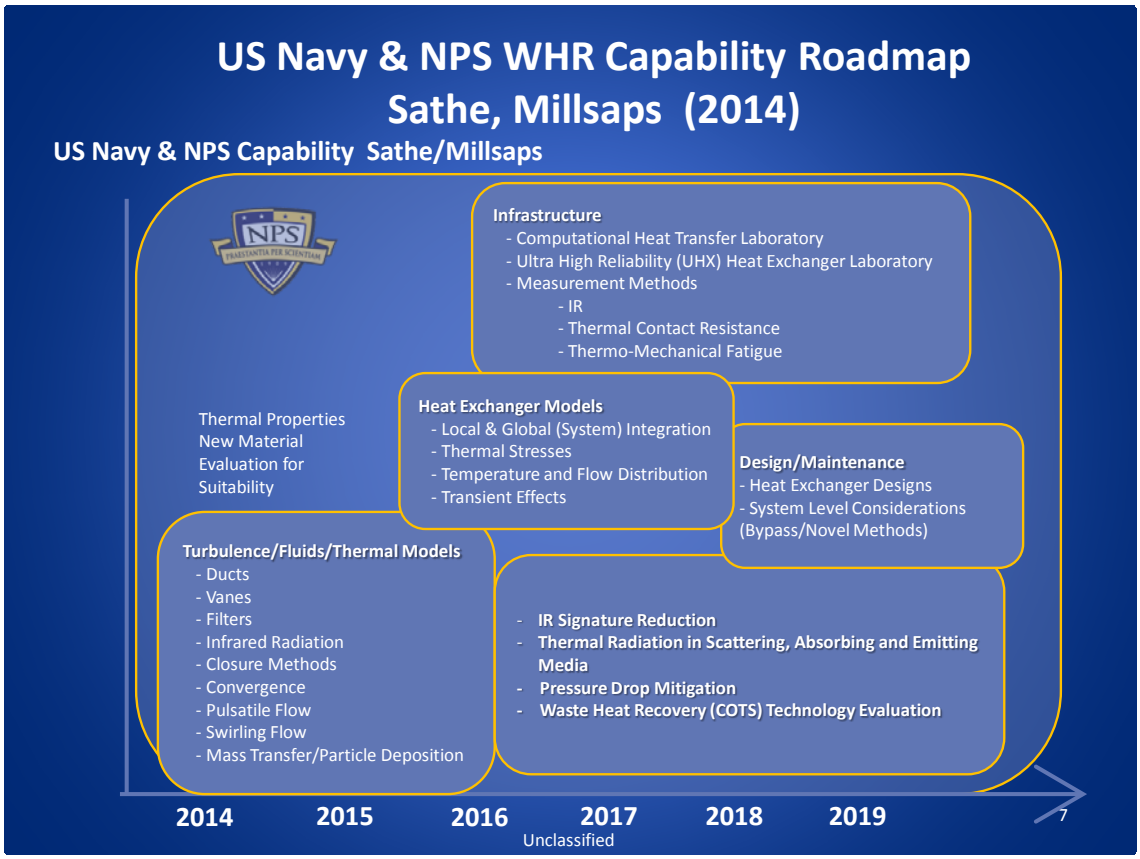

Figure 3. NPS, USN, and USMC Waste Heat Recovery System Roadmap (from Sathe & Millsaps, 2014).

Chapter V presents the results of analytical models that were evaluated over a wide range of WHRU length-to-tube diameter (L/d) ratios and water jacket diameter-to-tube diameter (D/d) to understand the effect of geometry on WHRU heat recovery and exhaust pressure drop performance. Evaluations of the models were made based on the ε-NTU method and correlations obtained from open sources such as heat transfer textbooks and handbooks.

Subsequently, Chapter VI presents the analysis and results from CFD models constructed using the ANSYS-CFX CFD package. CFD models were used in order to overcome the limitations of analytical models to investigate effects of water inlet and outlet placements, exhaust gas swirl, different tube materials and heat spreader feature. The parameters inspected were heat recovery rate, exhaust gas side pressure drop,

temperature profile, contours, as well as velocity vectors field in the exhaust gas and water domains.

Chapter VII discusses the findings and conclusions of this study. The chapter also includes recommendations and suggests future work to advance understanding on this topic. Finally, settings and results of ANSYS-CFX models used in this study are collated and provided in the Appendices.

A. SELECTION OF WHRU CONFIGURATION FOR STUDY

In order to understand the complex interactions and relationships between heat recovery, pressure drop, and temperature profile in exhaust gas WHRUs, two simple counter-flow WHRU configurations (exhaust jacket and water jacket) were initially considered to be used as the model to study the effect various features on performance and reliability.

A counter flow configuration was chosen over a parallel one due to higher heat transfer effectiveness and, more importantly, the smaller range of temperature differences between the hot and cold fluids throughout the WHRU length. The importance of gradual temperature profiles and gradients towards minimization of differential expansion and WHRU reliability was discussed in Chapter II. Comparison of the typical temperature profiles of counter flow versus parallel flow heat exchange is shown in Figure 4.

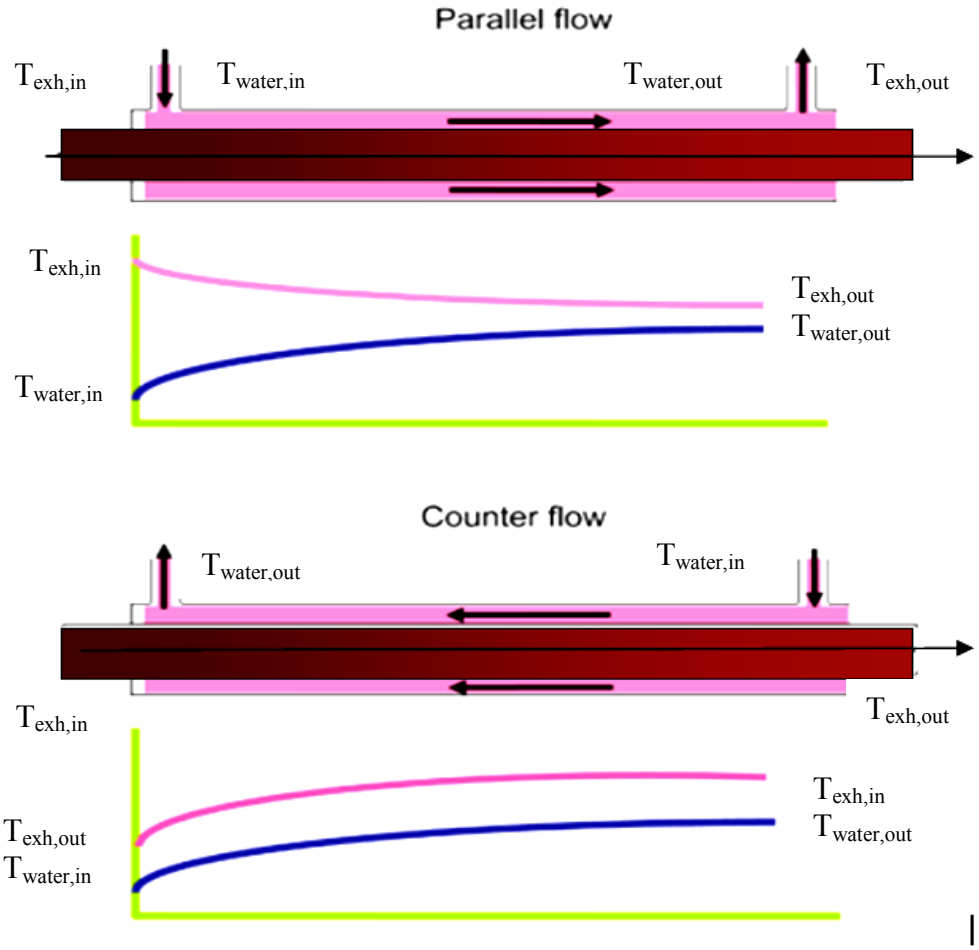

Figure 4. Comparison of typical temperature profiles for parallel flow (top) versus counter flow (bottom) heat exchange (after Longwin at http://www.longwin.com/).

The following considerations were used as criteria for the selection of the final counter flow WHRU configuration:

1. Ability to avoid adverse temperature profiles and gradients in order to improve WHRU reliability

2. Minimum impact on the performance of existing power plant in event of WHRU failure.

3. Ease of access for inspections and maintenance

4. Ease of retrofit onto exhaust stacks of existing power plants with minimum modifications or redesign

The water jacket was eventually chosen over the exhaust jacket configuration due to merits that are discussed in the following sections.

1. Exhaust Jacket WHRU Configuration

The exhaust jacket WHRU shown in Figure 5 is representative of how many WHRU are being configured. In the exhaust jacket configuration, the WHRU is placed inside the exhaust tube, with water inlet and outlet being the only connections going through the exhaust tube.

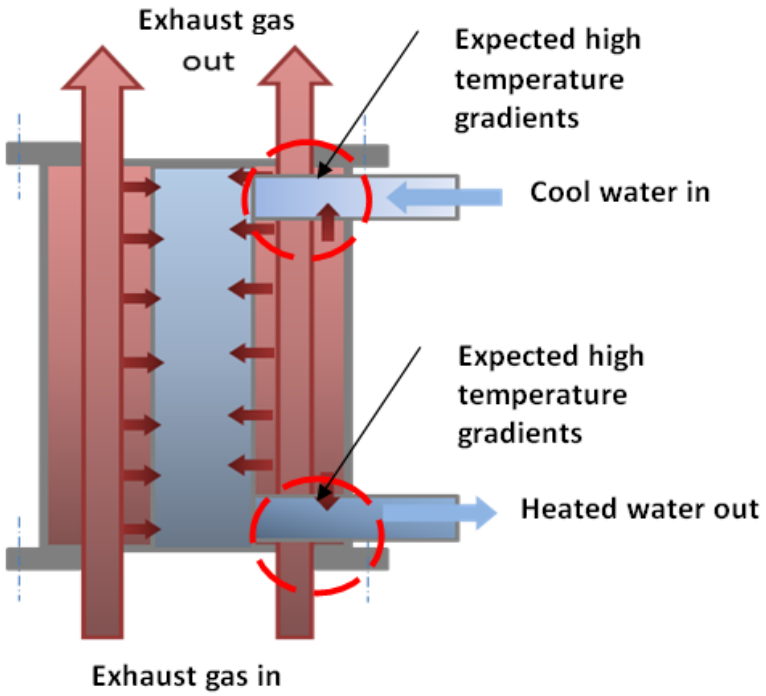

Figure 5. Schematic view of the counter-flow exhaust jacket WHRU configuration.

WHRUs used in the first generation WHRS of the USN and Canadian Navy was similarly placed within the exhaust gas stream (Breaux & Davies, 1978; Mastronarde, 1982). The Rankine Cycle Energy Recovery (or RACER); a WHRS explored by the USN for use onboard USN gas turbine powered ships also designed for its WHRU to be placed

within the exhaust tube (Halkola, Campbell, & Jung, 1983) in order to maximize its heat recovery.

The exhaust jacket configuration also allows several WHRUs to be placed inside the exhaust tube to increase heat recovery. However, doing this causes blockages and restricts the flow of exhaust stream through the exhaust tube. This increases the exhaust gas side pressure drop and back pressure which adversely impact the efficiency and operation of the power plant upstream as discussed in previously.

For a new WHRS system, allowance for this additional pressure drop can be incorporated into the design of the exhaust system. However, in the case of retrofit, a redesign of the engine intake and exhaust system might be required in order to mitigate the increased exhaust pressure drop. This would increase the capital cost, affecting the life time savings of the WHRS.

Adverse temperature profiles are also expected at the locations where the water inlet and outlet enter or exit the exhaust stack due to large temperature differences between water and exhaust gas. Thermal stresses arising from localized differential thermal expansions between the water pipes and exhaust stack could eventually result in cracks and leakages. In the event of a failure, a WHRU placed inside the exhaust tube of a power plant may also render the entire power plant to be non-operational. This is unacceptable in view of system readiness and availability requirements. This WHRU configuration also posed significant challenges when access for inspection, maintenance, or replacements is required. Based on these considerations, the exhaust jacket configuration was not selected.

2. Water Jacket WHRU Configuration

The water jacket WHRU configuration shown in Figure 6 is a simple layout in which a water jacket surrounds the exhaust tube of a power plant. Water is introduced into the jacket using an inlet pipe situated on top of the WHRU. Water flows down the jacket in a direction opposite to the exhaust gas flow, and exits the jacket through an outlet pipe situated at the bottom. Heat energy from the exhaust gas is transferred to the water through the exhaust tube.

One advantage of the water jacket configuration is the relative ease with which it can be retrofitted on the existing exhaust tube. The water jacket configuration allows existing exhaust tube dimensions to remain the same. There are also very little requirements for redesign or modification of the exhaust gas system. Heat energy from the exhaust gases is transferred to the heat transfer fluid in the water jacket through the exhaust tube section. This WHRU configuration has the potential to be scalable or can be constructed in a standard WHRU module and installed onto the required length of the exhaust tube. Potentially, lesser modifications should be required to implement this due to its simple design.

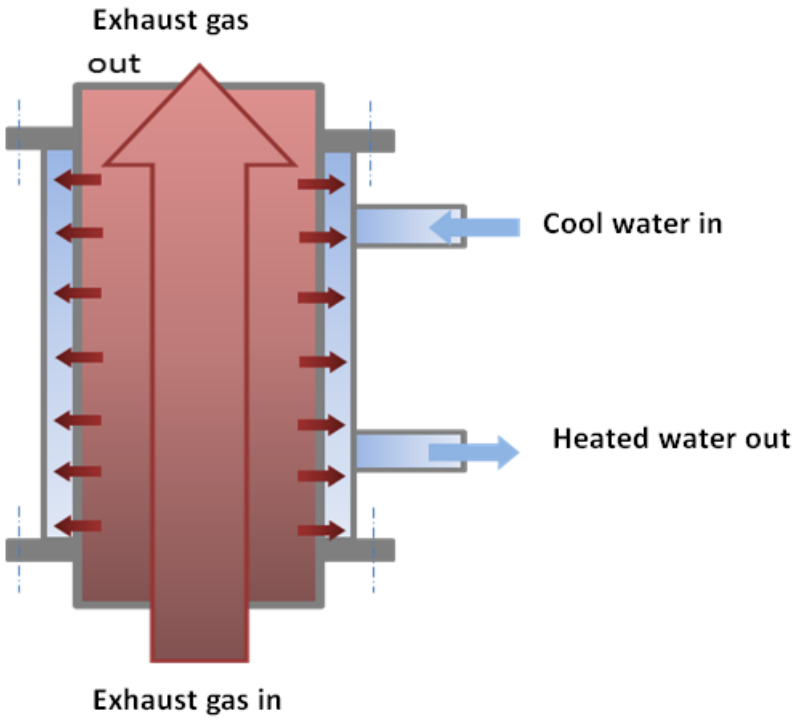

Figure 6. Schematic view of the counter-flow water jacket WHRU configuration.

The water jacket configuration also provides easy access to the WHRU for inspection and maintenance. In addition, no components were placed within the exhaust

tube. This avoided additional blockage or back pressure which could affect engine performance and operation.

The water jacket configuration allows the layout and configuration of the existing exhaust gas system to remain unchanged, avoiding the need for any redesign of the engine intake and exhaust system which could add cost and complexity to the WHR implementation on existing systems. Based on these merits, the water jacket WHRU configuration was eventually used for follow-on analytical and CFD modeling to investigate the effect of exhaust tube L/d ratio, D/d ratio, coolant inlet and outlet placements, exhaust gas swirling conditions, and tube materials (steel, copper, Inconel, and ceramic) on heat recovery performance

The literature review conducted found numerous researches on how recovery performance of concentric heat exchangers can be improved by adding swirl to the flow within the tube. Swirls within the tube were generated using swirl generators, such as helical inserts and fins within the flow, or snail entrance features as discussed earlier in Durmus (2002); Akpinar (2006); Agrawal and Sengupta (1993); Khalil, Zohir, and Farid, (2010); Kreith and Margolis (1959), Pardhi and Baredar (2012); Patel, Parmar, and Soni (2014); Sane, Taji, and Pachegaonkar (2014); and Masliyah and Nandakumar (1976). These enhancement techniques generally result in a pressure drop penalty that is higher than the heat recovery improvements. Based on the background information, this thesis proceeds to study how heat recovery, pressure drop, and temperature distributions within water jacket exhaust gas WHRU are affected by water jacket inlet and outlet placements, WHRU tube materials, or heat spreader features. Results from this study provide insight into how problems affecting the performance and reliability of WHRUs can be resolved.

B. CFD MODEL SETUP AND GEOMETRY

The model used for the CFD studies is shown in Figure 7 through Figure 11. Locations of inlets, outlets, and key parameters used to describe the WHRU geometry are included in these figures. In order to facilitate wider application of the results, non-dimensional analysis and non-dimensioned parameters were utilized and are discussed in Chapter IV.

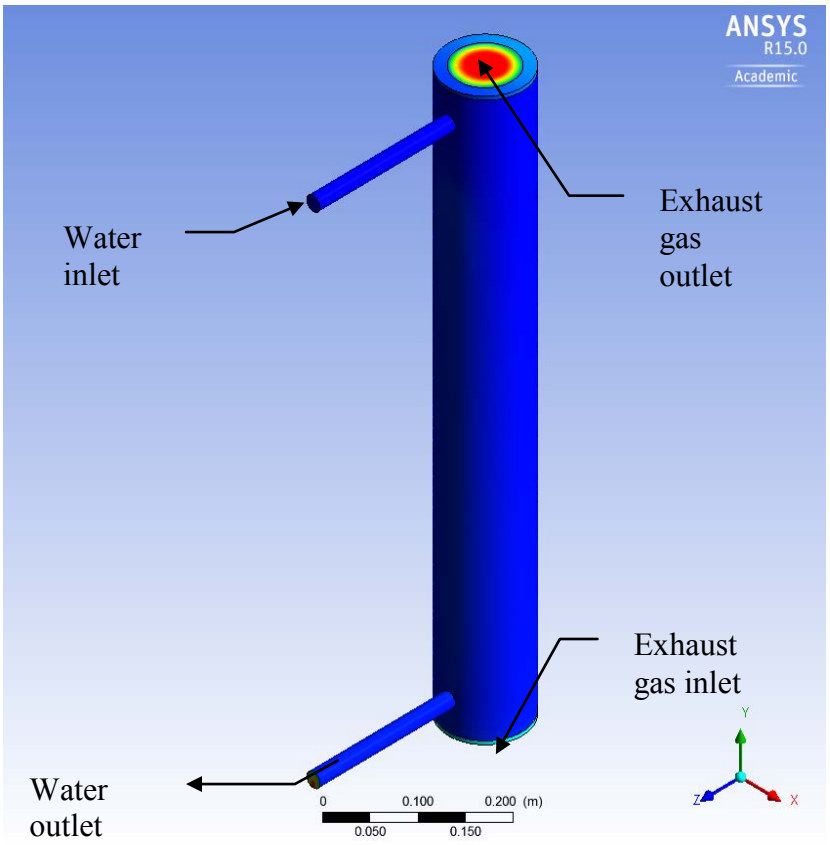

Figure 7. Isometric view of the CFD model used in the study.

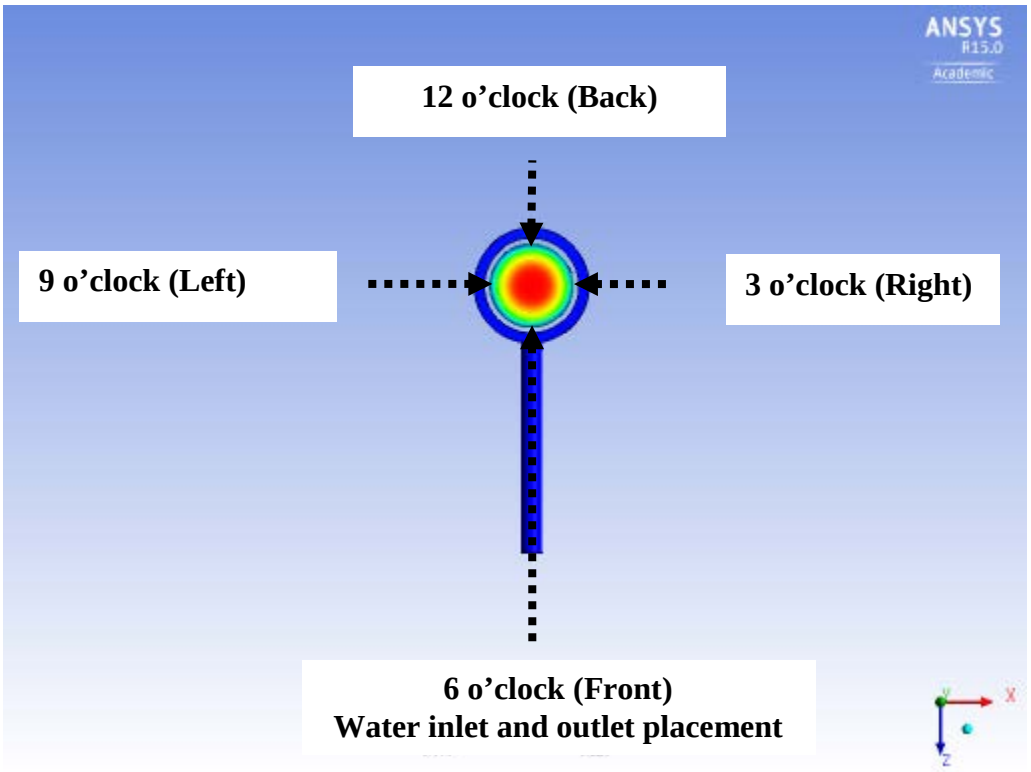

Figure 8. Top view of CFD model defining radial orientation of measurements locations.

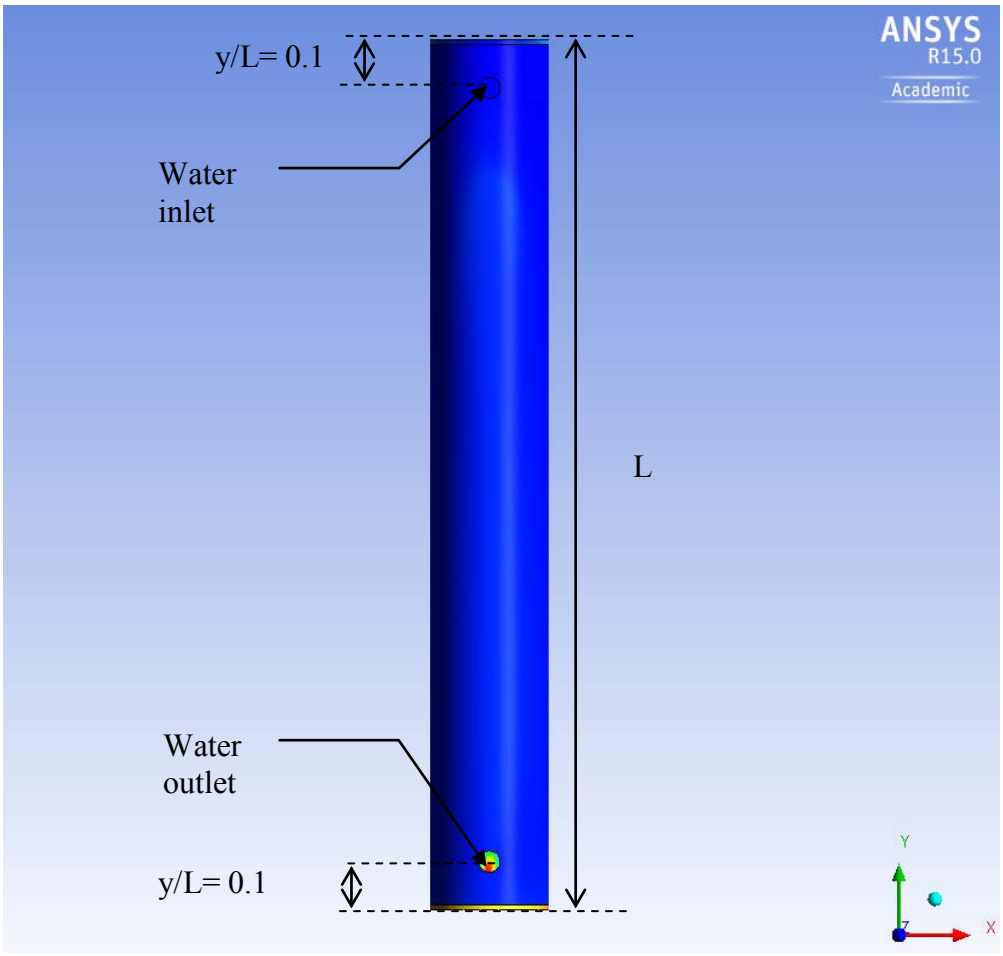

Figure 9. A 6 o'clock view of CFD model showing WHRU length (L) and locations of water inlet and outlet.

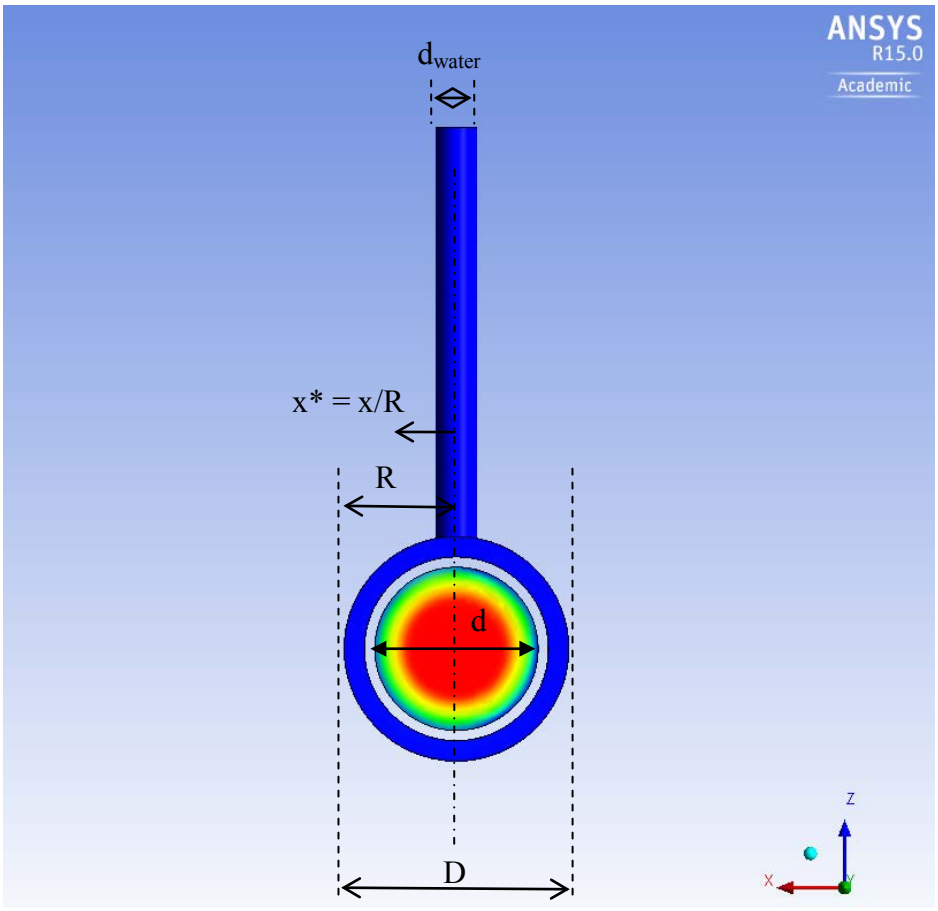

Figure 10. Top view of CFD model defining the water jacket diameter (D), jacket radius (R), exhaust tube diameter (d), and water inlet and outlet diameter (d_{water}).

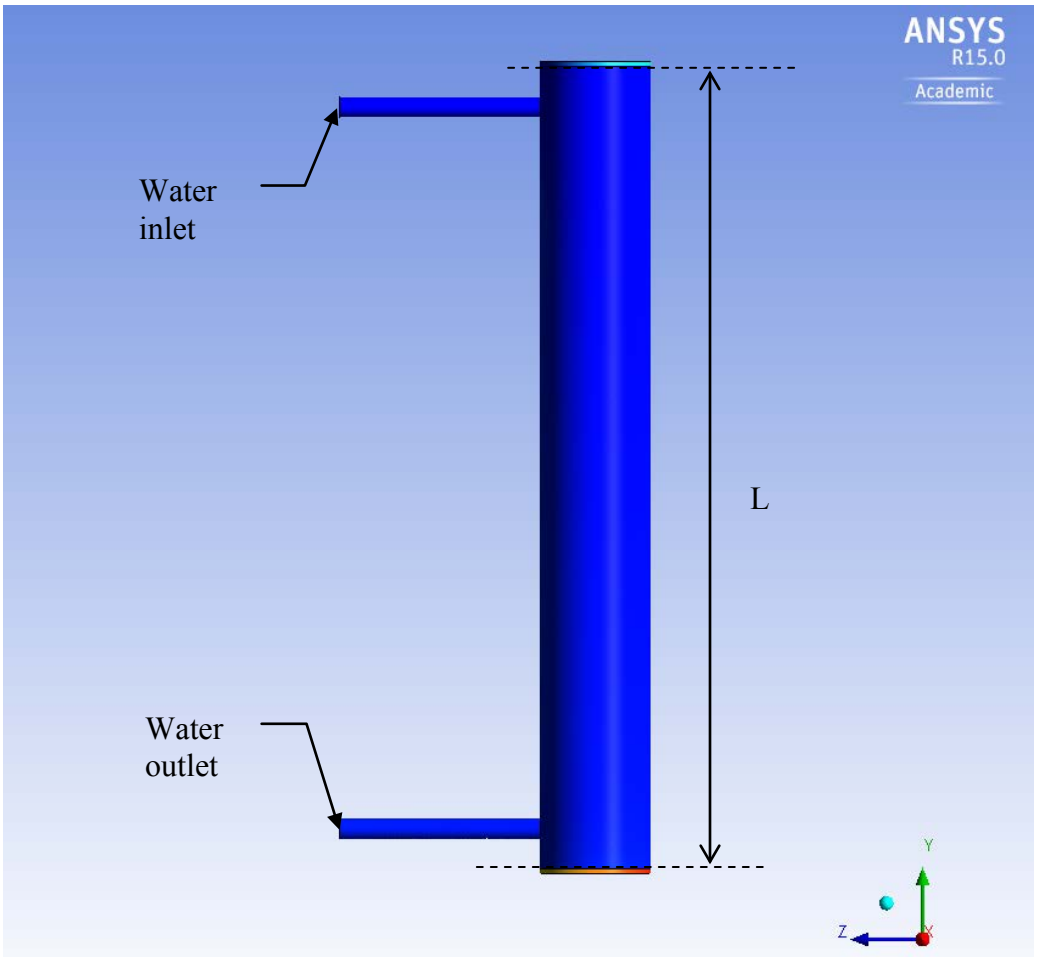

Figure 11. A 3 o'clock view of CFD model defining locations of water inlet and outlet.

THIS PAGE INTENTIONALLY LEFT BLANK

IV. GOVERNING EQUATIONS, NON-DIMENSIONAL ANALYSIS AND CORRELATIONS

The governing equations for continuity, momentum, and energy transport and conservation used for the CFD modeling are stated in this chapter. These equations are built into the algorithm of ANSYS-CFX. Additional information on the governing equation can be obtained from (ANSYS, 2013). Subsequently, non-dimensional analysis was conducted using the Buckingham Pi Theorem in order to reduce and identify the important parameters affecting heat recovery and pressure drop. In order for the studies to be applicable over a wider range of variables, parameters in this study have been non-dimensioned. Finally, the correlations used for the estimation of heat recovery and pressure in the water jacket WHRU are discussed.

A. GOVERNING EQUATIONS

The governing equations for mass, momentum, and energy transport used by ANSYS-CFX are shown here (ANSYS, 2013).

Continuity Equation

$$\frac{\partial \rho}{\partial t} + \nabla.(\rho \vec{U}) = 0 \tag{1}$$

Momentum Equations

$$\frac{\partial (\rho \vec{U})}{\partial t} + \nabla(\rho \vec{U} \otimes \vec{U}) = -\nabla p + \nabla.\tau + S_M \tag{2}$$

Thermal Energy Equation

$$\frac{\partial (\rho h)}{\partial t} + \frac{\partial \rho}{\partial t} + \nabla.(\rho \vec{U} h) = \nabla.(k \nabla T) + \vec{U} \nabla p + \tau : \nabla \vec{U} + S_E \tag{3}$$

where:

S_E and S_M are energy and momentum sources. For this study, no sources were present.

$\vec{U}$ is the velocity vector and is defined as:

$$\vec{U} = \begin{bmatrix} u_x \\ u_y \\ u_z \end{bmatrix} \tag{4}$$

τ is the stress tensor related to the strain rate by the following:

$$\tau = \mu(\nabla\vec{U} + (\nabla\vec{U})^T - \frac{2}{3}\delta\nabla\vec{U}) \tag{5}$$

and in equation (2)

$$\nabla(\rho\vec{U}\otimes\vec{U}) = \begin{bmatrix} \frac{\partial}{\partial x}(\rho U_x U_x) + \frac{\partial}{\partial y}(\rho U_y U_x) + \frac{\partial}{\partial z}(\rho U_z U_x) \\ \frac{\partial}{\partial x}(\rho U_x U_y) + \frac{\partial}{\partial y}(\rho U_y U_y) + \frac{\partial}{\partial z}(\rho U_z U_y) \\ \frac{\partial}{\partial x}(\rho U_x U_z) + \frac{\partial}{\partial y}(\rho U_y U_z) + \frac{\partial}{\partial z}(\rho U_z U_z) \end{bmatrix} \tag{6}$$

where $\tau : \nabla\vec{U}$ is the viscous dissipation which models the internal heating caused by viscosity in the fluid.

B. NON-DIMENSIONAL ANALYSIS

Numerous parameters affect heat recovery and exhaust gas side pressure drop. In order to reduce and identify the important parameters to the study, non-dimensional analysis was conducted using the Buckingham Pi Theorem. The geometry of the water jacket WHRU configuration was simplified using the layout shown in Figure 12 and was used as the basis for non-dimensional analysis.

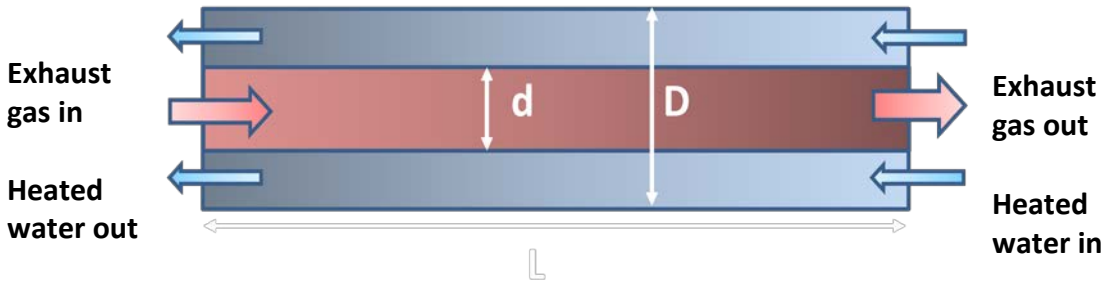

Figure 12. Water jacket WHRU configuration used for non-dimensional analysis.

1. Non-dimensional Exhaust Gas Side Pressure Drop

An estimation of pressure drop in the exhaust gas side is crucial as it translates directly to exhaust back pressure to the heat engine upstream. The pressure drop for the constant diameter exhaust tube was estimated using existing correlations for fluid flow in a pipe. Pressure loss (ΔP) in the exhaust tube for steady state flow is a function (ϕ) of the following parameters:

$$\Delta P = \phi(D, d, \bar{U}, L, \mu, \rho) \tag{7}$$

The dimensions of the aforementioned parameters are expressed in three basic dimensions, Force (F), Length (L) and Time (T), as shown in Table 1.

Table 1. Summary of parameters used for non-dimensional pressure loss analysis.

Parameters	Symbols	Dimensions
Pressure loss	ΔP	FL^{-2}
Jacket diameter	D	L
Tube diameter	d	L
Length of WHRU	L	L
Average fluid velocity	$\bar{U}$	$L\ T^{-1}$
Fluid dynamic viscosity	μ	$FL^{-2}T$
Fluid density	ρ	$FL^{-4}T^{2}$

The Buckingham Pi Theorem, the seven parameters in Equation (7), and three basic dimensions are used to generate four Pi numbers.

$$\pi_1 = \frac{\Delta P}{\rho \bar{U}^2} = \Delta P^* \tag{8}$$

$$\pi_2 = \frac{D}{d} \tag{9}$$

$$\pi_3 = \frac{L}{d} \tag{10}$$

$$\pi_4 = \frac{\mu}{\rho \bar{U} D_{eff}} = \frac{1}{\mathrm{Re}} \tag{11}$$

where D_{eff} for the exhaust tube is d, and (D – d) for the water jacket.

The non-dimensional pressure drop (ΔP^*) is a function (ϕ) of the parameters shown here:

$$\Delta P^* = \frac{\Delta P}{\rho \bar{U}^2} = \phi\left(\frac{D}{d}, \frac{L}{d}, \frac{1}{\mathrm{Re}}\right) \tag{12}$$

This also happens to be the reciprocal of the Euler number which characterizes the ratio of local pressure drop to dynamic pressure due to fluid friction in conduits (Yarin, 2012). A Euler number of 1 corresponds to a perfect frictionless flow. As such, lower ΔP^* values correspond to lower pressure drops and are influenced by D/d, L/d, and the Reynolds number of the flow.

Another useful form of non-dimensional pressure drop given by Munson, Young, Okiishi, and Huebsch (2009) is shown in Equation (13). It is a ratio of pressure to viscous force and is useful during the investigation of flows at features which involve abrupt changes in geometries such as inlets and outlets.

$$\Delta P^{**} = \frac{\Delta P D_{eff}}{\mu \bar{U}} \tag{13}$$

2. Non-Dimensional Heat Recovery (Based on Exhaust Gas Side)

The steady state heat recovery rate (q_{exh}) at the gas side for the water jacket WHRU is a function (ϕ) of the following parameters:

$$q_{exh} = \phi(\rho_{exh}, D, d, L, \mu_{exh}, C_{p,exh}, \mathrm{k}_{exh}, \bar{U}_{exh}, T_{exh}, T_{water}) \qquad (14)$$

The dimensions of the above parameters expressed in four basic dimensions, Mass (M), Length (L), Time (T) and Temperature (θ) are shown in Table 2.

Table 2. Summary of parameters used for non-dimensional heat transfer (q*).

Parameters	Symbols	Dimensions
Heat transfer	q_{exh}	ML^2T^{-3}
Density of exhaust gases	ρ_{exh}	ML^{-3}
Water jacket diameter	D	L
Exhaust tube diameter	d	L
Length of heat exchanger	L	L
Dynamic viscosity of exhaust gases	μ_{exh}	$ML^{-1}T^{-1}$
Constant pressure specific heat capacity of exhaust gas	$C_{p,exh}$	$L^2T^{-2}\,\theta^{-1}$
Thermal conductivity of exhaust gas	k_{exh}	$MT^{-3}L\,\theta^{-1}$
Mean velocity of exhaust gas flow	$\bar{U}_{exh}$	$L\,T^{-1}$
Temperature of exhaust gas	T_{exh}	θ
Temperature of water	T_{water}	θ

Using the 11 parameters listed in Equation (14) and four basic dimensions, seven Pi numbers were generated and are shown here:

$$\pi_1 = \frac{q_{exh}}{\rho_{exh} d^2 \bar{U}_{exh}^3} \tag{15}$$

$$\pi_2 = \frac{L}{d} \tag{16}$$

$$\pi_3 = \frac{D}{d} \tag{17}$$

$$\pi_4 = \frac{\mu_{exh}}{\rho_{exh} d \bar{U}_{exh}} = \frac{1}{\mathrm{Re}_{exh}} \tag{18}$$

$$\pi_5 = \frac{C_{p,exh} T_{exh}}{\bar{U}_{exh}^2} \tag{19}$$

$$\pi_6 = \frac{k_{exh} T_{exh}}{\rho_{exh} d \bar{U}_{exh}^3} \tag{20}$$

$$\pi_7 = \frac{k_{exh} T_{water}}{\rho_{exh} d \bar{U}_{exh}^3} \tag{21}$$

Therefore, the non-dimensional heat transfer equation is expressed as follows:

$$\frac{q_{exh}}{\rho_{exh} D^2 \bar{U}_{exh}^3} = f\left(\frac{L}{d}, \frac{D}{d}, \frac{\mu_{exh}}{\rho_{exh} d \bar{U}_{exh}}, \frac{C_{p,exh} T_{exh}}{\bar{U}_{exh}^2}, \frac{k_{exh} T_{exh}}{\rho_{exh} d \bar{U}_{exh}^3}, \frac{k_{exh} T_{water}}{\rho_{exh} d \bar{U}_{exh}^3}\right) \tag{22}$$

$$\pi_6 \frac{1}{\pi_5} = \frac{k_{exh} T_{exh}}{\rho_{exh} d \bar{U}_{exh}^3} \frac{\bar{U}_{exh}^2}{C_{p,exh} T_{exh}} = \frac{k_{exh}}{C_{p,exh} \rho_{exh} d \bar{U}_{exh}} = \frac{k_{exh}}{C_{p,exh} \mu_{exh}} \frac{\mu_{exh}}{\rho_{exh} d \bar{U}_{exh}} = \frac{1}{\mathrm{Pr}_{exh}} \frac{1}{\mathrm{Re}_{exh}} \tag{23}$$

Multiplying π_6 with the reciprocal of π_5 gives a combination of the reciprocal of the Prandtl number and Reynolds number. The Prandtl number compares the momentum and thermal diffusivity of the fluid, while the Reynolds number compares inertia force to the friction forces of the fluid.

Multiplying π_1 with the reciprocal of π_5 results in the non-dimensional heat transfer rate, q^*:

$$q^* = \pi_1 \frac{1}{\pi_5} = \frac{q}{\rho_{exh} D^2 \bar{U}_{exh}^3} \frac{\bar{U}_{exh}^2}{C_{p,exh} T_{exh}} = \frac{q}{\rho_{exh} D^2 \bar{U}_{exh} C_{p,exh} T_{exh}} = \frac{\frac{\pi}{4} q}{\rho_{exh} \frac{\pi}{4} D^2 \bar{U}_{exh} C_{p,exh} T_{exh}} = \frac{\frac{\pi}{4} q}{\dot{m}_g C_{p,exh} T_{exh}} \quad (24)$$

The non-dimensional heat recovery is a function of the following parameters shown as follows:

$$q^* = \frac{\frac{\pi}{4} q}{\dot{m}_{exh} C_{p,exh} T_{exh}} = f\left(\frac{1}{\mathrm{Re}_{exh}}, \frac{L}{d}, \frac{D}{d}, \mathrm{Pr}_{exh}\right) \quad (25)$$

I subsequently expressed the non-dimensional heat recovery as a percentage of maximum recoverable heat energy for the given temperature based effectiveness - NTU method in Incropera, Bergman, Lavine, and Dewitt (2011) for better insight into the heat recovery performance. The equation is defined as:

$$q^* = \frac{q_{exh}}{\dot{m}_{exh} C_{p,exh} (T_{exh,in} - T_{water,in})} \quad (26)$$

C. NON–DIMENSIONAL PARAMETERS

In order to allow results of the study to be applicable for a wide range of geometry and parameters of corresponding models, parameters and variables are non-dimensioned. This also allows the number of experimental runs or analyses to be reduced through application of similitude without the restrictions of physical units. In addition, non-dimensioned parameters provide insights into the relative significance of one parameter over another.

In order to define horizontal positions with respect to radius (R) of the WHRU jacket along the X coordinate, the following non-dimensional parameter was used.

$$x^* = \frac{x}{R} \tag{27}$$

Similarly, to define horizontal positions with respect to radius (R) of the WHRU jacket on the Z-coordinate, the following non-dimensional parameter was used.

$$z^* = \frac{z}{R} \tag{28}$$

In order to define the vertical position with respect to the WHRU length (L), the following non-dimensional parameter was used.

$$y^* = \frac{y}{L} \tag{29}$$

Thickness (t) of the materials such as the tube wall is also non-dimensioned with respect to the tube diameter (d) via the following expression:

$$t^* = \frac{t}{d} \tag{30}$$

The following is the non-dimensional parameter of the jacket diameter (D) with respect to the exhaust tube (d) which is kept unchanged throughout the study. This parameter is used to study the effect of geometry on heat recovery and pressure losses.

$$d^* = \frac{D}{d} \tag{31}$$

Another non-dimensional parameter used in this research to study the effect of geometry is the WHRU length to the tube diameter ratio.

$$L^* = \frac{L}{d} \tag{32}$$

Temperature is non-dimensioned against the difference between the inlet temperatures of the exhaust gas ($T_{exh,in}$) and water ($T_{water,in}$), and is defined as:

$$T^* = \frac{T - T_{water,in}}{T_{exh,in} - T_{water,in}} \tag{33}$$

Therefore T* = 1 at the exhaust gas inlet, and T* = 0 at water inlet.

The thermal conductivity of fluids and solids used in the study was non-dimensioned against the thermal conductivity of air; $k_{c,air}$ = 0.0261 W/mK and is obtained from the ANSYS material model used for CFD modeling. The non-dimensional thermal conductivity is defined in Equation (34).

$$k^* = \frac{k}{k_{air}} \tag{34}$$

The Reynolds number gives the ratio of inertia to viscous forces. For a circular tube, it is defined as:

$$\mathrm{Re} = \frac{\rho \bar{U} D_{eff}}{\mu} = \frac{4\dot{m}}{\pi \mu D_{eff}} \tag{35}$$

where D_{eff} for the exhaust tube is the diameter (d). For the water jacket, D_{eff} is the difference (D - d) between the jacket diameter (D) and exhaust tube diameter (d) for the water jacket.

The ratio of Reynolds number of water to exhaust gas flow is shown here:

$$R_{\mathrm{Re}} = \frac{\mathrm{Re}_{water}}{\mathrm{Re}_{exh}} \tag{36}$$

The Prandtl number (Pr) of a fluid compares the momentum to thermal diffusivities, relating the momentum and thermal boundary layers, and is defined as:

$$\mathrm{Pr} = \frac{\mu C_p}{k} = \frac{\upsilon}{\alpha} \tag{37}$$

where υ = momentum diffusivity [m^2/s] and α = Thermal diffusivity [m^2/s].

In heat transfer, the Prandtl number of the fluid represents the relative thickness of the momentum and thermal boundary layers. A fluid with a Prandtl number less than one is thermal diffusivity dominant. Heat is diffused faster compared to the velocity (momentum) of the fluid. Air and exhaust gases values around 0.7 to 0.8. Momentum diffusivity dominates when the Prandtl number is higher than one. This is the case in liquid such as water or oil. At 300K degrees Celsius, water has a Prandtl number of around 5.8. As a reference, commercial heat transfer fluids such as Paratherm HR™ (Paratherm, n.d.) have a Prandtl number of about 450.

D. NUSSELT NUMBER CORRELATION

The Nusselt number (Nu) is the ratio of convection to pure conduction heat transfer and is defined in Equation (38).

$$Nu = \frac{hD_{eff}}{k} \tag{38}$$

Different Nusselt number correlations exist for different flow regimes and shape of conduits. The flow for this study involves turbulent flow in circular tubes and circular annulus. The Gnielinski correlation which is valid for $0.5 < Pr < 2{,}000$ and $3{,}000 < Re_D < 5x10^6$ was used to estimate the turbulent flow Nusselt number for both water and exhaust gas flow in this study. The correlation is defined as:

$$Nu = \frac{(f/2)(\mathrm{Re}_b - 1000)\,\mathrm{Pr}}{1 + 12.7(f/2)^{1/2}(\mathrm{Pr}^{2/3} - 1)} \tag{39}$$

where f is the "Filonerko Fanning friction factor" from page 133 of Kakac and Liu (2002). It is used to estimate the friction factor for turbulent flow for circular conduits. The correlation is valid for $3{,}000 < Re < 10^6$ and is defined as:

$$f = [1.58Ln(\mathrm{Re}) - 3.28]^{-2} \tag{40}$$

where f decreases with increasing Reynolds number as plotted in Figure 13.

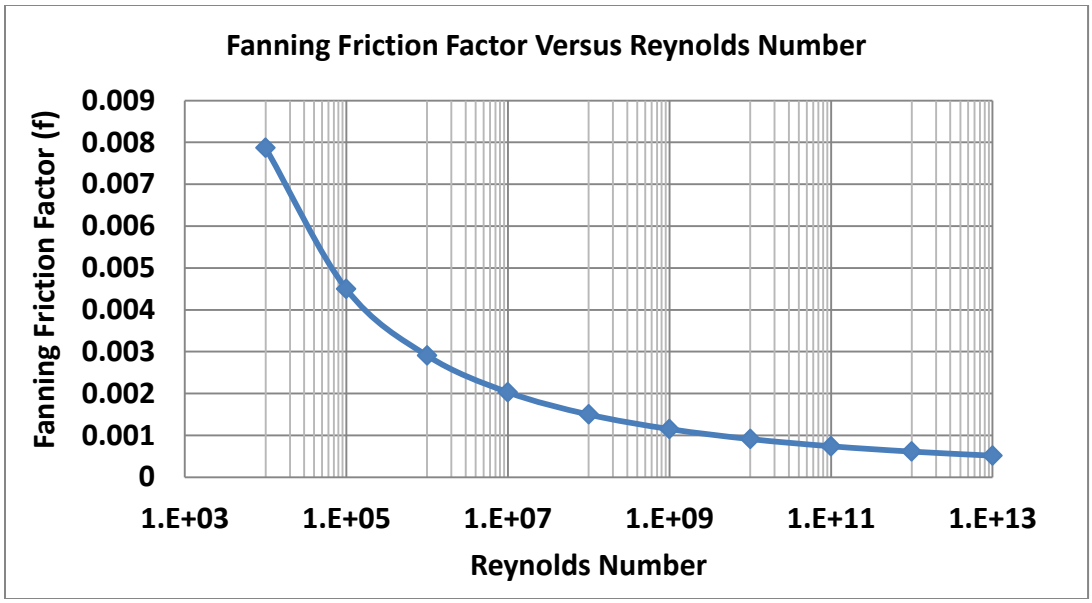

Figure 13. "Filonerko Fanning friction factor" versus Reynolds number (applicable for both water or exhaust gas flow).

E. PRESSURE LOSS ESTIMATION

The study assumed the surfaces in the WHRU to be smooth. The smooth line correlation shown in Equation 41 is used to estimate the pressure drop in the circular pipes and annulus; f is obtained using the "Filonerko fanning friction factor" discussed earlier. During actual operation, roughness increases the friction factor and needs to be taken into account.

$$\Delta P = \frac{2 f L \rho \bar{U}_m^2}{D_{eff}} \tag{41}$$

F. HEAT RECOVERY ESTIMATION (USING EFFECTIVENESS-NTU METHOD)

The effectiveness- NTU (ε-NTU) method was used to estimate the heat recovery in analytic models (Incropera, Bergman, Lavine, & Dewitt, 2011). In the study, the heat capacity of the exhaust gas (C_{exh}) is smaller than the water (C_{water}) and is assigned as the minimum heat capacity (C_{min}). The maximum possible heat recovery rate in the WHRU is estimated using Equation (42).

$$q_{\max} = C_{\min}(T_{exh,in} - T_{water,in}) \tag{42}$$

The effectiveness (ε) of the heat recovery is defined as:

$$\varepsilon = \frac{q}{q_{\max}} = \frac{C_h(T_{exh,in} - T_{exh,\text{out}})}{C_{\min}(T_{exh,in} - T_{water,\text{in}})} = \frac{C_h(T_{water,out} - T_{water,in})}{C_{\min}(T_{exh,in} - T_{water,\text{in}})} \tag{43}$$

The effectiveness relationship for counter flow and parallel flow is a function of the NTU and C_r and is shown in Equation (44) and Equation (45). C_r is ratio of minimum heat capacity to maximum heat capacity.

$$\varepsilon_{counterflow} = \frac{1 - \exp[-\text{NTU}(1 - \text{C}_r)]}{[1 - C_r \exp[-\text{NTU}(1 - \text{C}_r)]} \tag{44}$$

$$\varepsilon_{parallel} = \frac{1 - \exp[-\text{NTU}(1 + \text{C}_r)]}{[1 + C_r]} \tag{45}$$

NTU is calculated based on the overall heat transfer coefficient ($\tilde{U}_{overall}$), minimum heat capacity, and heat exchange area.

$$NTU = \frac{\tilde{U}_{overall} A}{C_{\min}} \tag{46}$$

where the overall heat transfer coefficient is estimated using the heat transfer coefficient equation shown in Equation (47). In order to simplify the calculations, no thermal resistance from fouling was considered. The contribution from the thermal conductivity

of the tube wall was also neglected due to the relatively small contribution (Incropera, Bergman, Lavine, & Dewitt, 2011).

The overall heat transfer coefficient is influenced primarily by the exhaust gas heat transfer coefficient.

$$\frac{1}{\tilde{U}_{overall}A} = \frac{1}{h_{exh}A} + \frac{t}{k_{\text{tube}}A} + \frac{1}{h_{water}A} \tag{47}$$

Once the NTU is obtained, the effectiveness is calculated and the actual heat recovery for each case is then calculated using Equation (48).

$$q = \varepsilon C_{\min}(T_{exh,in} - T_{water,in}) \tag{48}$$

V. ANALYTICAL STUDY

An analytical study was used to estimate of the amount of heat recovery and pressure drop for the water jacket WHRU using correlations and methods discussed in Chapter IV. The estimates were calculated based on exhaust tube dimensions and exhaust gas flow conditions of the USMC's MEP803A DG and USN's 501-K17 SSTG over a range water jacket to exhaust tube diameter ratio (D/d), Length to exhaust tube ratio (L/d), and Exhaust Reynolds number. Results from the estimates provide insight into the effects of WHRU geometry on heat recovery and pressure loss performance.

Calculations were made over a D/d range from 1.3 to 3.3 with exhaust tube diameter (d) kept constant while the water jacket diameter was varied. This is equivalent to retrofitting an existing exhaust tube with water jacket WHRUs of different diameters. WHRU L/d was varied from 5 to 1000. Similarly, WHRU length was varied while the tube diameter was held constant.

Calculations were made using an exhaust gas Reynolds number of 20,000 to 400,000 which covers the range expected from USMC's MEP803A DGs and USN's 501K SSGTGs. Constant exhaust gas and water inlet temperatures of 773K and 300K were used and are representative of parameters that would be expected during operations. Non-dimensional parameters such as heat recovery (q*) and exhaust pressure drop (ΔP^*) were used to present the results.

A. ASSUMPTIONS AND IDEALIZATIONS FOR ANALYTICAL STUDY

In order to facilitate the analytical study, the following assumptions and idealizations were used (Shah & Sekulic, 2002):

- steady state
- negligible heat losses to the surrounding
- no heat sinks or sources in the WHRU tube wall or fluids
- fluid temperature is uniform over every flow cross section
- no phase changes of the heat transfer fluid flowing through the WHRU
- fluid properties of each fluid are constant throughout the WHRU
- entry velocity and temperature to the WHRU on the fluid side are uniform
- fluid and overall heat transfer coefficients are constant (independent of temperature, time, and position) throughout the WHRU
- heat transfer surface area is distributed uniformly on each fluid side
- the fluid flow rate is uniformly distributed through the WHRU on each fluid side. No uneven flow, flow stratification, flow bypassing, or flow leakages occur in either the exhaust or water stream. The flow condition of either fluid domain is characterized by the mean velocity at any cross section.
- longitudinal heat conduction in the fluid and in the wall is negligible only 1-D heat conduction

The analytical model was not able to account for the effects due to water inlet and outlet locations, tube thermal conductivity, exhaust swirl, or other design features such as heat spreaders.

B. EFFECT OF GEOMETRY ON WHRU PERFORMANCE

This section investigates how heat recovery and pressure drop were affected by the geometry of the water jacket WHRU. Two non-dimensional geometric variables were varied to achieve this. The variables were the water jacket-to-exhaust tube diameter ratio (D/d) and WHRU length-to-exhaust tube diameter ratio (L/d). Exhaust tube diameter (d) was held constant while the D and L were varied.

1. Effect on Non-dimensional Heat Recovery (q*)

The effects of L/d, D/d, and exhaust Reynolds number on heat recovery are presented in Figure 14 through Figure 19. Non-dimensional heat recovery (q*) from D/d = 1.11 to 3.33 and L/d ratios from 5 to 1,000 were evaluated at exhaust Reynolds number of 2,000, 200,000, and 400,000. This allowed a study on the effect of geometry on heat recovery at exhaust flow corresponding to USMC DG at rated condition, USN SSGTG at 50% rated condition, and 100% rated condition. These results are plotted in Figure 14 through Figure 16.

The heat recovery results were also presented from another perspective in Figure 17 through Figure 19. Heat recovery results from L/d ratios ranging from 5 to 1,000, and exhaust gas Reynolds numbers ranging from 20,000 to 400,000 were calculated at D/d ratios of 1.25, 1.54, and 2.0. This allowed the effect of L/d and exhaust Reynolds number to D/d ratios to be compared.

Generally heat recovery increases with higher L/d ratio due to greater area available for heat transfer. Figure 17 through Figure 19 presents the effect of L/d on heat recovery performance over the range of exhaust gas Reynolds number at three different D/d ratios. Highest heat recovery (q*) was achieved for a WHRU with the highest L/d ratios. The maximum possible heat recovery was achieved if the length of the WHRU was long enough, i.e., L/d=1,000. However, once the maximum heat recovery is achieved (q*=1), further increase of WHRU length did not improve the heat recovery. On the contrary, additional pressure drop at the exhaust gas side was incurred. This causes back pressure, negatively impacting the performance and fuel consumption of the power plant upstream.

In addition, water jacket WHRU with high L/d ratios may not be feasible due to space constraints onboard ships or out in the battlefield. Similarly a D/d ratio which is too low would also result in excessively high pressure drop in the water side.

In general, smaller D/d ratios improve heat recovery. This is shown in Figure 14 through Figure 16. The WHRU with a smaller D/d ratio has smaller spaces in the water jacket, which results in better heat transfer between the exhaust tube wall and the water.

An interesting trend observed is that heat recovery at Re_{exh} = 20,000 shown in Figure 14 shows that L/d ratio improved heat recovery more quickly compared to a decrease in D/d ratios. This result is applicable to circumstances pertaining to USMC's DG. However, at the high exhaust Reynolds number of 400,000 shown in Figure 16 heat recovery improvement due to D/d reduction increased more rapidly. As such, a low D/d ratio would result in better heat recovery improvement in a WHRU for the USN SSGTG than for the USMC DG. It was also observed that q* increased more sharply at D/d less than two.

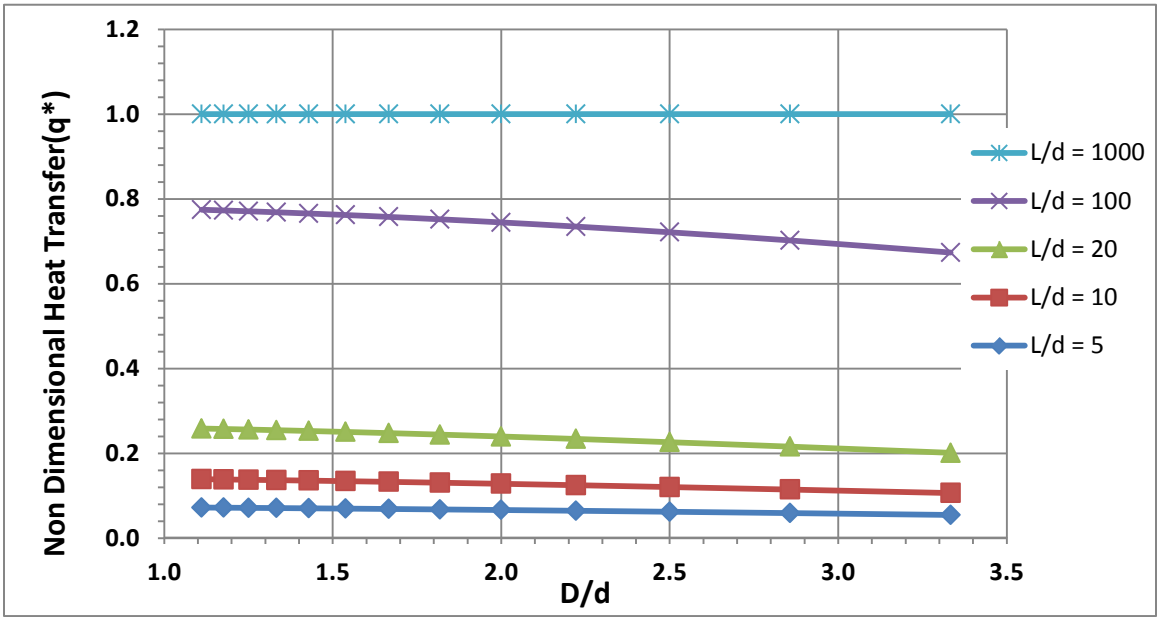

Figure 14. Comparison of non-dimensional heat transfer (q*) at exhaust gas Reynolds number = 20,000 for D/d from 1.3 to 3.3 and L/d from 5 to 1,000.

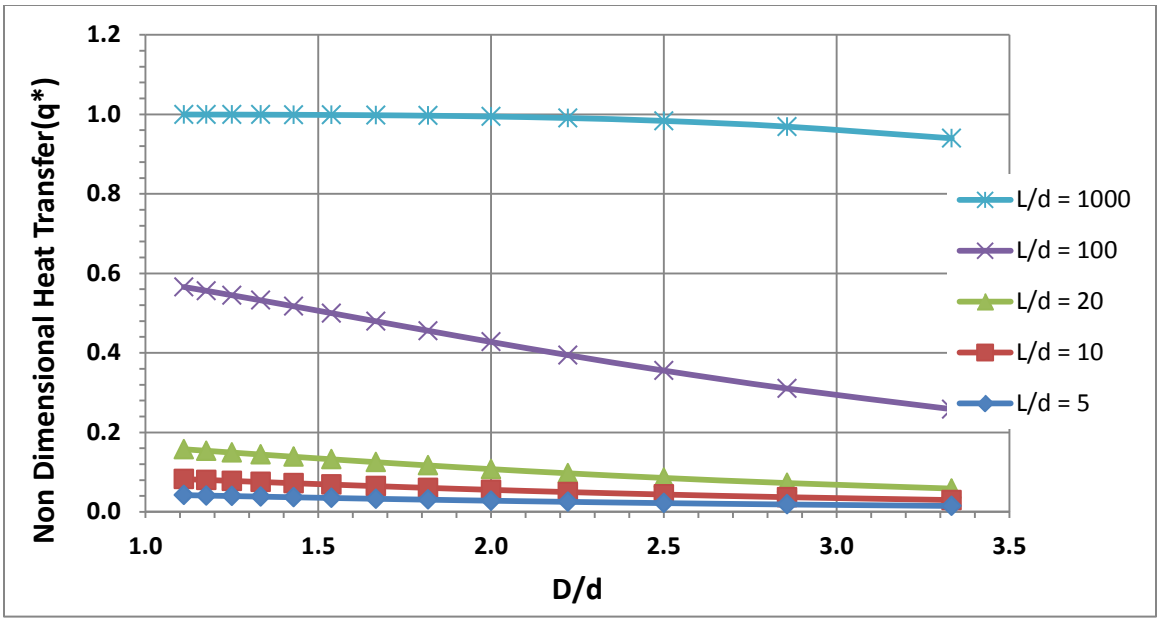

Figure 15. Comparison of non-dimensional heat transfer (q*) at exhaust gas Reynolds number = 200,000 for D/d from 1.3 to 3.3, and L/d from 5 to 1,000.

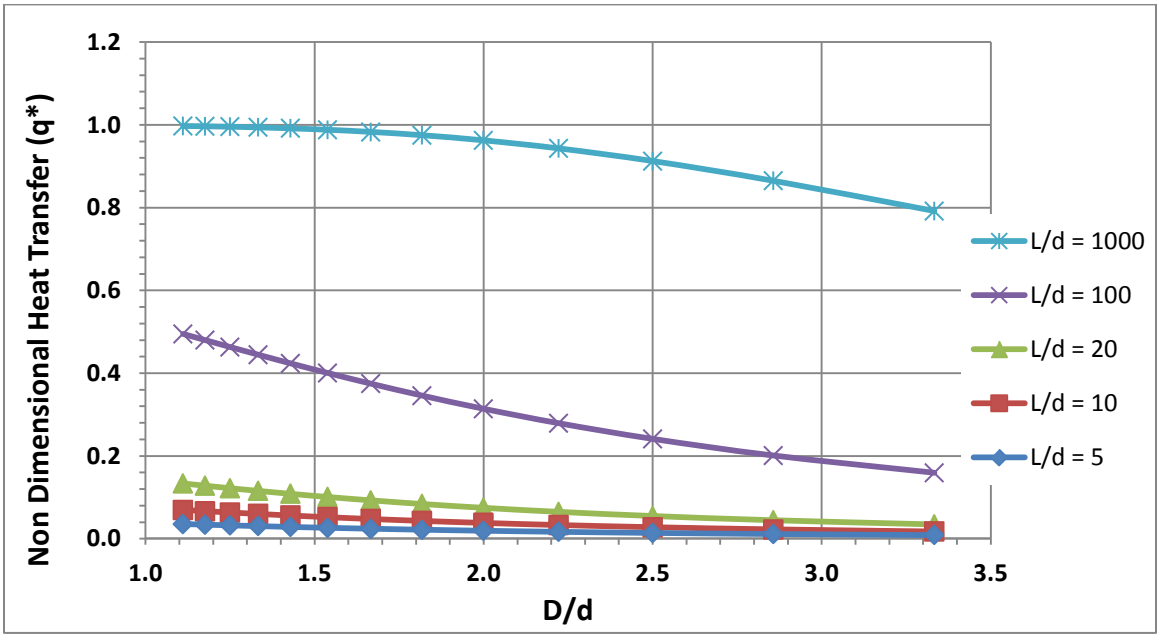

Figure 16. Comparison of non-dimensional heat transfer (q*) at exhaust gas Reynolds number = 400,000 for D/d from 1.3 to 3.3, and L/d from 5 to 1,000.

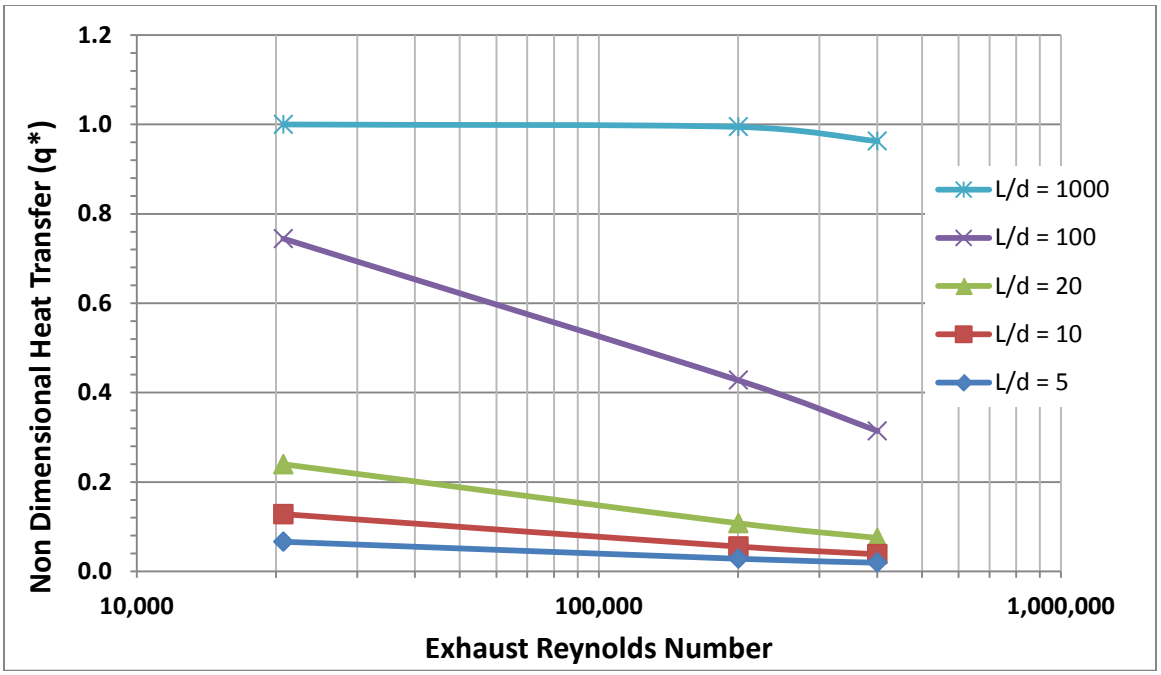

Figure 17. Comparison of non-dimensional heat transfer (q*) at D/d= 2 for L/d from 5 to 1000, Re_{exh} from 20,000 to 400,000.

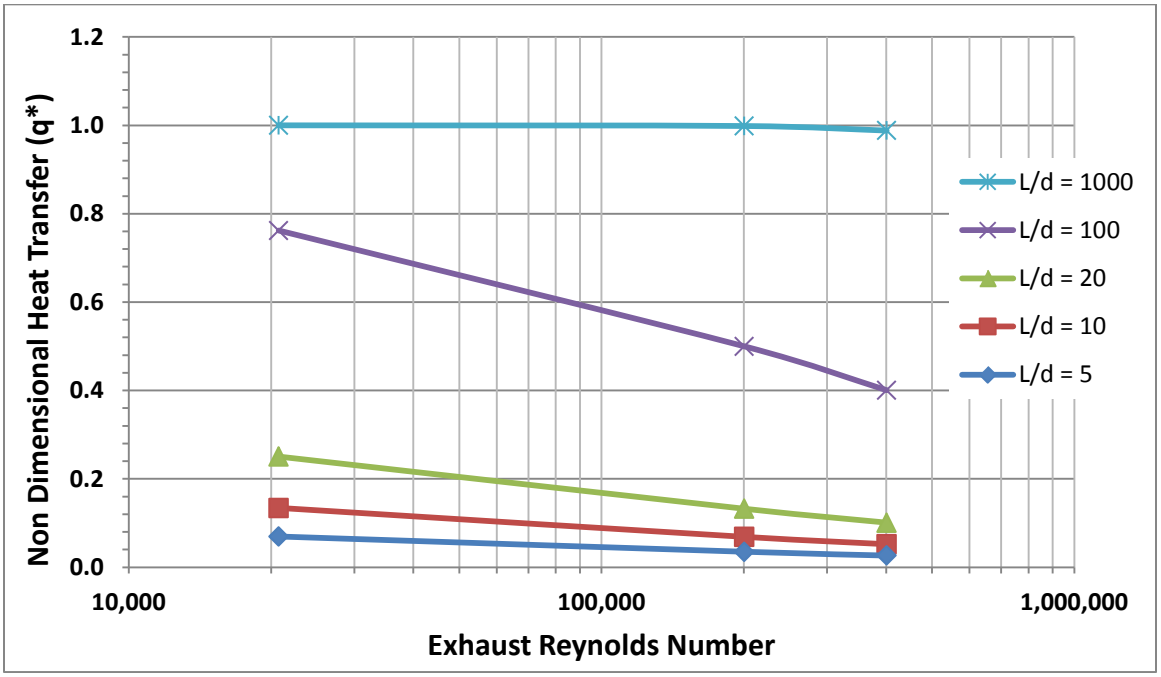

Figure 18. Comparison of non-dimensional heat transfer (q*) at D/d= 1.54 for L/d from 5 to 1,000, and Re_{exh} from 20,000 to 400,000.

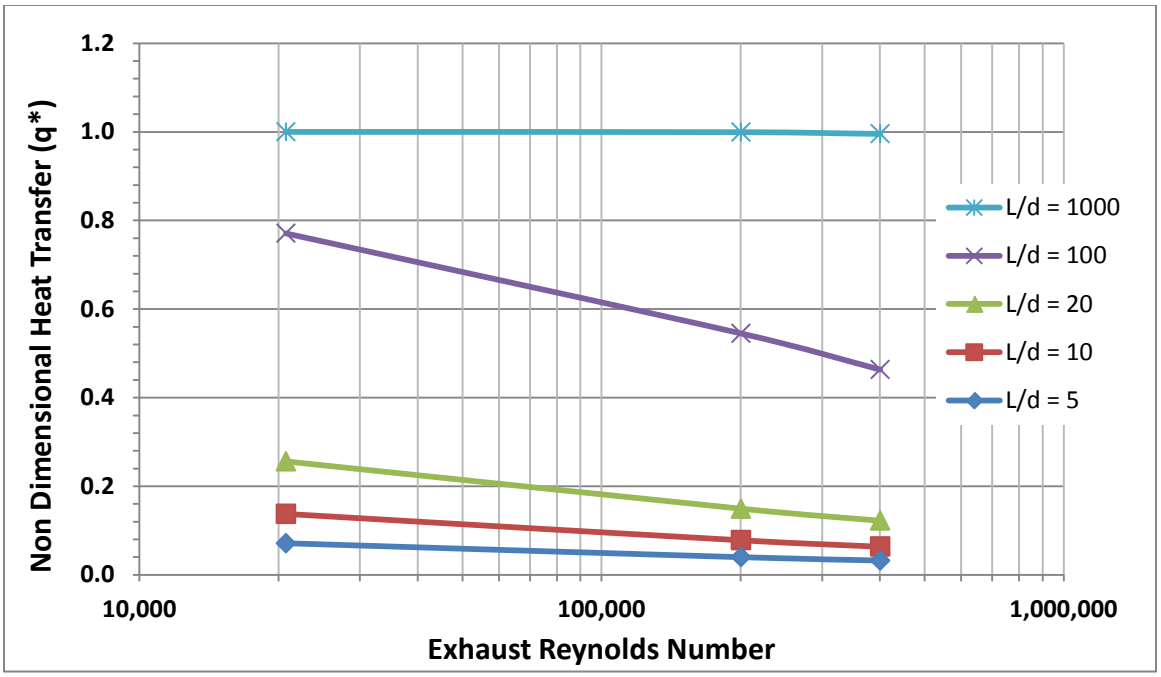

Figure 19. Comparison of non-dimensional heat transfer (q*) at D/d= 1.25 for L/d from 5 to 1,000, and Re_{exh} from 20,000 to 400,000.

2. Effect on Non-dimensional Pressure Drop (ΔP*) Performance

With the exhaust tube diameter (d) being held constant, the exhaust gas side pressure drop is only dependent on L/d ratio and exhaust gas Reynolds number. The results of the analytical calculations are shown in Figure 20. The non-dimensional pressure drop, exhaust Reynolds number, and L/d ratios exhibit a linear relationship when plotted on a log-log scale.

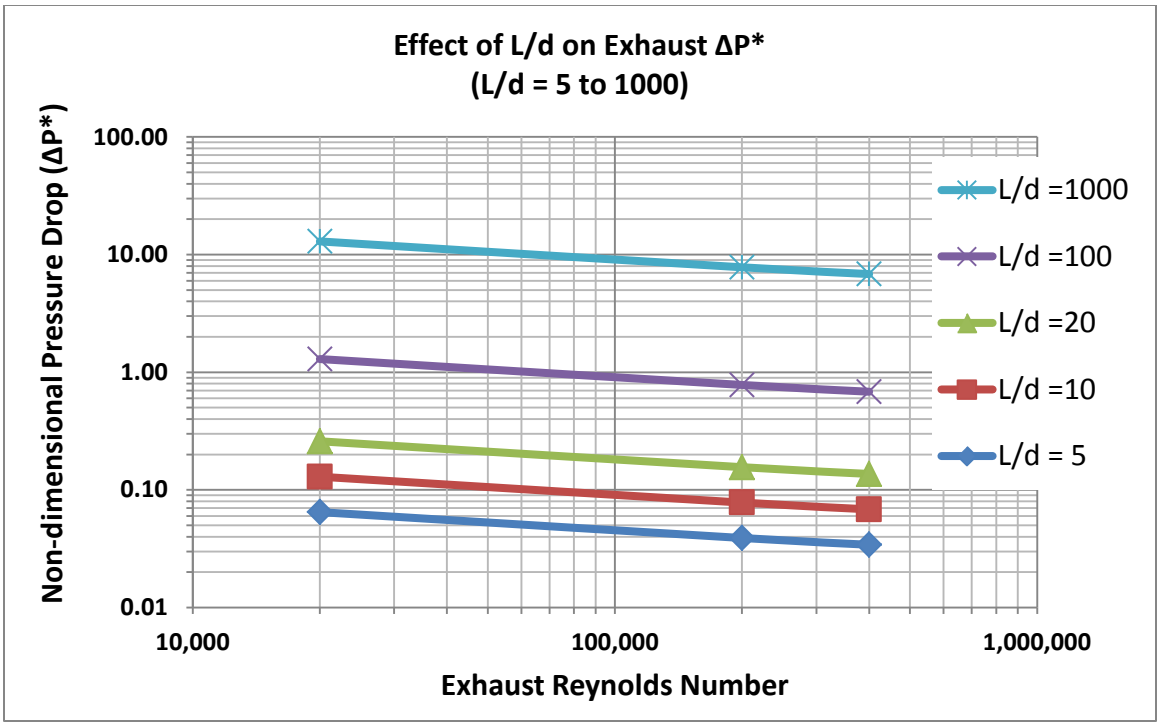

Figure 20. Comparison of non-dimensional heat transfer (q*) at D/d= 1.25, L/d from 5 to 1,000, and Exhaust Gas Reynolds Number from 20,000 to 400,000.

3. Limitations of Analytical Study

The analytical study was able to generate heat recovery and pressure drop results over a wide range of WHRU L/d, D/d ratios, and exhaust gas Reynolds numbers. These results provided an understanding of how WHRU performance (heat recovery and exhaust side pressure drop) are affected by changes in WHRU geometry and exhaust Reynolds number. However, the analytical study was unable to provide any resolution of the temperature profiles within the WHRU. The analytical model was also unable to account for the effects due to water inlet and outlet locations, tube thermal conductivity, exhaust swirl, or other design features such as a heat spreader. These limitations were resolved by the use of CFD modeling and will be discussed in Chapter VI.

4. Range of L/d Ratio, D/d Ratio and Exhaust Reynolds Number for CFD Study

Given the space constraints onboard ships and dimensions of exhaust tubes, WHRUs with L/d of 100 or 1,000 may not be feasible. As such, more realistic L/d ratios of 5, 10, and 20 were used in this study using CFD. The CFD models were based on a D/d ratio of 1.25. The exhaust gas Reynolds number of 20,000 to 400,000, reflective of the exhaust flow in the USN SSGTG and USMC DG, was used.

THIS PAGE INTENTIONALLY LEFT BLANK

VI. COMPUTATIONAL FLUID DYNAMICS (CFD) MODEL ANALYSIS

The ANSYS-CFX CFD package was used for the CFD study. CFD models for WHRU with D/d = 1.25 and tube thickness of t* = 0.0625 were constructed and used to investigate the effects of L/d and other WHRU features on heat recovery, pressure drop performance, and temperature profiles within the WHRU. The exhaust Reynolds number and water Reynolds number for the runs ranged from 20,000 to 400,000. The water Reynolds number was held constant at 8,300. Inlet exhaust temperature and inlet water temperature were kept constant at $T_{exh,in}$ = 773K and $T_{water,in}$ = 300K, respectively. The corresponding non-dimensional temperatures were T* = 1 and T*= 0, respectively, and represented the maximum and minimum temperatures in the study.

A. ANSYS-CFX RUNS

An overview of the ANSYS-CFX runs is tabulated in 0A sample of setup, inputs, and outputs for the CFD model run 4 are provided in Appendix A.

Table 3. Overview of CFD runs conducted in ANSYS-CFX (D/d=1.25, t* = 0.0625)

Run No.	L/d	Exhaust Swirl condition	Water inlet/outlet placement	Re_{exh}	Re_{water}	Tube Material	Added Feature
1 2 3 4	10	No Swirl	Center line	20,000 100,000 200,000 400,000	8,300	Steel	Nil
5 6 7 8	5	No Swirl	Center line	20,000 100,000 200,000 400,000	8,300	Steel	Nil
9 10 11 12	20	No Swirl	Center line	20,000 100,000 200,000 400,000	8,300	Steel	Nil
13 14 15 16	10	Axial + Tangential Velocity	Center line	20,000 100,000 200,000 400,000	8,300	Steel	Nil
17 18 19 20	10	Axial + Tangential + Radial Velocity	Center line	20,000 100,000 200,000 400,000	8,300	Steel	Nil
21 22 23 24	10	No Swirl	Center line	20,000 100,000 200,000 400,000	8,300	Steel	Steel heat spreader of y/L=0.1 placed at exhaust gas inlet
25 26 27 28	10	No Swirl	Center line	20,000 100,000 200,000 400,000	8300	Inconel 625	Nil
29 30 31 32	10	No Swirl	Center line	20,000 100,000 200,000 400,000	8300	Copper	Nil
33 34 35 36	10	No Swirl	Center line	20,000 100,000 200,000 400,000	8300	Pyroceram	Nil
37 38 39 40	10	No Swirl	Inlet at x/R=0.8, Outlet at x/R= -0.8	20,000 100,000 200,000 400,000	8,300	Steel	Nil
41 42 43 44	10	No Swirl	Inlet and outlet on opposite sides of Center line	20,000 100,000 200,000 400,000	8,300	Steel	Nil

Each ANSYS model is made up of three domains. Two fluids domains were used to model the exhaust gas flow in the tube and the water flow in the water jacket respectively. A solid domain was used to model the exhaust tube section between the water and exhaust gas.

The domains were first created using SOLIDWORKS and then imported into ANSYS-CFX as "Parasolids" for assembly, meshing, and pre-solver setup using different modules within ANSYS-CFX. Details of specific domains and boundary conditions were defined in the pre-solver module through the assignment of different material models, and fluid and thermal properties. The "Ideal Air model" sub-model was used to model the exhaust gas, while the "water at 25^{o} C" sub-model was used to model the water domain. The "Steel" material model was used for the solid WHRU tube. After setup, the CFD models were sent to the CFX-Solver for solution.

Upon successful solution (achieving target residual), parameters such as temperatures, velocity, and pressures were generated using the CFX-Post's function calculator. Sampling points were also assigned to specific locations or a specific profile, i.e., along the tube length at the "3 o'clock" position, to obtain local measurements of parameters such as temperature. Parameters such as fluid inlet and outlet temperatures and pressure were also exported to MS EXCEL for follow-on calculation and plotting of heat transfer, pressure loss, and pumping power.

1. Model Meshing

The models were meshed using 'Automatic Meshing method' and 'Program Controlled Inflation' options with nine inflation layers. Figure 21 shows a screen shot of the settings in CFX-Meshing. The summary of the mesh sizes for the various models is shown in 0

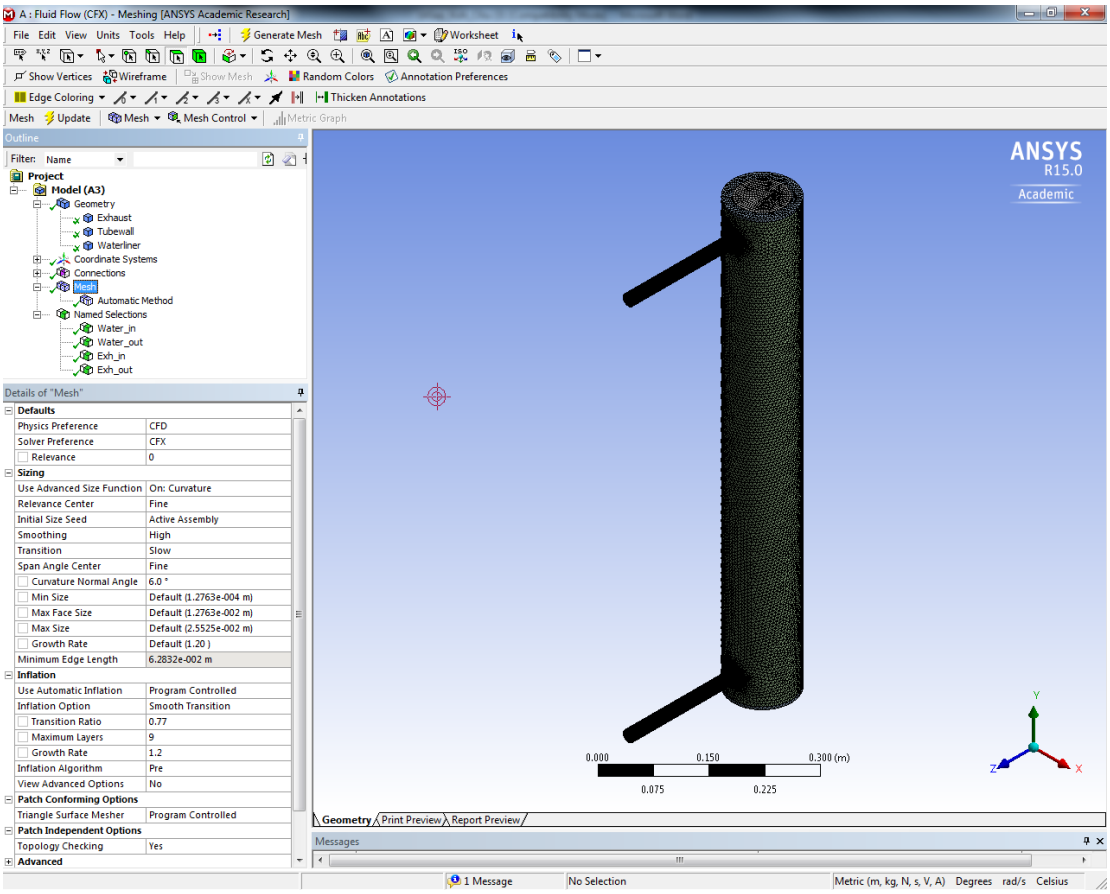

Figure 21. Screen shot of completed meshing in CFX-Meshing for "Baseline" model using automatic meshing method and program controlled inflation settings.

Table 4. Meshing details of various ANSYS-CFX models.

Model Name	Total Nodes	Total elements	Water Domain Nodes	Water Domain Elements	Tube Domain Nodes	Tube Domain Elements	Exhaust Domain Nodes	Exhaust Domain Elements
Baseline	531,790	1,206,992	386,297	981,704	34,733	121,110	110,760	104,178
Swirl_A								
Swirl_B								
Baseline_Inconel625								
Baseline_Copper								
Baseline_Pyroceram								
LD_5	436,251	1,018,979	347,791	887,850	18,978	65,363	69,482	65,766
LD_20	572,162	1,317,430	306,322	886,254	68,208	245,991	197,632	185,185
Shift	561,818	128,515	416,325	105,986	34,733	121,110	110,760	104,178
Baseline_Slug	544,070	1,233,127	386,190	981,969	45,316	145,723	112,564	105,435
Opposite	523,936	1,187,963	378,453	962,667	34,723	121,118	110,760	104,178

2. Heat Transfer Model

Heat transfer is modeled between the exhaust, water, and the WHRU tube domain using the ANSYS-CFX's "Thermal Energy" model, which models the transport of enthalpy through the fluid domain using conduction and convection. The Total Energy model was not selected because viscous heating was not expected to be significant in this study.

3. Turbulence Model

The standard K-epsilon (K-ε) model in ANSYS-CFX was used to model the turbulence for all the runs. This model is based on the Reynolds Averaged Navier-Stokes (RANS) and is widely accepted and implemented for turbulence modeling (Patankar, 1980). The K-ε model is known to be stable, accurate, and numerically robust, and is

considered to be the standard model in the CFD industry. The K-ε model in CFX also uses the scalable wall-function approach which allows solutions on arbitrarily fine near-wall grids to be made. This increased robustness and accuracy of the solutions over standard wall functions (ANSYS, 2013).

B. MODEL VALIDATION AND SENSITIVITY ANALYSIS

All models were validated by ensuring the overall mass and the energy entering and leaving the controlled surfaces (inlets and outlets) were balanced. In all the cases, energy balances better than 0.019% were achieved. The worst case had an energy imbalance of less than 0.045%. The details of the energy balance of the all the CFD model runs are collated in Appendix B.

Mass averaged values of inlet and outlet temperatures, specific heat capacity, and mass flow rates were used to verify conservation of mass within the controlled volume. A sensitivity analysis was conducted to find out the effect of different meshing size and solver target residual error value on the result accuracy of energy balance and the resolution. Runs using three meshing levels (250,000, 500,000, and 1,500,000 nodes) and three levels of CFX solver target residual error values (1E-4, 1E-5, and 1E-6) were conducted using a model with L/d =10, D/d= 1.25, t/d=0.0625 subjected to the same fluid flow conditions. No significant improvement in accuracy for output parameters and energy balance were found when the higher residual error values of 1E-6 were used over 1E-5. Models using a meshing size of 1,500,000 nodes provided slightly better resolution in temperatures contours and profiles than models with 500,000 nodes. The model with 250,000 nodes provided the least resolution in terms of contours but took the least amount of time to achieve solution convergence. The models with increasing mesh sizes took increasing amounts of time run. CFD models with a meshing size of 500,000 nodes and solver residual target error value of 1E-6 offered optimum balance of accuracy, resolution, and processing time.

In addition to validation using mass and energy balance, the results from the CFD models were validated using the corresponding results from the analytical models. The results are compared in Table 5 and plotted in Figure 22. Generally, the heat recovery

results from the CFD and analytical models agree. They exhibited the same trend and are within the same orders of magnitude. Higher q* is achieved at higher L/d and a lower exhaust Reynolds number. At higher Reynolds numbers of 400,000, q* from the CFD models is 6% to 26% lower than the results obtained from analytical models. At lower Reynolds numbers of 20,000, q* from the CFD models are 6% to 24% higher than in analytical models.

As a whole, a difference of up to 26% exists between the results from the CFD and analytical model. The difference increased with higher L/d ratio and Reynolds numbers. However, it is not unreasonable to expect some differences between the CFD and analytical models, considering the simplifications and assumptions associated with the analytical model. The difference between the water inlet and outlet placements of the CFD and analytical models could also contribute toward the difference. One also needs to keep in mind that uncertainty of approximately $\pm$10% also exists in the analytical correlations used in Incropera, Bergman, Lavine, and Dewitt (2011), and Kakac and Liu (2002). The range of uncertainty is also included in Figure 22 for reference.

Table 5. Comparison of non-dimensional heat recovery (q*) between analytical and CFD models of L/d = 5, 10, 20; Re_{exh} = 20,000, 200,000 to 400,000; D/d=1.25, t*=0.0625; no Exhaust swirl, centerline water inlet/outlet placement, Re_{water} = 8,300.

L/d	**5**			**10**			**20**		
Re_{exh}	CFD	Analytical	% Difference	CFD	Analytical	% Difference	CFD	Analytical	% Difference
20,000	0.089	0.071	24%	0.154	0.138	12%	0.272	0.256	6%
200,000	0.041	0.040	2%	0.070	0.078	-10%	0.126	0.149	-16%
400,000	0.030	0.032	-6%	0.050	0.063	-21%	0.090	0.122	-26%

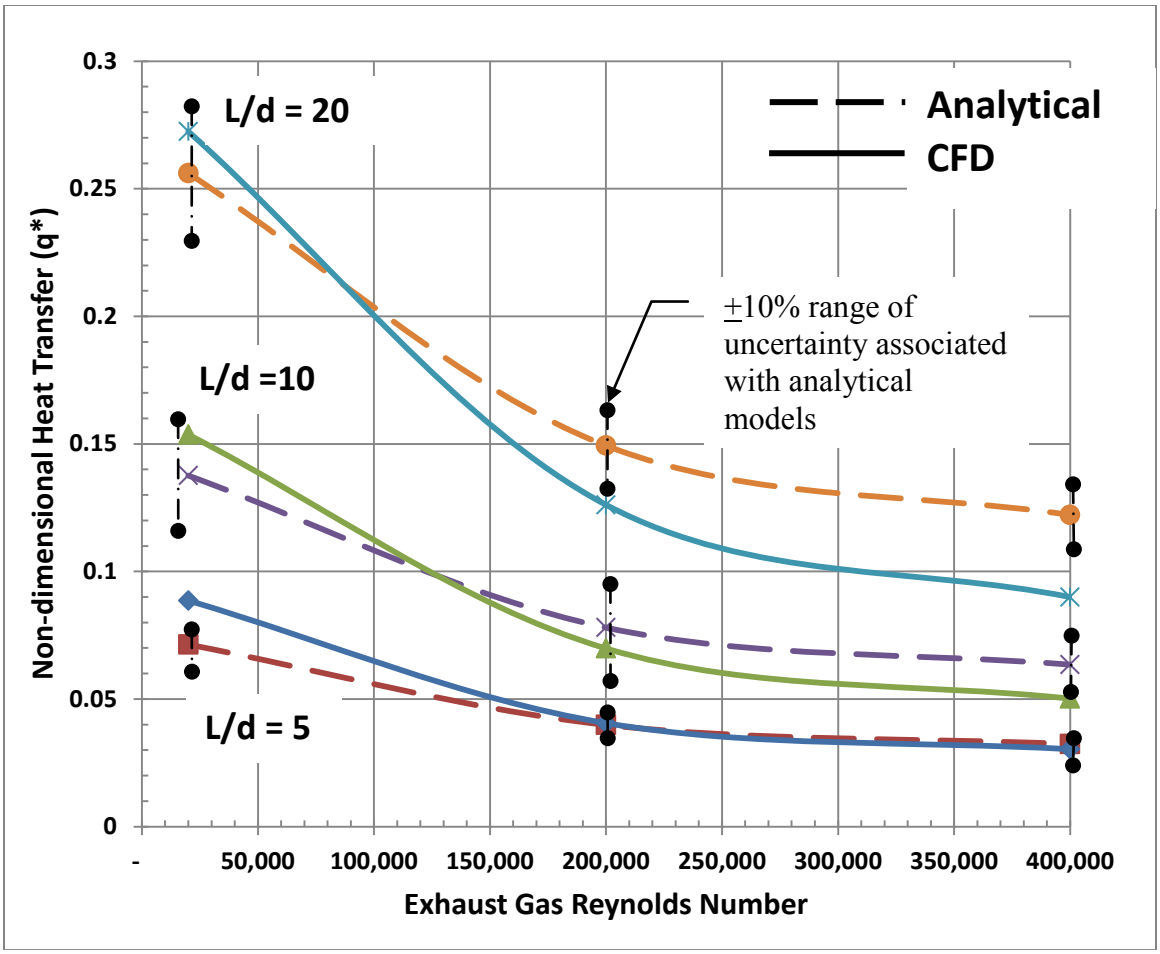

Figure 22. Comparison of non-dimensional heat recovery (q*) between analytical and CFD models of L/d = 5, 10 and 20 with Re_{exh} from 20,000 to 400,000. D/d=1.25, t*=0.0625; no exhaust swirl, centerline water inlet and outlet placement with Re_{water} = 8,300.

1. Effect of WHRU Length to Tube Diameter Ratio on Non-dimensional Heat Recovery

The effects of WHRU length on non-dimensional heat recovery (q*), pressure drop (ΔP*), and WHRU tube temperatures were investigated using CFD models with L/d ratios of 5, 10, and 20. A constant D/d ratio of 1.25 was maintained. The model runs were conducted at exhaust gas Reynolds numbers ranging from 20,000 to 400,000. This range was used as it covered the type of exhaust flow regime expected in USMC MEP 803A DG and USN 501K SSGTG. Figure 22 illustrates the effect of the three L/d ratios on q* with all other parameters kept similar. Higher q* was achieved at higher L/d for the same

Reynolds number. This was expected as more available area for heat transfer is available with higher L/d. Using the model with L/d = 10 as benchmark, increasing L/d to 20 increased q* from 68% to 81%. Reducing L/d to 5 decreased q* from 41% to 46%.

2. Effect of WHRU Length to Tube Diameter Ratio on Non-Dimensional Pressure Drop (ΔP*)

Figure 23 illustrates the effect of different L/d on ΔP* with all other parameters kept the same. For the same exhaust Reynolds number, higher ΔP* were encountered with a WHRU with higher L/d. Using a WHRU with L/d = 10 as the baseline for comparison, increasing L/d to 20 increased the ΔP* by 96%. A reduction of L/d to 5, decreased ΔP* by 45%. This result was expected as frictional loss is proportional to WHRU length.

It was also observed that ΔP* decreases as the exhaust Reynolds number increases. For the all CFD models, ΔP* leveled off at Reynolds numbers of 150,000 to 200,000. This result was expected since the flow was modeled over smooth surfaces. This trend can be explained by an inspection of the pressure loss equation in Chapter IV.E, and the relationship between the Fanning friction factor and Reynolds number shown in Figure 13.

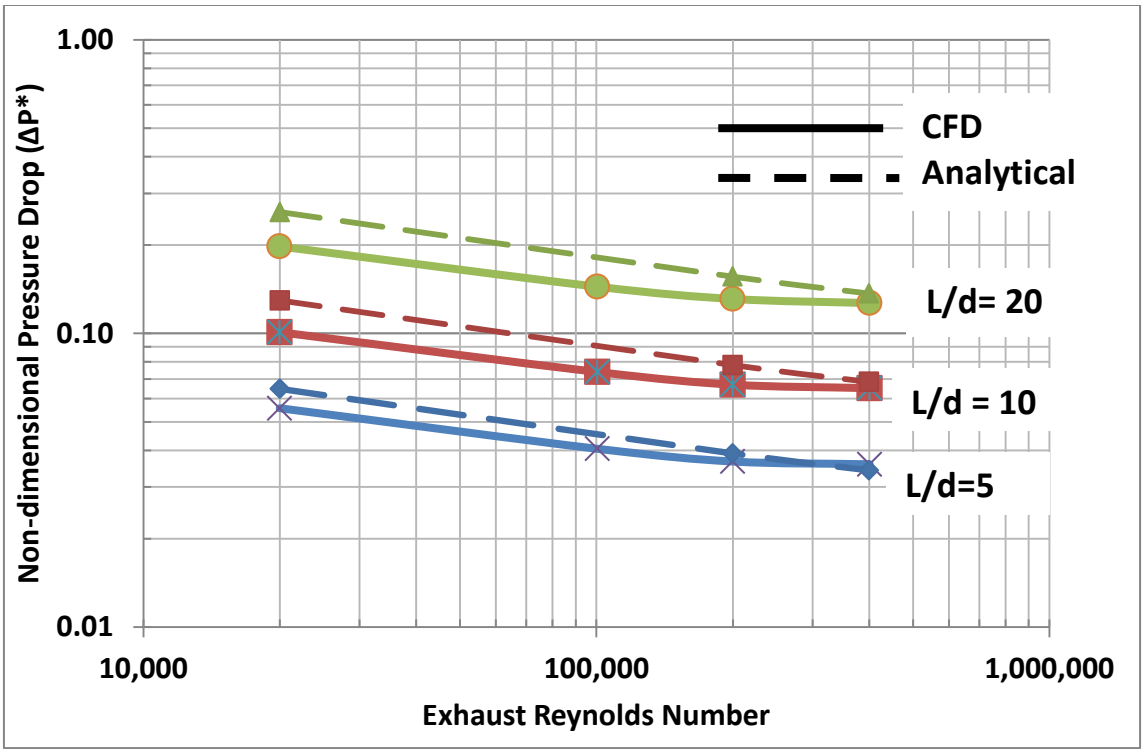

Figure 23. Comparison of non-dimensional pressure drop (ΔP*) between analytical and CFD models of L/d = 5, 10, 20; Re_{exh} from 20,000 to 400,000; D/d=1.25, t*=0.0625, no exhaust swirl, centerline water inlet/outlet placement, Re_{water} = 8,300.

C. EFFECT OF L/D ON WHRU TUBE TEMPERATURE PROFILE

CFD models allowed temperature profiles in the WHRU to be examined. The temperature profiles within WHRU models of L/d ratios of 5, 10, and 20 were compared at exhaust Reynolds numbers ranging from 20,000 and 400,000, which correspond to the flow regime expected in the exhaust stack of the USMC MEP801A DG and USN 501K SSGTG. Temperatures were measured along the length of the WHRU tube at 3, 6, 9, and 12 o'clock positions as shown in Figure 24.

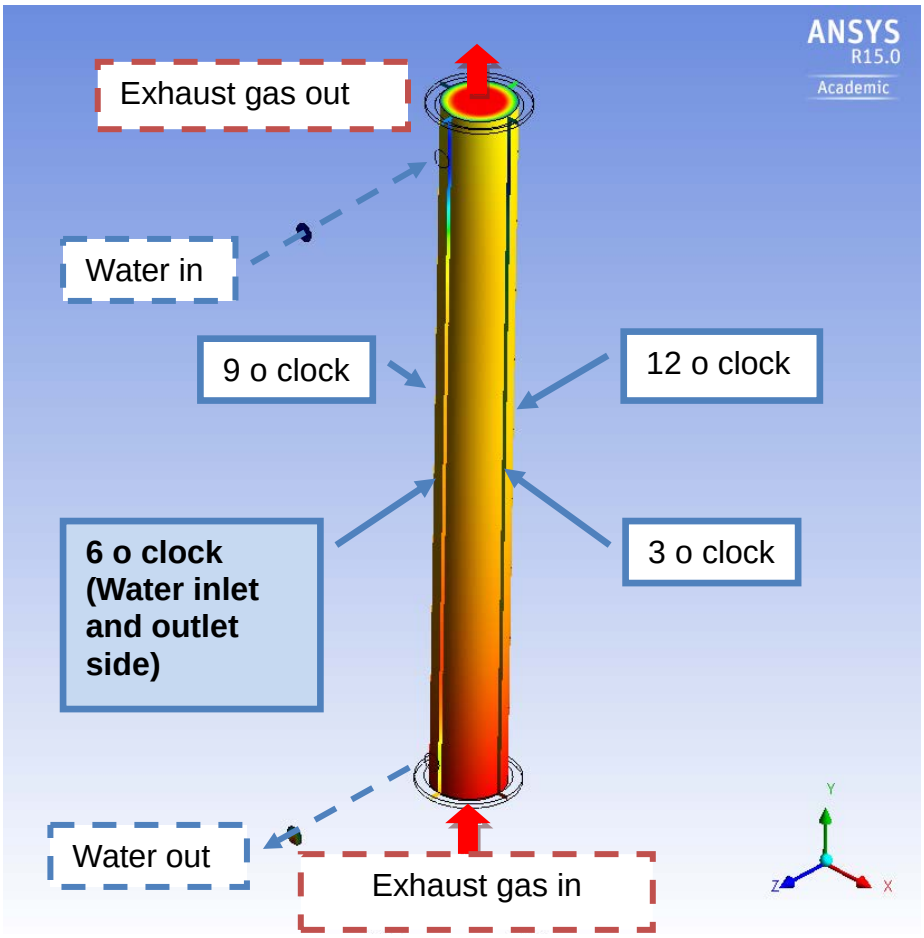

Figure 24. Isometric view showing locations where temperature measurements are made on WHRU tube with reference to inlets and outlets of exhaust and water flow.

The temperatures were non-dimensionalized and normalized using the difference of inlet temperatures of exhaust gas and water found in Equation (33). The non-dimensionalized temperatures were plotted to gain insights into the longitudinal and radial temperature distributions. The temperature profiles for L/d of 5, 10, and 20 are shown in Figures 25, 27, and 29, respectively. The corresponding temperature contours are shown in Figures 26, 28, and 30.

Figures 25, 27, and 29 show that the shape of the temperature profile is affected by L/d ratios and exhaust Reynolds number. Generally higher exhaust gas Reynolds numbers increase tube temperatures and amplify temperature differences. At Re_{exh} of 400,000, the sharpest temperature gradients were observed.

For a WHRU with L/d = 5 (shown in Figure 25), the largest difference occurs at the lower half of the WHRU where the exhaust inlet and water outlet are situated. The tube temperature contours for model with L /d = 5 evaluated at Re_{exh} = 400,000 are shown in Figure 26. The adverse temperature profile between the 6 o'clock and 12 o'clock is clearly shown.

When L/d is increased to 10 (shown in Figure 27), this difference is most prominent in the middle of the tube. The large temperature difference within the WHRU is also shown in the plots in Figure 28.

For WHRU with L/d = 20 (shown in Figure 29), the most prominent temperature differences occur at the upper end of the exhaust tube near the location of the exhaust outlet and the water inlet. Temperature contours of a model with L/d=20 evaluated at Re_{exh} = 400,000 is shown in Figure 30. Once again adverse temperature profiles can be seen in the temperature contours plots.

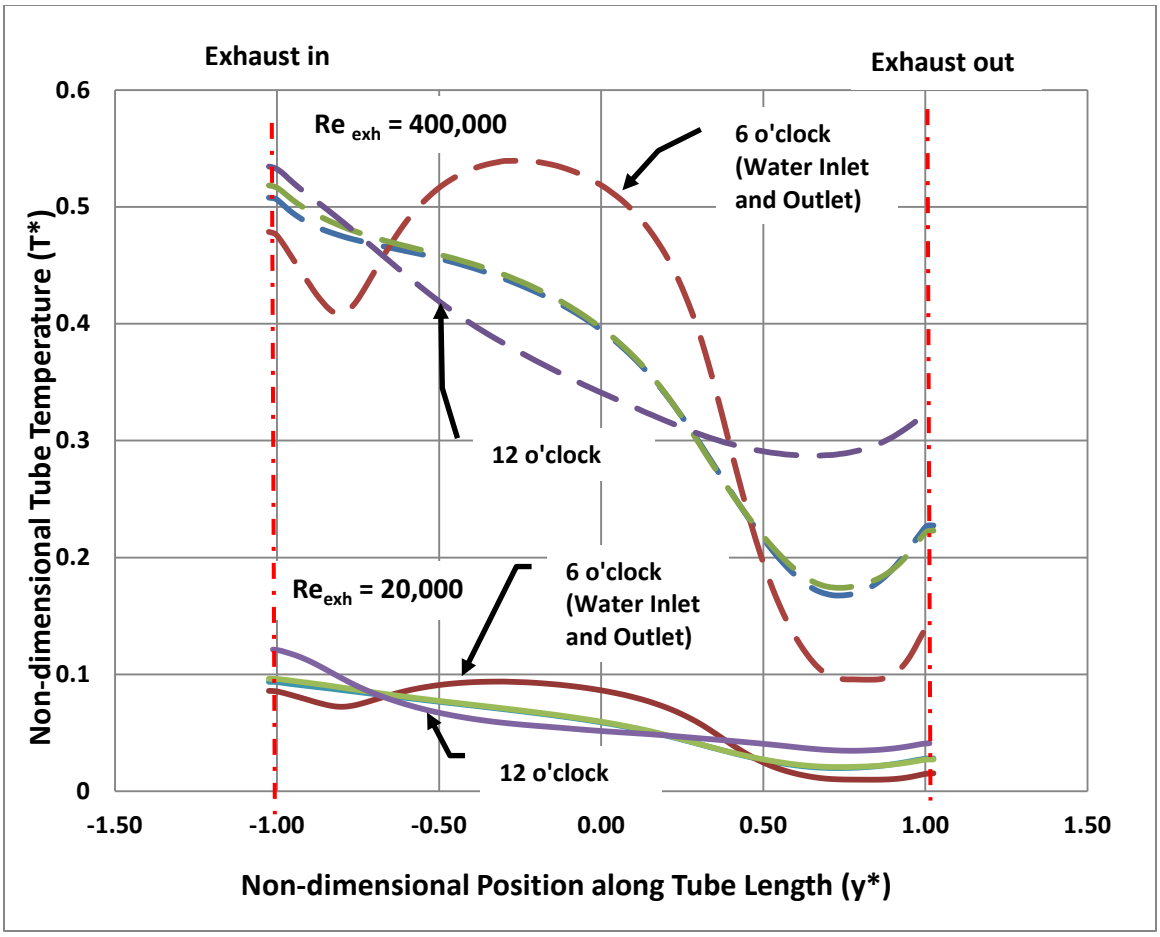

Figure 25. Tube temperature profile for WHRU of L/d= 5 at Re_{exh} = 20,000 and 400,000, D/d=1.25, t*=0.0625, no exhaust swirl, centerline water inlet/outlet placement, Re_{water} = 8,300.

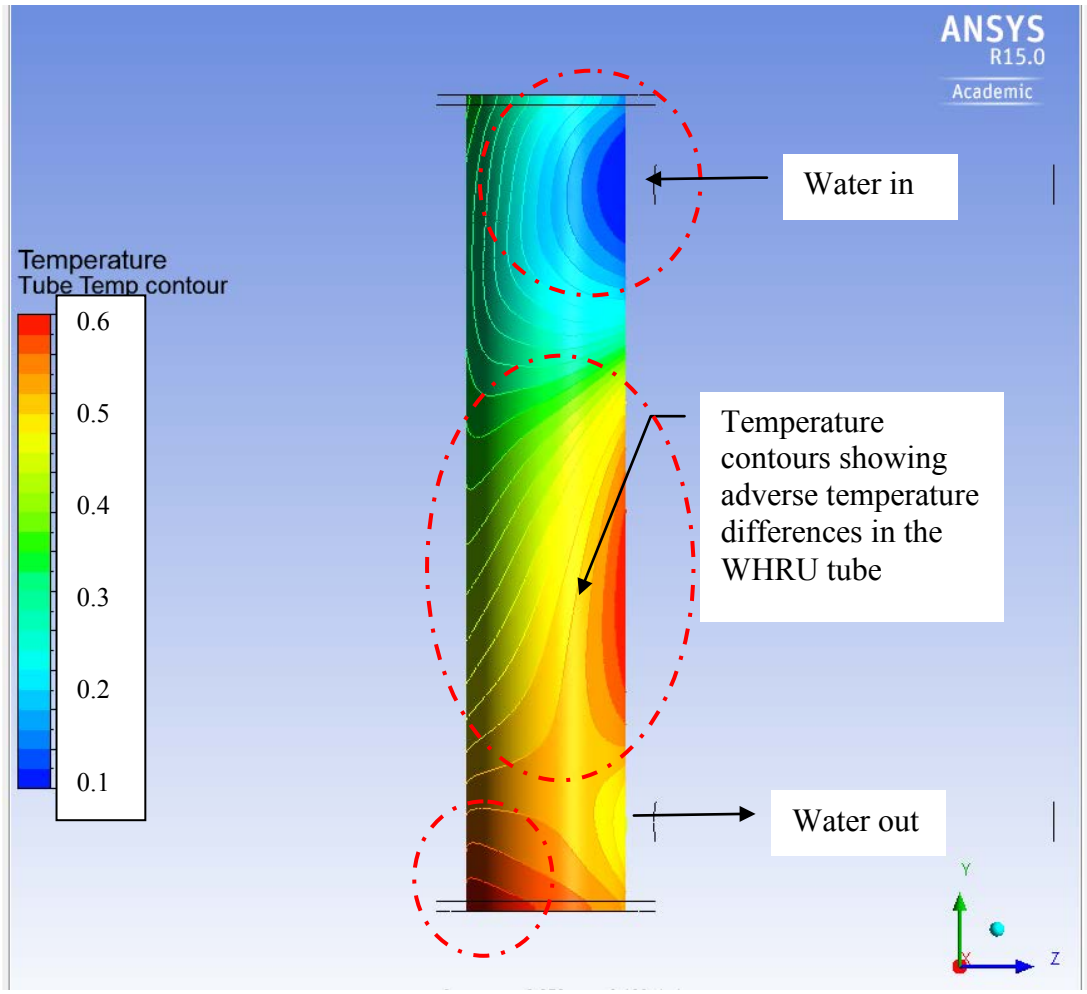

Figure 26. Tube temperature contours from 9 o'clock for WHRU with L/d = 5, D/d=1.25, t*=0.0625 at Re_{exh} = 20,000 and 400,000 with no exhaust swirl and centerline water inlet/outlet placement. Re_{water} = 8,300.

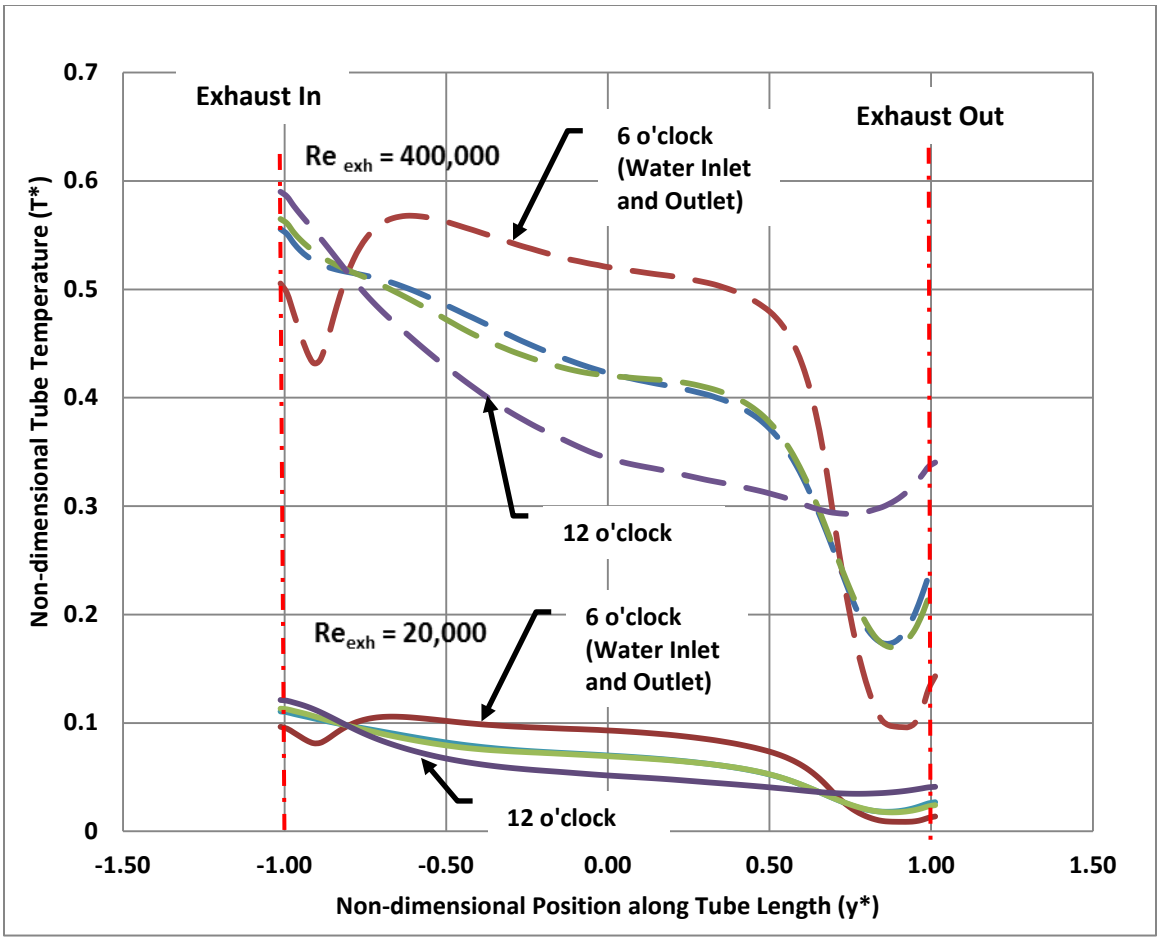

Figure 27. Tube temperature profile for WHRU with L/d = 10, D/d=1.25, t*=0.0625 at Re_{exh} = 20,000 and 400,000 with no exhaust swirl and centerline water inlet/outlet placement. Re_{water} = 8,300.

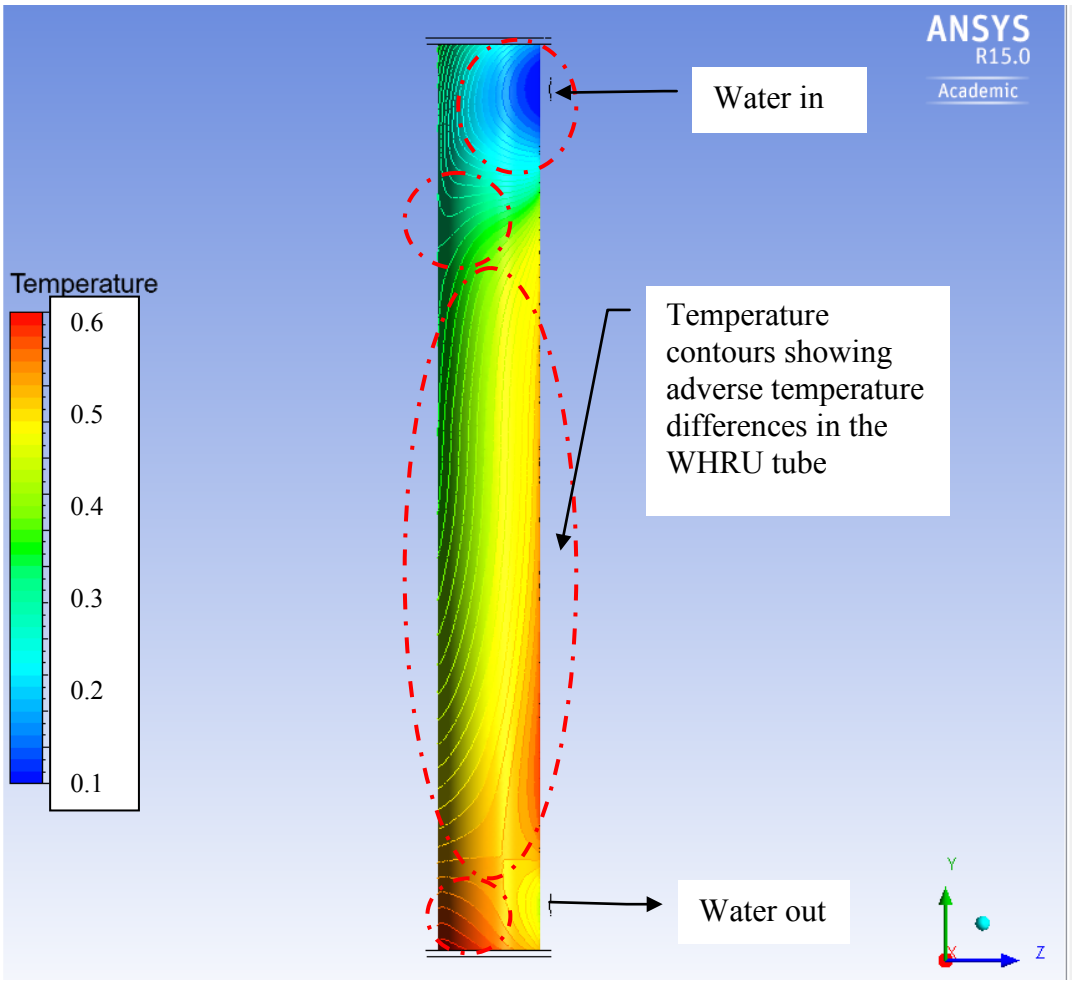

Figure 28. Tube temperature contours from 9 o'clock for WHRU with L/d = 10, D/d=1.25, t*=0.0625 at Re_{exh} = 20,000 and 400,000 with no exhaust swirl and centerline water inlet/outlet placement. Re_{water} = 8,300.

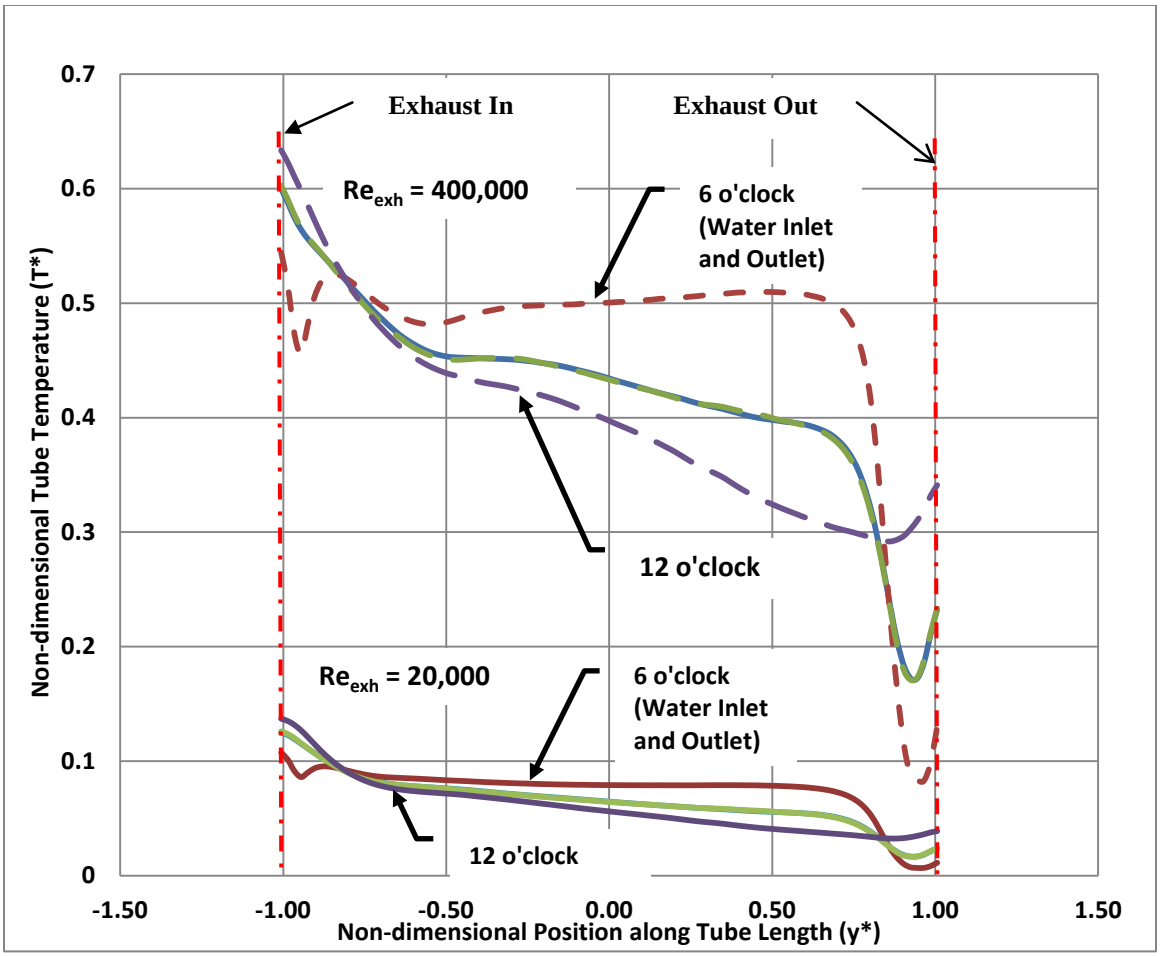

Figure 29. Tube temperature profile for WHRU with L/d = 20, D/d=1.25, t*=0.0625 at Re_{exh} = 20,000 and 400,000 with no exhaust swirl and centerline water inlet/outlet placement. Re_{water} = 8,300.

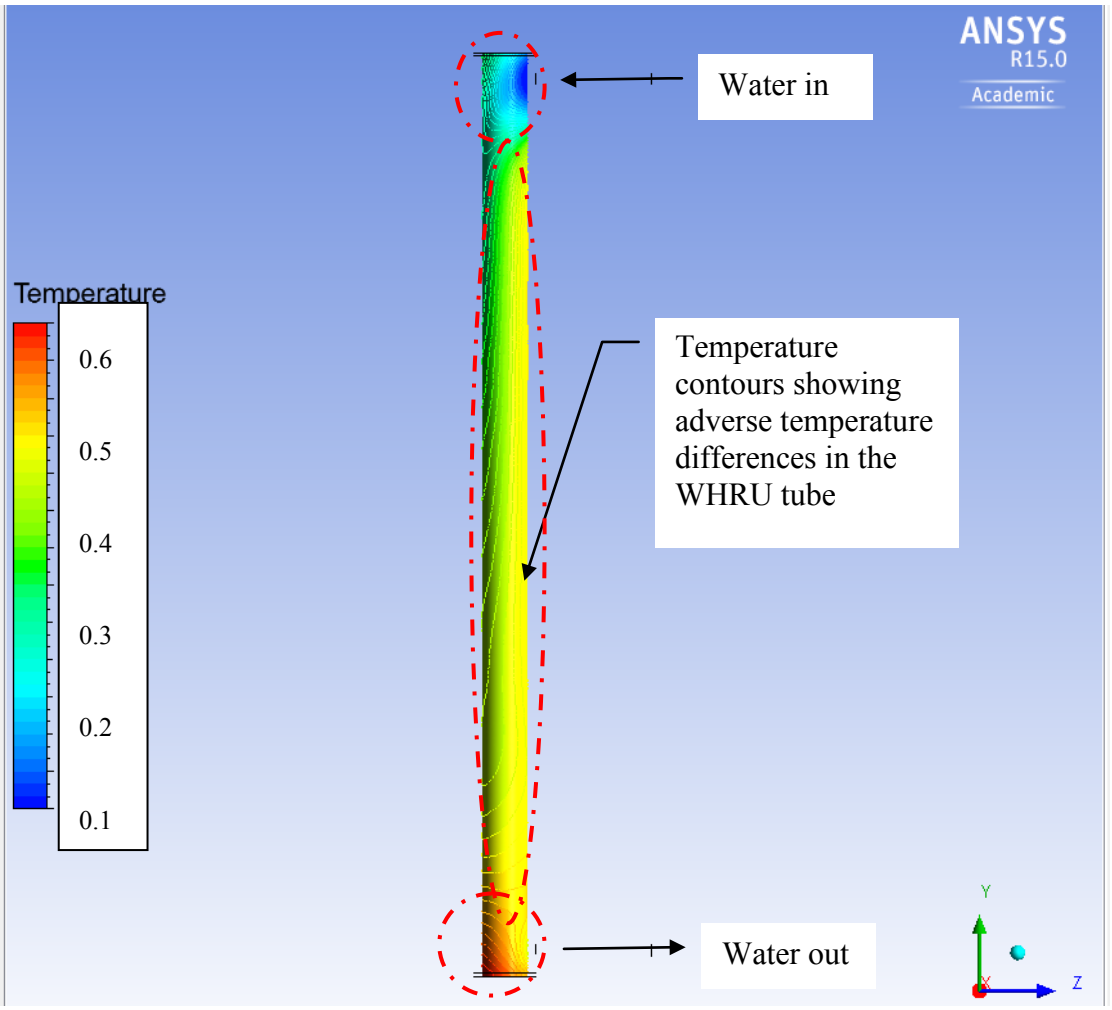

Figure 30. Tube temperature contours from 9 o'clock for WHRU with L/d = 20, D/d=1.25, t*=0.0625 at Re_{exh} = 20,000 and 400,000 with no exhaust swirl and centerline water inlet/outlet placement. Re_{water} = 8,300 showing temperature contours of the WHRU tube from different angles.

D. TEMPERATURE PROFILE AT 6 O'CLOCK AND 12 O'CLOCK

One of the key findings of this study was revealed when the water streamline in the water jacket was examined. The water streamlines shown in Figure 31 revealed the flow within the water jacket to be highly uneven. Most of the water entering the water jacket was channeled towards the 12 o'clock location, while minimum amount of water was channeled to the 6 o'clock profiles. This caused uneven heat transfer and the adverse temperature profile between the 6 o'clock and 12 o'clock profiles. Water flow along the 3 o'clock and 9 o'clock profiles were almost equal.

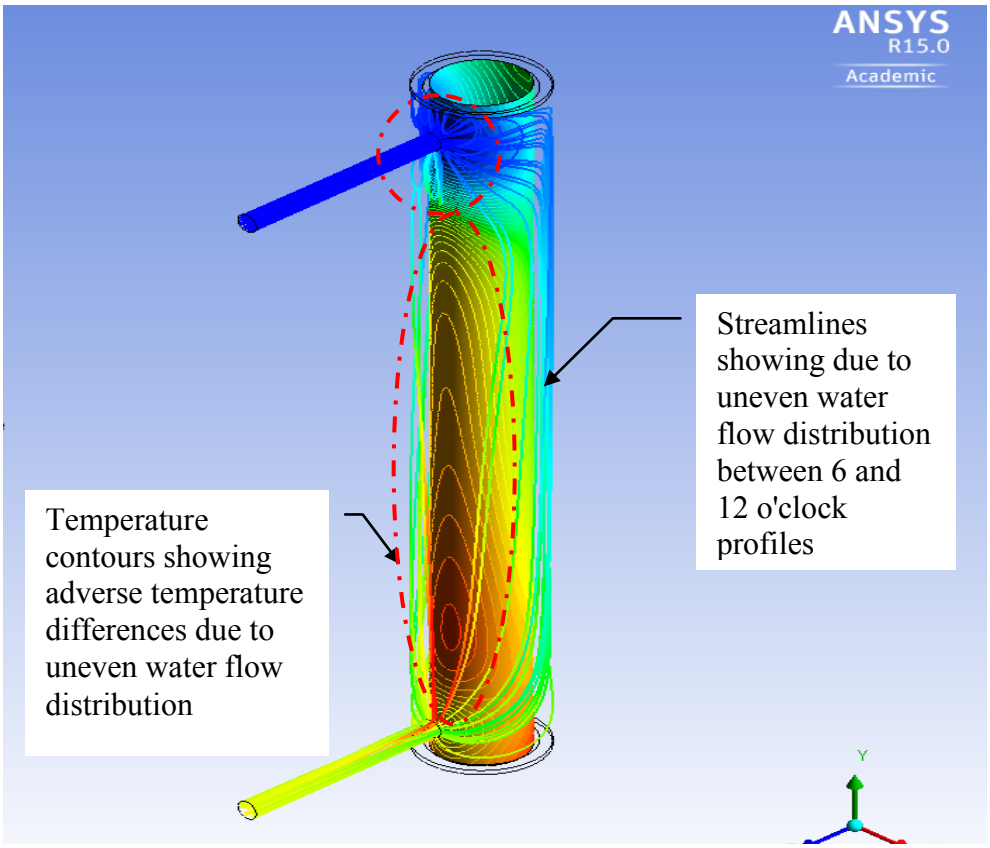

Figure 31. Water streamlines depicting non-uniformity of water flow inside water jacket of a WHRU of L/d =10, D/d=1.25 with centerline water Inlet/outlet placements at Re_{water} = 8,300.

The large temperature differences between the 6 o'clock and 12 o'clock profiles were also observed for all three L/d ratios. This difference was the most pronounced at Re_{exh}=400,000. The 6 o'clock profile is also the side where the water inlet and outlet were located. In order to facilitate comparison, the 6 o'clock and 12 o'clock temperature profiles WHRU of for L/d = 5, 10, and 20 at Re_{exh} of 400,000 are plotted in Figure 32.

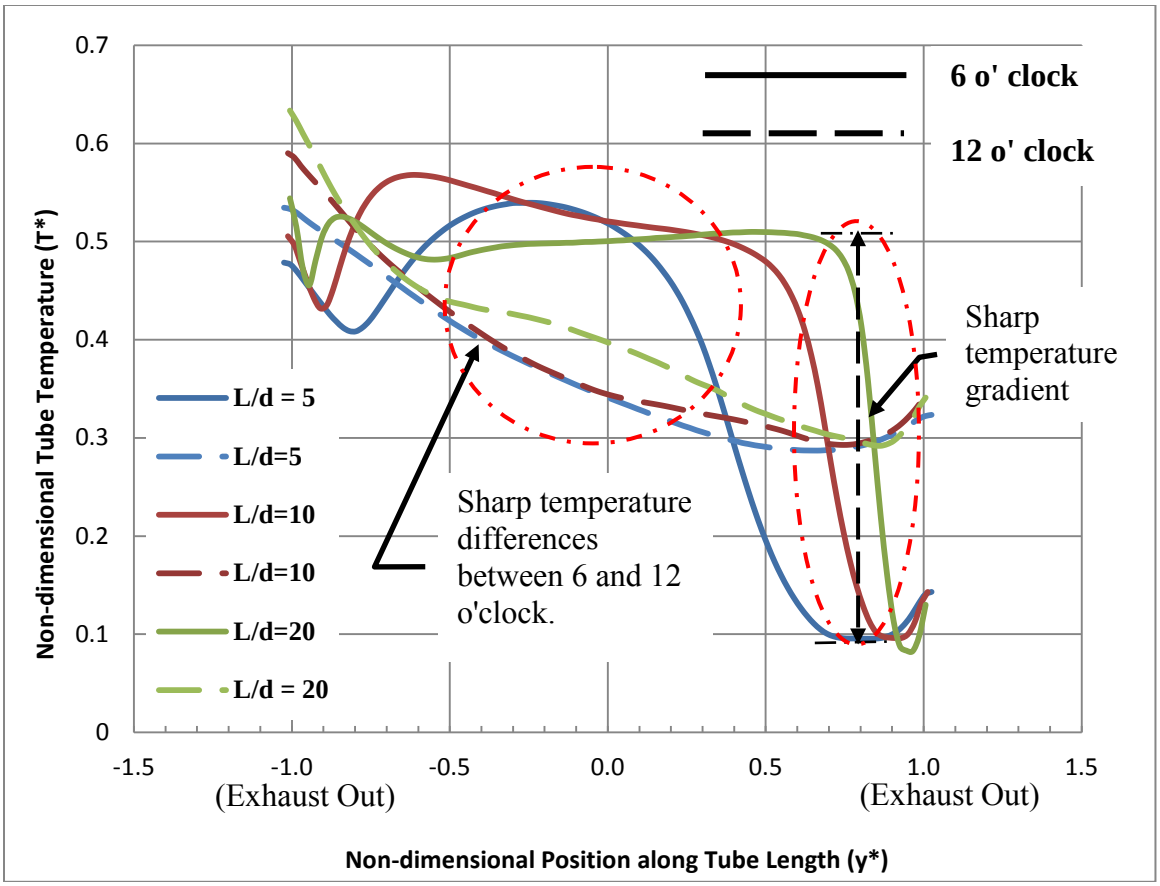

Figure 32. Comparison of temperature profile at 6 o'clock and 12 o'clock at Re_{exh} = 400,000 for WHRU of L/d = 5, 10, and 20.

Adverse temperature profiles can give rise to localized thermal stresses due to differential expansions in the tube. This has been identified to be a main reason for WHRU failures. In Figure 31, large temperature variations are observed both axially and radially. Differential stresses are produced both longitudinally as well as radially along the tube and could severely impact the reliability of WHRUs. During transient loadings such as startups, shutdowns, or load changes, these stresses could potentially be amplified due to transient and unsteady temperature differences.

E. EFFECTS OF EXHAUST SWIRL

In actual operation, exhaust gases are naturally non-uniform and swirling. As opposed to conditioning to produce uniform exhaust streams into the WHRU, swirl in the exhaust gas stream could increase heat transfer or starve regions due to flow recirculation.

Intrusive swirl generators such as helical inserts were used to increase heat transfer through the production of swirl in the flow stream (Patel, Parmar, & Soni, 2014). However, the placement of such devices inside an existing exhaust tube also introduces blockage resulting in a pressure drop that is higher than the heat recovery improvement. In order to mitigate this, the study explored the idea of using "non-intrusive" swirl generators such as guide vanes to induce swirl in the exhaust stream. These devices could be positioned at suitable positions upstream of the WHRU.

In order to investigate this effect using CFD models, a model of L/d = 10, D/d= 1.25, t*=0.0625 with a centerline placement of water inlet and outlet was used. Different axial, tangential, and radial velocity components were introduced to the inlet exhaust flow of the models to simulate the swirl that would have been induced by the "non-intrusive" swirl generators. Three exhaust swirl conditions were investigated in this thesis over exhaust Reynolds numbers ranging from 20,000 to 400,000 while the water Reynolds number was held constant at 8,300. The total mass flow rate was kept constant for the three swirl conditions. The details of the swirl conditions are tabulated in Table 6.

Table 6. Summary of exhaust swirl conditions in the study.

Swirl Condition	Unit Vector magnitude of Axial Velocity Component (U_y)	Unit Vector magnitude of Tangential Velocity Component (U_Θ)	Unit Vector Magnitude of Radial Velocity Component (U_r)
No Swirl Condition	1	0	0
Swirl Condition A	1	1	0
Swirl Condition B	1	1	1

1. Effect of Exhaust Swirl on Non-dimensional Heat Recovery (q*)

As shown in results plotted in Figure 33, a WHRU with exhaust flow incorporating axial and tangential velocity components of equal magnitude (swirl condition A) increased heat recovery by 22% to 36% compared to an exhaust flow with only an axial velocity component (no swirl condition). Subsequent increase of swirl through the introduction of equivalent magnitude axial, tangential, and radial velocity component (swirl condition B) increased heat recovery by 40% to 52%. This amounted to a 10% to 17% increase over "swirl condition A." The highest heat recovery improvements were obtained at low Reynolds numbers of 20,000 for all three cases.

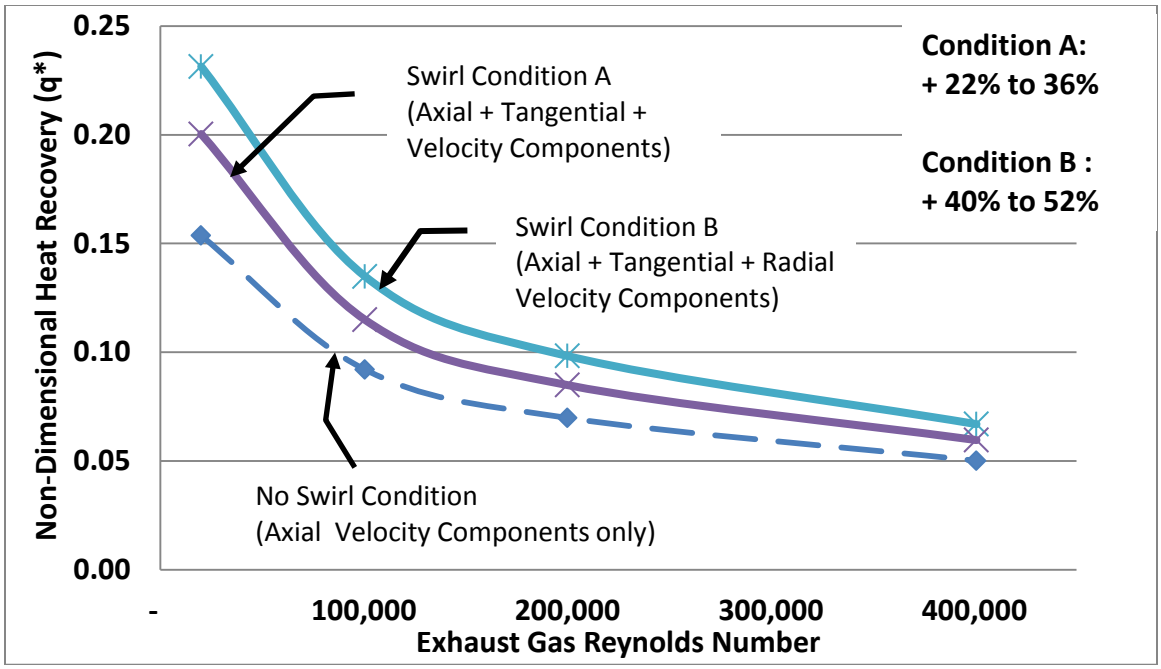

Figure 33. Comparison of non-dimensional heat recovery (q*) at exhaust swirl conditions specified in Table 6. L/d = 10; Re_{exh} = 400,000; Re_{water} = 8,300.

2. Effect of Exhaust Swirl on Non-dimensional Pressure Drop (ΔP*)

Despite the improvement in heat recovery, the introduction of swirl into the exhaust flow stream increased pressure drop at a higher proportion. The pressure drop results are shown in Figure 34. Flow with axial and tangential velocity components of equal magnitude (swirl condition A) increased non-dimensional pressure drop by 137% to 148%. An increase in the exhaust swirl (swirl condition B) resulted in an exhaust side pressure drop that is 540% to 740% higher than an exhaust flow with swirl.

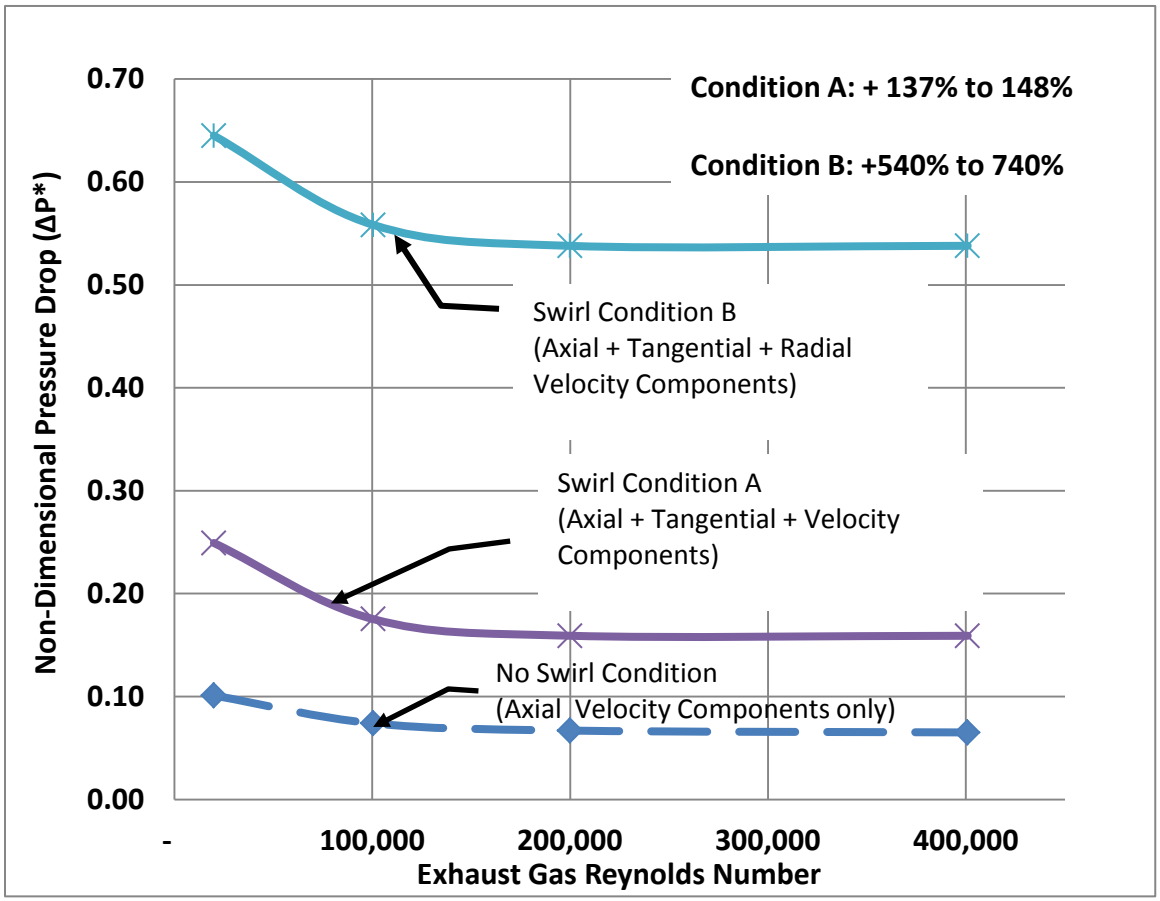

Figure 34. Effect of three different exhaust swirl conditions (specified in Table 6) on exhaust side non-dimensional pressure drop for WHRU of L/d = 10, D/d=1.25 with centerline water inlet/outlet placements.

3. Effect of Exhaust Swirl on Tube Temperature Profile

The tube wall temperature profiles of a WHRU (L/d = 10, D/d = 1.25, t*=0.0625, Re_{exh} = 400,000) with exhaust swirl condition A (axial and tangential velocity components) and exhaust swirl condition B (axial, tangential, and radial velocity components) were plotted against the temperature profile of an equivalent WHRU without exhaust swirl in Figure 35 and Figure 37, respectively.

The results from the CFD models showed that the shape of the temperature profile remained relatively unchanged with increased exhaust swirl. However, the higher average temperatures of WHRU were recorded when more swirl was imparted to the exhaust gas flow within the exhaust tube. Swirl condition B, the exhaust flow condition with the most amount of swirl, produced the highest increase in temperatures. Temperature increase of up to 41%, 36%, 41%, and 47% were recorded in 3, 6, 9, and 12 o'clock positions, respectively. Swirl condition A, which had relatively moderate swirl conditions, increased temperatures by 29%, 34%, 33%, and 27% in the 3, 6, 9, and 12 o'clock positions, respectively.

The increase in tube temperature can be attributed to the effectively longer path taken by the exhaust stream. In swirling flows, the exhaust streams undertake a helical path shown in Figure 36 instead of a straight axial path through the exhaust tube. In addition, the centrifugal forces and the secondary motion induced by the swirl of the exhaust gases reduced the thickness of the exhaust gas boundary layers in the tube resulting in higher tube temperatures and better heat recovery (Sane, Taji, & Pachegaonkar, 2014). For the three flow conditions studied, the greatest temperature differences occurred between measurements at 6 o'clock and 12 o'clock throughout the entire WHRU length. In addition to the global difference, adverse temperature gradients were also observed locally at y/L = from 0.5 to 1. This trend of temperature profiles is present in WHRU with or without swirling exhaust gas flows.

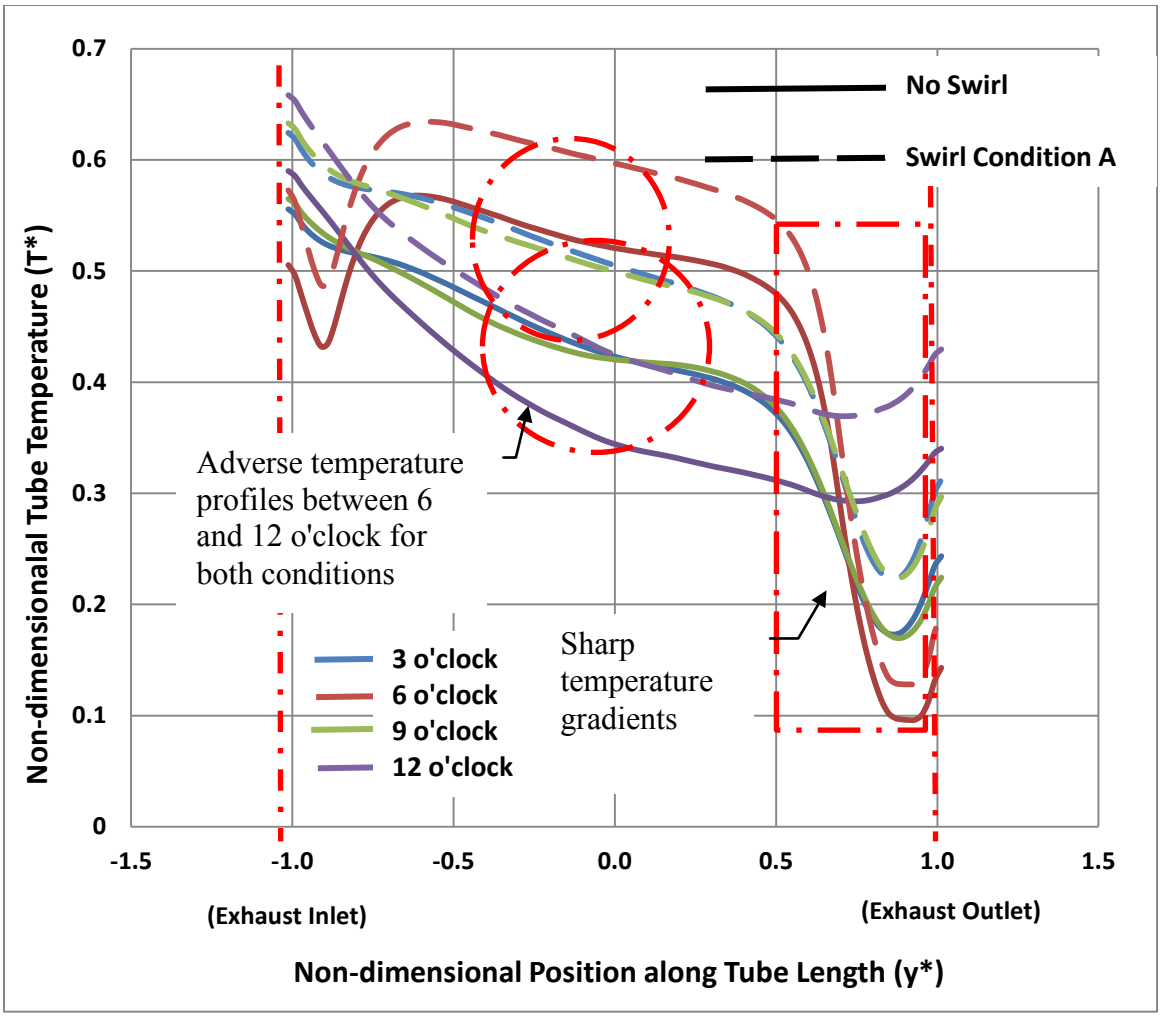

Figure 35. Comparison of tube temperature profiles between WHRU with swirl condition A (axial plus tangential velocity components) with a WHRU with no exhaust swirl (axial velocity component only). WHRU has L/d = 10, D/d=1.25, t*=0.0625, and centerline water inlet and outlet placement, Re_{exh} = 400,000, Re_{water} = 8,300.

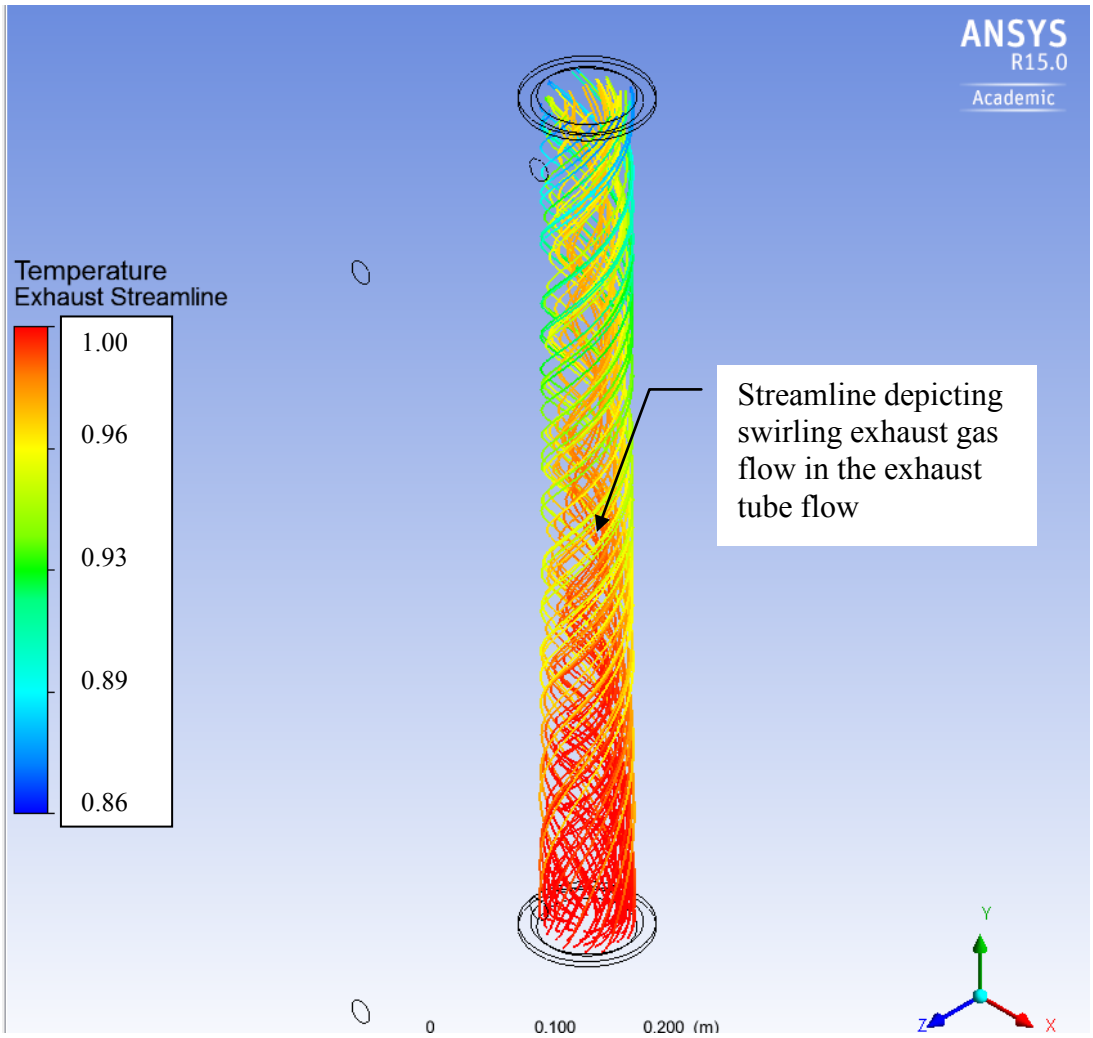

Figure 36. Streamline depicting the helical exhaust gas stream associated with swirl condition B (axial + tangential + radial velocity components) in a WHRU of L/d = 10. D/d=1.25, t*=0.0625 at Re_{exh} = 400,000.

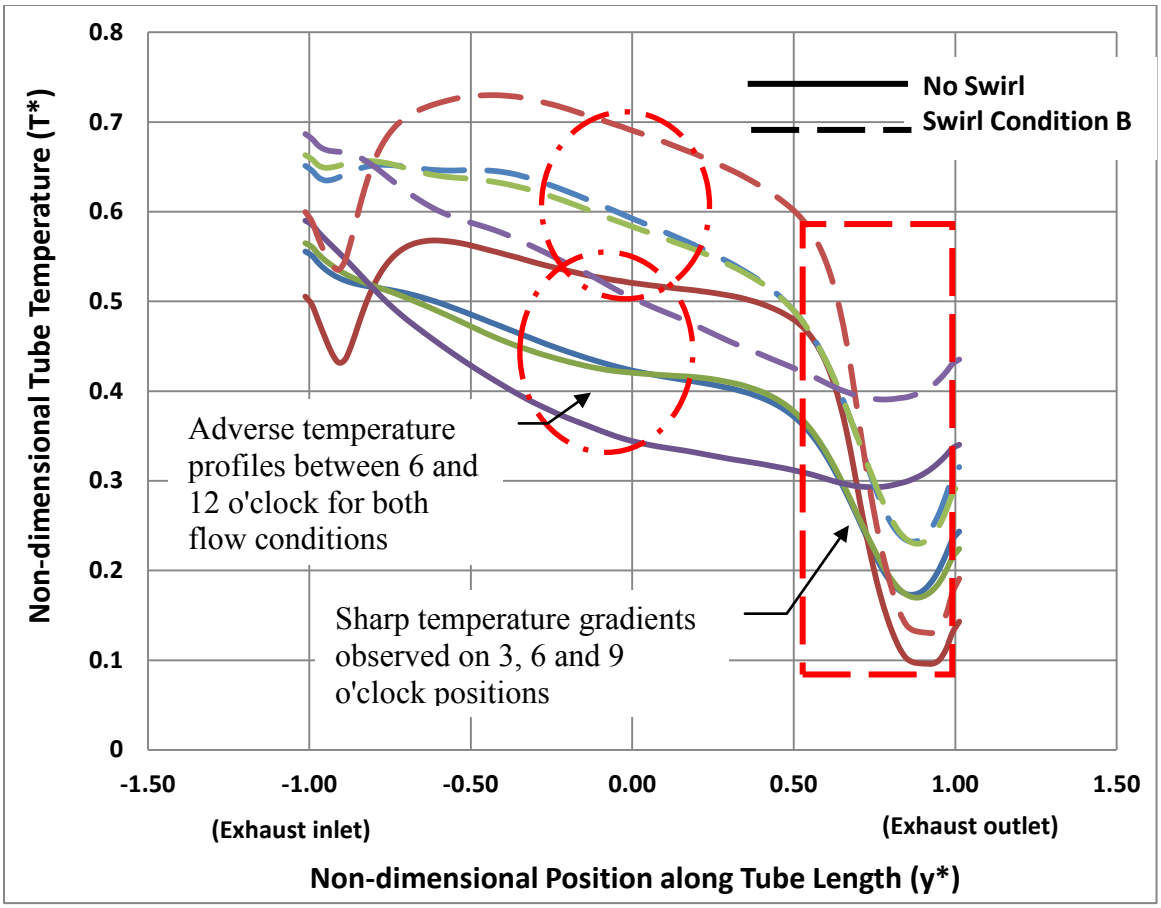

Figure 37. Comparison of tube temperature profile between WHRU with swirl condition B (axial, tangential, and radial velocity components) with a WHRU with only axial velocity component swirl at L/d = 10, D/d=1.25, t*=0.0625, centerline water inlet and outlet placement, Re_{exh} = 400,000, Re_{water} = 8,300.

The results from this section signify that swirling of the exhaust gas flow in the exhaust tube have minimum effects on the shape of the temperature profiles. The addition of swirl in the exhaust flow stream increased the average temperatures and did not mitigate the adverse temperature profiles within the WHRU. As such, swirling of exhaust gases does not contribute toward the improvement of WHRU reliability.

Additionally, the increase in heat recovery achieved through the swirling of exhaust gases comes at a higher pressure drop penalty. As discussed earlier, additional pressure drop in the exhaust gas system negatively impacts the performance and fuel consumption of the heat engine upstream.

F. EFFECT OF DIFFERENT TUBE MATERIAL

The effect of material thermal conductivity on tube temperature profile, heat recovery, and exhaust side pressure drop were studied. Four materials (steel, Inconel625, copper, and "Pyroceram" ceramic) of varying thermal conductivity were used in this study. The intention was to find out if high thermal conductivity can be used to mitigate high temperature gradients within the WHRU.

Steel is one of the most common materials used for construction. It has been used as the baseline material for the CFD models in this study. Inconel 625 was also chosen to be studied as it is a material used for the fabrication of WHRU tubes or engine components constantly in contact with exhaust gas. "Pyroceram" is a ceramic that has the lowest thermal conductivity among the four materials studied. "Pyroceram" is used in high temperature applications such as industrial plants. Copper, on the other hand, has the highest thermal conductivity and provides insights as to whether materials with high thermal conductivity can be used to mitigate adverse temperature and improve waste heat recovery at the same time. The dimensional and non-dimensional thermal conductivity (k_c*) of the four materials is tabulated in Table 7. Thermal conductivity of exhaust gas is assumed to be the same as air at 0.0261 W/mK. Thermal conductivity of air was obtained from the ANSYS material model used for CFD modeling.

Table 7. Comparison of thermal conductivity for carbon steel, Inconiel625, copper, and "Pyroceram."

Material Name	**Thermal Conductivity [W/mK]**	**Non-dimensional Thermal Conductivity ($k^* = k / k_{air}$)**
Carbon Steel (Used as benchmark for comparison) (ANSYS, 2013)	60	2,299
Inconel 625 (Special Metals Corporation, 2013)	17	651
Copper (ANSYS, 2013)	400	15,326
"Pyroceram" (Incropera, Bergman, Lavine, & Dewitt, 2011)	3	115

A CFD model of L/d=10, D/d=1.25, t*=0.0625 and centerline water inlet and outlet placement with purely axial exhaust gas flow was used for the study. The corresponding properties were set up in ANSYS-Pre for the corresponding runs.

1. Effect on Non-dimensional Heat Recovery (q*)

Using steel WHRU tubes as the benchmark for comparison and using copper as the tube material increased heat recovery marginally by 1% to 5%. Inconel 625 resulted in a 1% to 8% reduction in heat recovery, while the use of "Pyroceram" reduced heat recovery by 8% to 35%. With the exception of "Pyroceram," the use of copper or Inconel 625 as material for the WHRU tube had a relatively small impact on heat recovery. The heat recovery results from the CFD modeling are plotted in Figure 38.

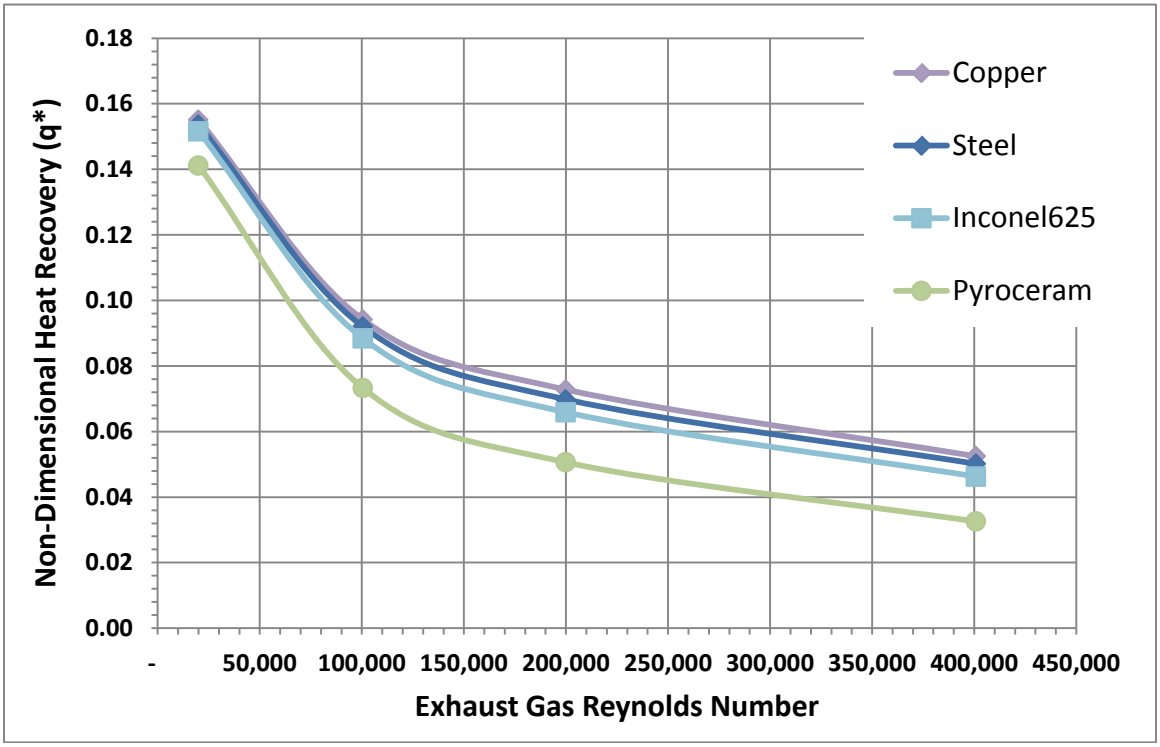

Figure 38. Comparison of non-dimensional heat recovery (q*) for WHRU with tubes made of copper, steel, inconel625 and "Pyroceram"/. L/d = 10, D/d=1.25, t*=0.0625. Re_{exh} from 20,000 to 400,000 with no exhaust swirl, centerline water inlet and outlet placement at Re_{water} = 8,300.

2. Effect on Non-dimensional Pressure Drop (ΔP*)

As shown in Figure 39, the use of the different tube materials had no significant impact on the exhaust gas pressure drop. The results are also reflective of the type of behavior expected in fluid undergoing force convection, as opposed to natural convection where thermal conductivity of the tube material will play a bigger role in the pressure drop. The results are additional indicators of the correct working of the CFD model.

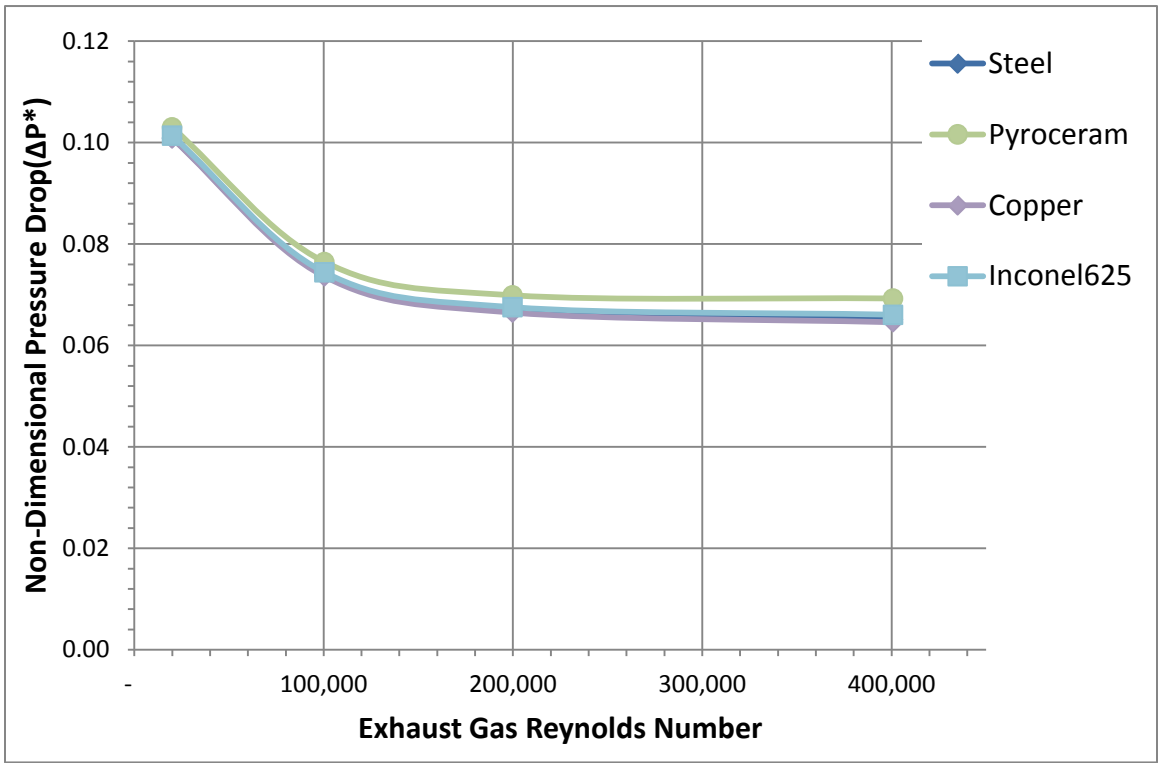

Figure 39. Comparison of non-dimensional pressure drop (ΔP*) for WHRU with tubes made of copper, steel, inconel625 and "Pyroceram"/. L/d = 10, D/d=1.25, t*=0.0625. Re_{exh} from 20,000 to 400,000 with no exhaust swirl, centerline water inlet and outlet placement at Re_{water} = 8,300.

3. Effect on WHRU Tube Temperature Profile

The temperature profiles of CFD models with steel, Inconel 625, copper, and "Pyroceram" are plotted in Figure 40, Figure 41, and Figure 42. These results shown were from CFD models which were evaluated at Re_{exh} = 400,000. The highest temperature gradients and differences were obtained during those run and were representative of exhaust conditions in USN's SSGTG.

a. Inconel 625 Tube

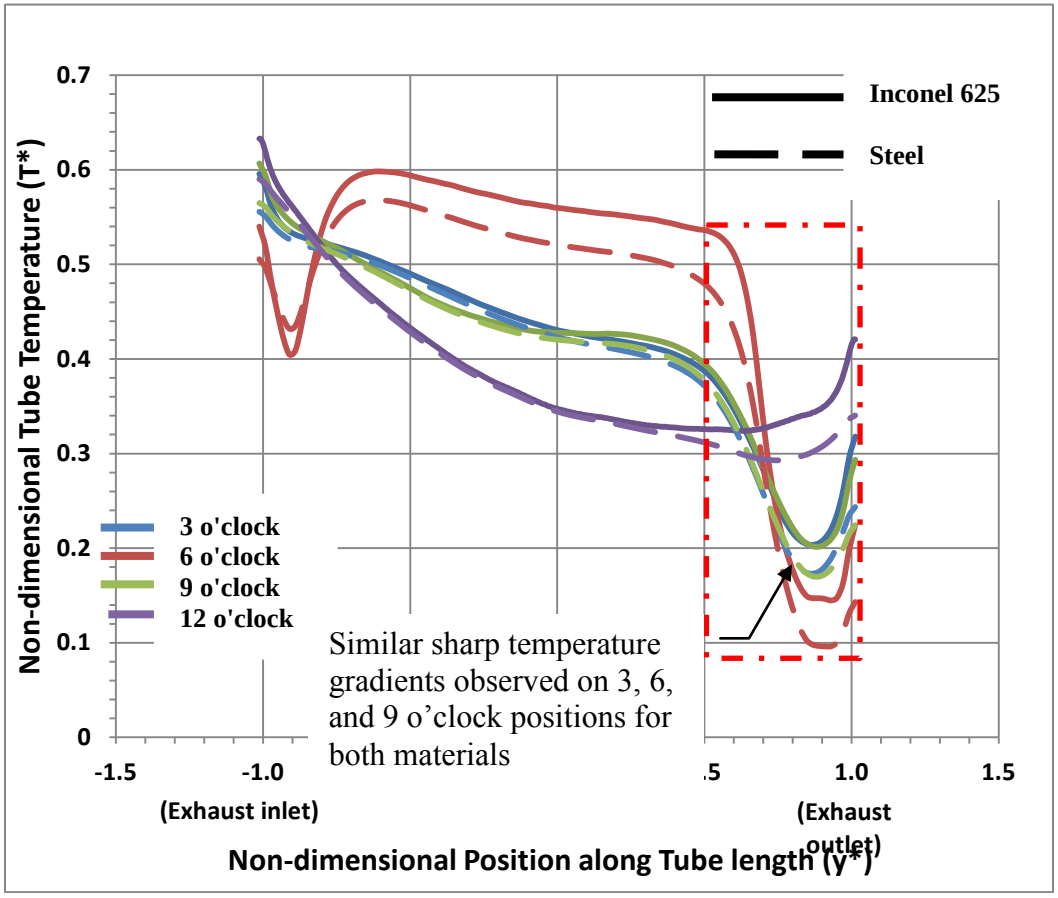

Figure 40. Comparison of tube temperature profile between Inconel 625 and steel WHRU of L /d =10, D/d=1.25, t* = 0.0625 with centerline inlet and outlet placement, no exhaust swirl, Re_{exh} = 400,000, Re_{water} = 8,300.

As illustrated in Figure 40, the temperature profiles of the Inconel 625 and steel WHRUs are similar, with the biggest temperature differences between the 6 o'clock and

12 o'clock positions. However, the Inconel 625 WHRU exhibited higher local temperature differences at y/L = -1.0 to -0.8 and y* = 0.8 to 1.0. The average temperature of the Inconel 625 WHRU was also higher than the steel WHRU. Adverse temperature profiles and sharp temperature gradients were not mitigated by the use of Inconel 625.

b. Copper Tube

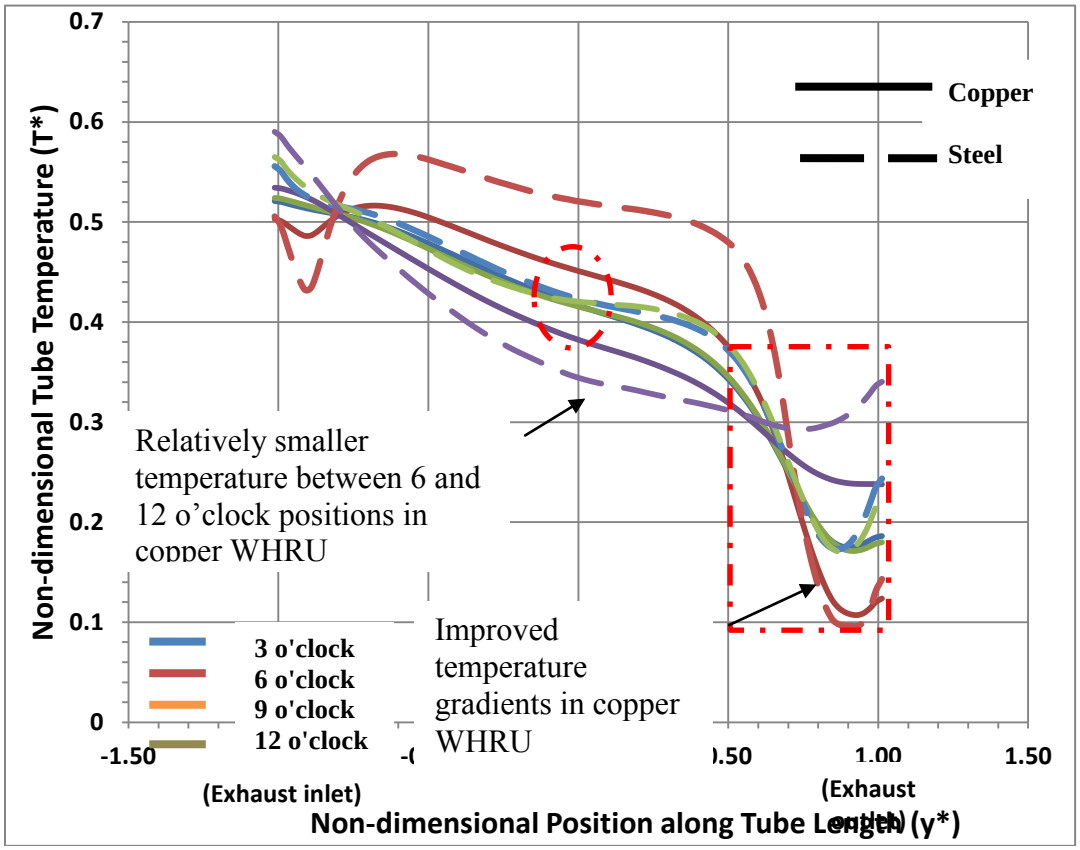

Figure 41. Comparison of tube temperature profile between copper and steel WHRU of L /d =10, D/d=1.25, t* = 0.0625 with centerline inlet and outlet placement, no exhaust swirl, Re_{exh} = 400,000, Re_{water} = 8,300.

Figure 41 compares the temperature profile of the copper WHRU against the steel WHRU. Results show copper WHRU to have temperature profiles which are relatively more favorable towards the improvement of WHRU reliability.

The use of copper contributes toward the mitigation of adverse temperature profiles within the WHRU. The familiar temperature difference between the 6 and 12

o'clock positions of the steel and Inconel 625 WHRU were reduced. Steel WHRU has a temperature difference up to 22% of maximum temperature range in the WHRU, while the maximum temperature difference for copper WHRU is 13% of the maximum range constituting to a 41% reduction of temperature difference. The sharp temperature gradients at y*=0.5 and 1.0 observed in steel and Inconel 625 were reduced by 25%.

The results indicate shows that material with high thermal conductivity can be used to mitigation adverse temperature profiles and gradients and improve WHRU reliability. Heat recovery performance is also increased marginally with no exhaust gas side pressure drop penalty.

c. "Pyroceram" Ceramic Tube

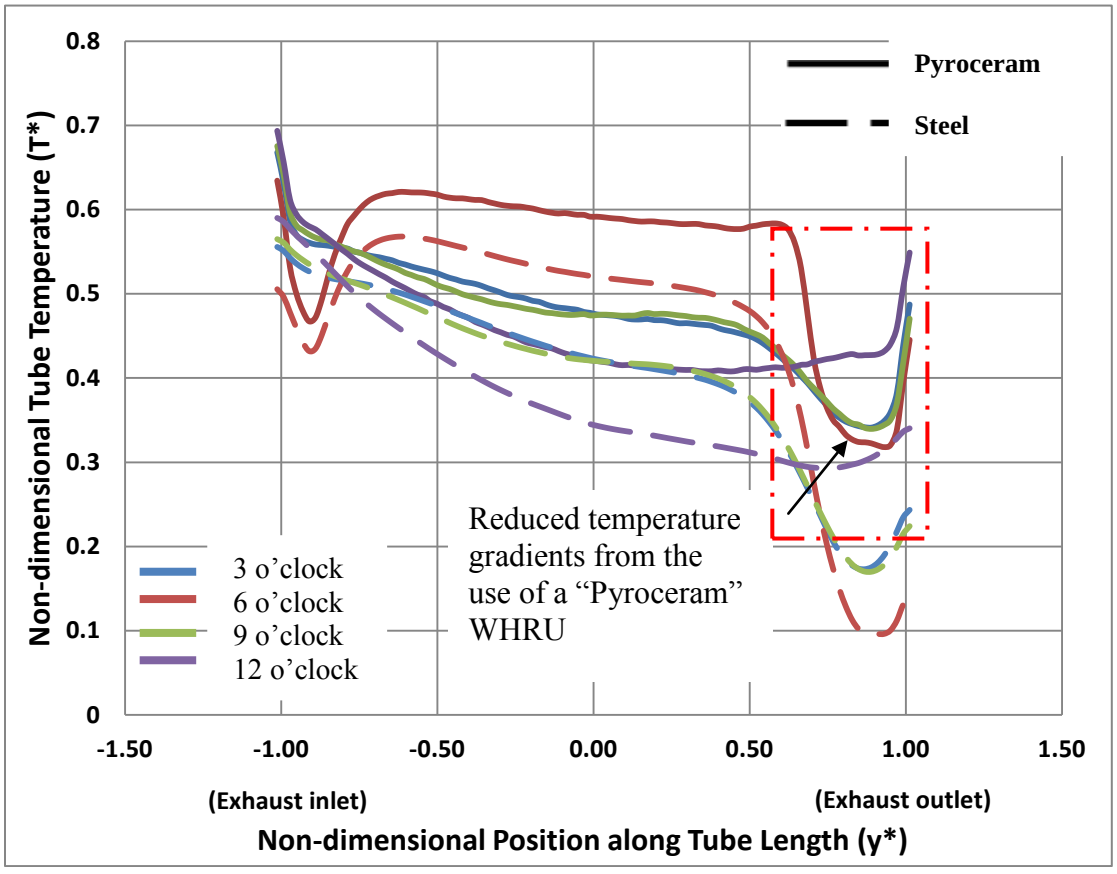

Figure 42. Comparison of tube temperature profile between Pyroceram and steel WHRU of L /d =10, D/d=1.25, t* = 0.0625 with centerline inlet and outlet placement, no exhaust swirl, Re_{exh} = 400,000, Re_{water} = 8,300.

"Pyroceram" being a ceramic possesses the lowest thermal conductivity among the four materials studied and is commonly used in ultra-high temperature applications. The results plotted in Figure 42 shows "Pyroceram" WHRU to have a smaller temperature gradient present between y* = 0.5 to 1.0 as compared to a steel WHRU. However, the highest average tube temperatures were recorded for the "Pyroceram" WHRU. The adverse temperature profile, especially between 6 o'clock and 12 o'clock positions of the WHRU, still remains as shown in Figure 42. The use of "Pyroceram" or materials with equivalently low thermal conductivity may be able to contribute marginally towards the mitigation of adverse temperature profiles and gradients.

d. Comparison of Tube Wall Temperature Profile at 6 O'Clock

The 6 o'clock tube wall temperature profiles of all four materials were plotted in Figure 44 in order to better compare the effect of material on temperature profiles and gradients. The average wall temperature of the copper WHRU tube was found to be lowest. The temperature gradient near the exhaust outlet (y*=0.5 to 1.0) was also more gradual compared to WHRU tube made of steel and Inconel 625. Interestingly, the temperature gradient for "Pyroceram" was also found to be more gradual compared to WHRU tubes made of steel and Inconel 625, despite having the highest average temperature. Based on the results, material with either very high or very low thermal conductivity seems to be more beneficial toward the mitigation of adverse temperature profiles and improvement of WHRU reliability.

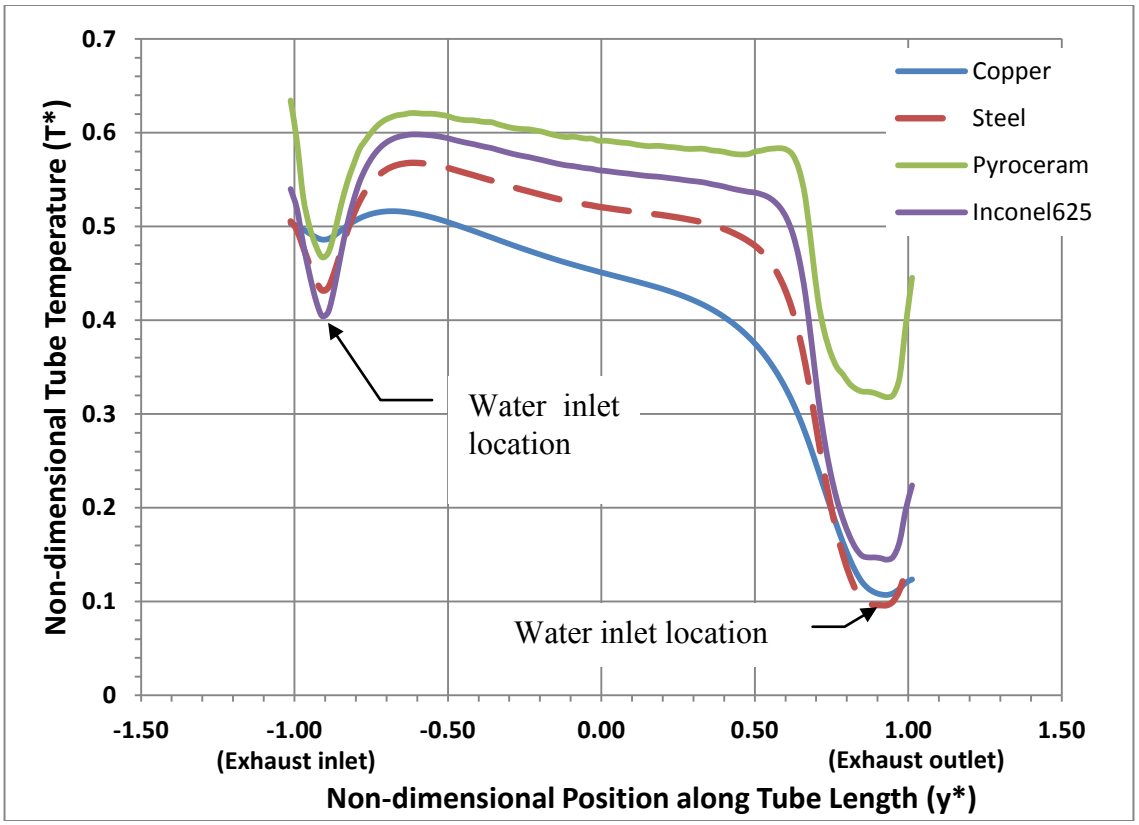

Figure 43. Comparison of 6 o'clock tube wall temperature profiles for WHRU tube made of copper, steel, "Pyroceram" and Inconel 625.

G. EFFECT OF SOLID HEAT SPREADER FEATURE

The adverse temperature profile in the WHRU was caused by poor distribution of water flow in the water jacket. One of the areas identified, shown in Figure 44, is the location near the water outlet and exhaust gas inlet.

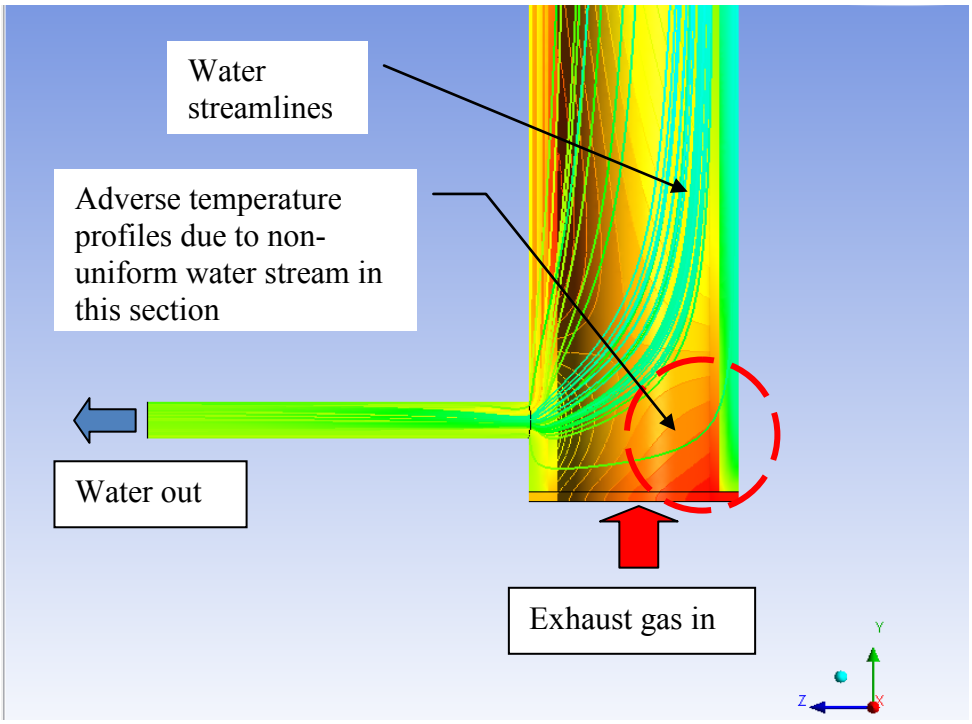

Figure 44. The 3 o'clock view of adverse temperature profiles due to non-uniform flow of water stream (shown by water streamlines) at the exhaust inlet section of a WHRU without the heat spreader feature.

In order to improve the temperature profile, the idea of a "heat spreader" feature was conceived. The intent was to use the additional conductive heat transfer associated with a solid section to achieve a more uniform heat transfer so as to improve the temperature profile. The heat spreader feature that was added is an additional solid annulus section placed in the water jacket of the WHRU at the exhaust gas inlet of the WHRU. These are shown in Figure 45 and Figure 46. The heat spreader thickness is 10% of the WHRU length (y*=0.1) and can potentially be fabricated from different materials. In this study, steel was used as the baseline material. Materials with either very high thermal conductivity such as copper or very low thermal conductivity such as "Pyroceram" could be used in future studies. A WHRU model of L/d=10, D/d=1.25, t*=0.0625 with centerline water inlet and outlet placements at Re_{exh}=400,000 with no exhaust swirl condition was used for this study.

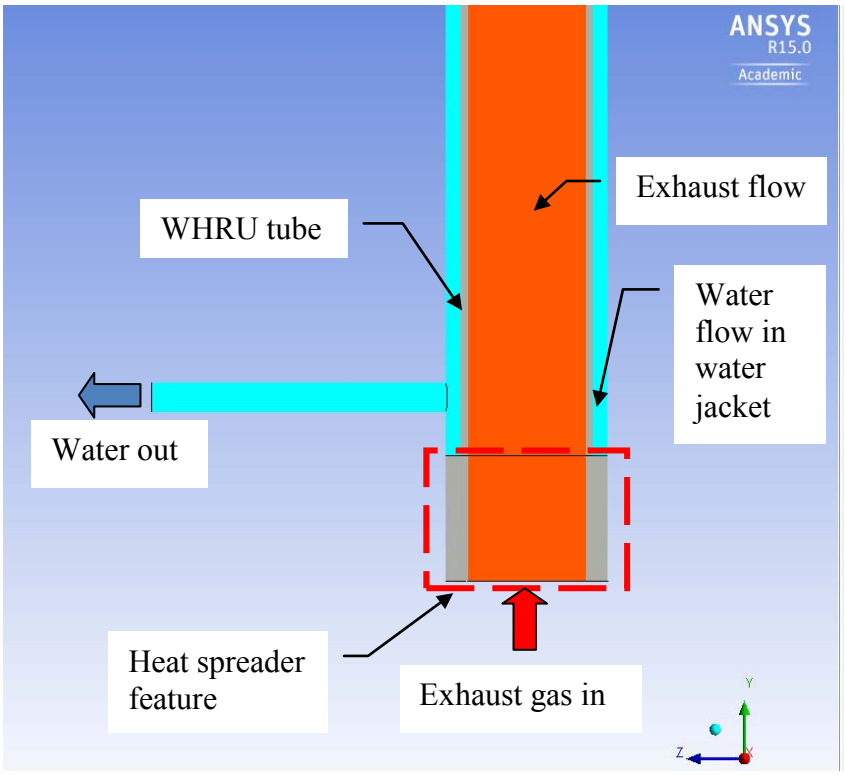

Figure 45. The 3 o'clock view of steel heat spreader feature near the exhaust inlet of the water jacket WHRU.

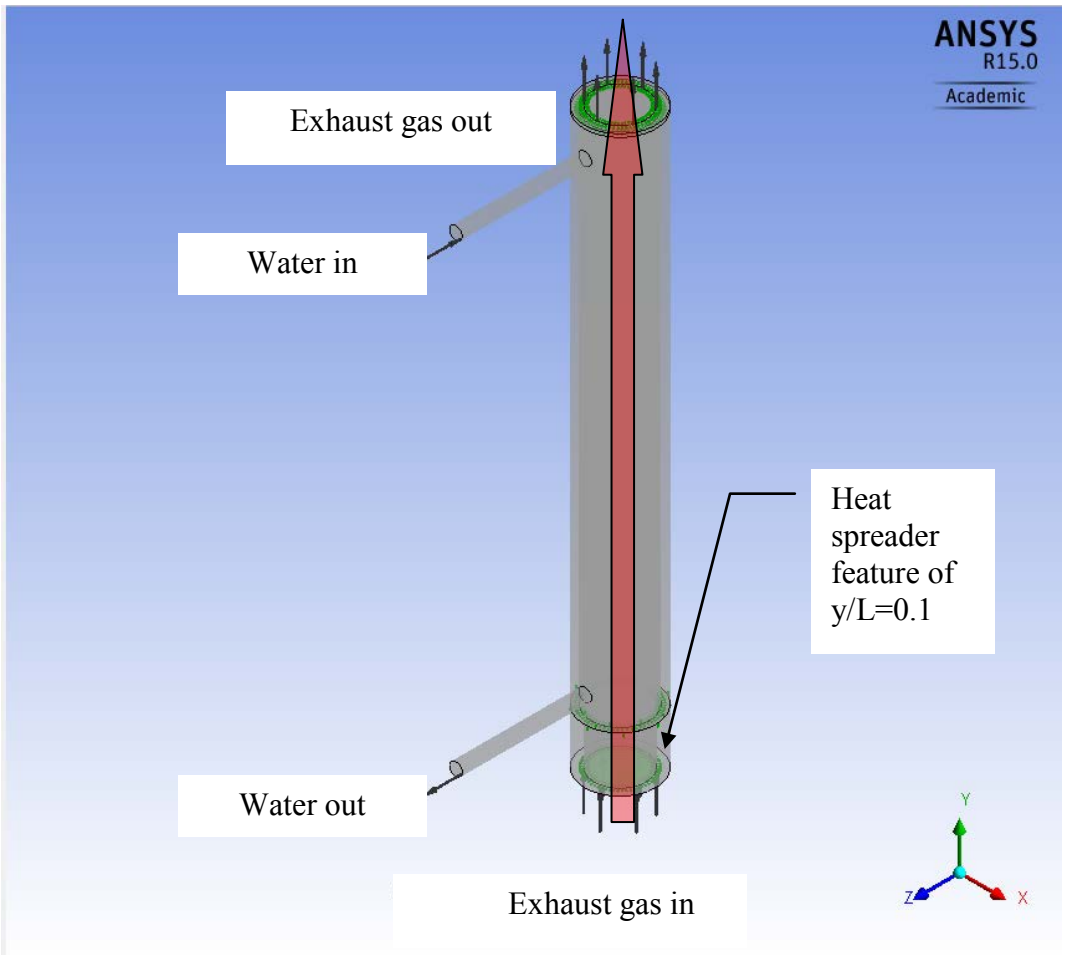

Figure 46. Isometric view of water jacket WHRU with steel heat spreader feature.

1. Effect on Non-dimensional Tube Temperature Profile

The temperature profiles of the WHRU with and without the heat spreader feature are shown in Figure 47. The results show that the use of a heat spreader actually had a detrimental effect on the temperature profile instead. The temperature gradients at the exhaust inlet section increased sharply for both Re_{exh} of 20,000 and 400,000 as highlighted by the red-dotted rectangle in Figure 47. This adverse temperature profile would result in increased thermal stresses and decrease reliability of the WHRU.

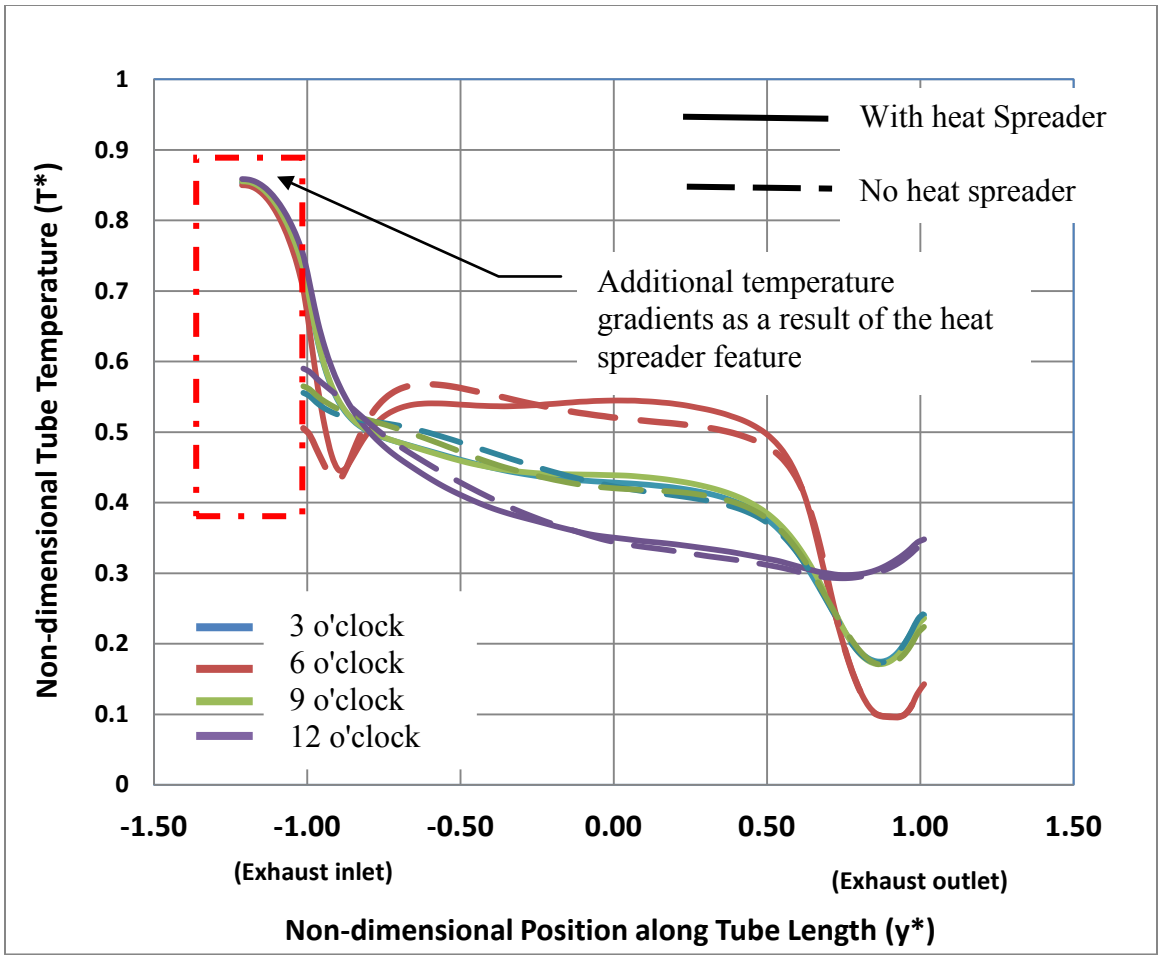

Figure 47. Comparison of tube temperature profile between WHRU with and without heat spreader feature at Re_{exh} = 20,000 and 400,000. For WHRU of L/d =10, D/d=1.25, t* = 0.0625, centerline water inlet and outlet placement with no exhaust swirl condition, Re_{water} = 8,300.

2. Effect on Non-dimensional Heat Recovery (q*)

The use of a heat spreader improved heat recovery marginally by 3% to 7% when compared to a similar model without the heat spreader. The highest improvement was seven percent when the exhaust Reynolds number was at 20,000 in Figure 48. The marginal improvement diminishes with increasing exhaust Reynolds number.

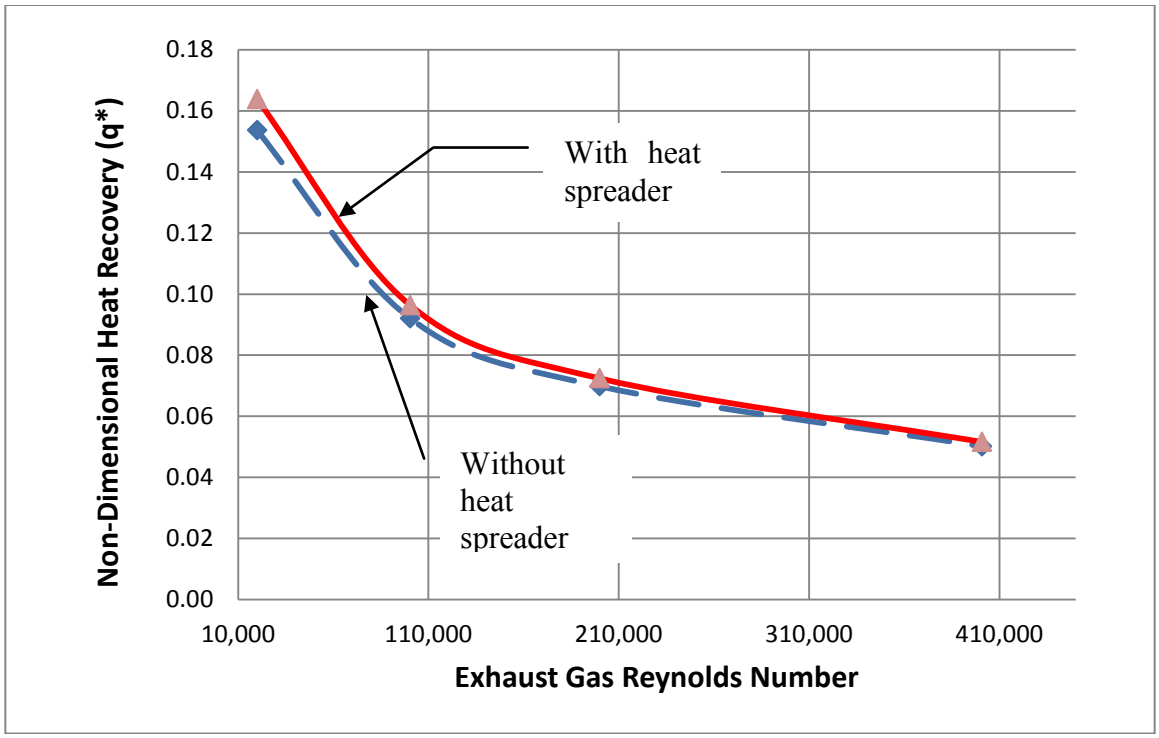

Figure 48. Effect of 0.1y* heat spreader on non-dimensional heat recovery (q*) for WHRU with L/d = 10, D/d=1.25, t*=0.0625, no exhaust swirl, centerline water inlet/outlet placement, Re_{exh} between 20,000 and 400,000; Re_{water} = 8,300.

3. Effect on Non-dimensional Pressure Drop (ΔP*)

A 12% increase in exhaust side pressure drop was registered with the WHRU fitted with a heat spreader shown in Figure 49. As there was no significant change to the exhaust flow stream throughout the majority of the WHRU length, the increase in pressure drop can be attributed to the additional length of y* = 0.1 from the heat spreader section.

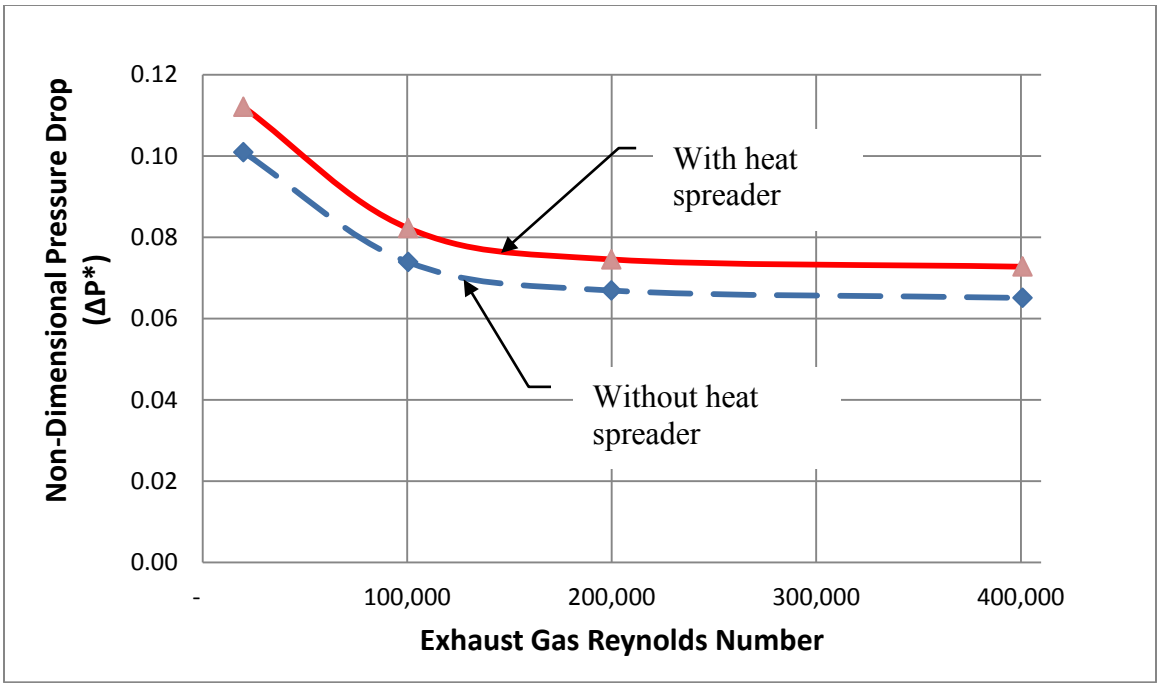

Figure 49. Effect of 0.1y* heat spreader on non-dimensional pressure drop (ΔP*) for WHRU with L/d = 10, D/d=1.25, t*=0.0625, no exhaust swirl, centerline water inlet/outlet placement, Re_{exh} between 20,000 and 400,000; Re_{water} = 8,300.

Although the heat spreader feature was able to demonstrate some potential to improve heat recovery performances, the adverse effect on the temperature profile near the exhaust inlet location would have resulted in increased thermal stresses within the WHRU. This has a significant negative impact on the reliability on the WHRU.

H. EFFECT OF WATER INLET AND OUTLET PLACEMENTS

In addition to studying the features related to WHRU geometry, exhaust gas flow, and tube material, the effect of three types of water inlet and outlet placements on heat recovery, exhaust pressure drop, and tube temperature profiles were also investigated. The CFD models used for the analysis were based on L/d = 10, D/d = 1.25 and t* = 0.0625. No swirls were introduced in the exhaust flow stream. The Reynolds number of exhaust gas flow was varied from 20,000 to 400,000 in order to reflect the exhaust flow expected in the USMC DG and USN SSGTG. The water Reynolds number was held

constant at 8,300. The diameter of the water inlet and outlet was held constant for all models used in this study.

The first type of water inlet and outlet placement (placement Type 1) is shown in Figure 50 and Figure 51. This is the default water placement used by previous CFD models in this study. Water inlet and outlet are located on the centerline on the 6 o'clock side. Water inlet is located y*= -0.1 from the end of the exhaust outlet, while the water outlet is located y*=0.1 from the exhaust inlet's end. WHRU with this placement option can be easily manufactured and could be one of the reasons why this type of inlet and outlet placement is commonly used in the industry.

The second type of placement (placement Type 2) is shown in Figure 52. Water inlet is located on the centerline of the 6 o'clock side, while water outlet is located on the centerline of the 12 o'clock side of the WHRU. Water placement Type 2 aims to improve the water flow in the water jacket so as to mitigate adverse tube temperature gradients and improve reliability. Similar to placement Type 1, this placement option is also prevalent in the industry.

The third type of placement, placement Type 3, is shown in Figure 53 through Figure 55. It was created with the water inlet and outlet laterally shifted by x*= $\pm$0.8 from the centerline. This simple shift of water inlet and outlet improved the water flow in the water jacket, which in turn mitigated the temperature profile and improved WHRU performance. Placement Type 3 is not as common, possibly due to the increased complexity in manufacturing.

1. Placement Type 1 (Baseline): Centerline Water Inlet and Outlet on Same Side of WHRU

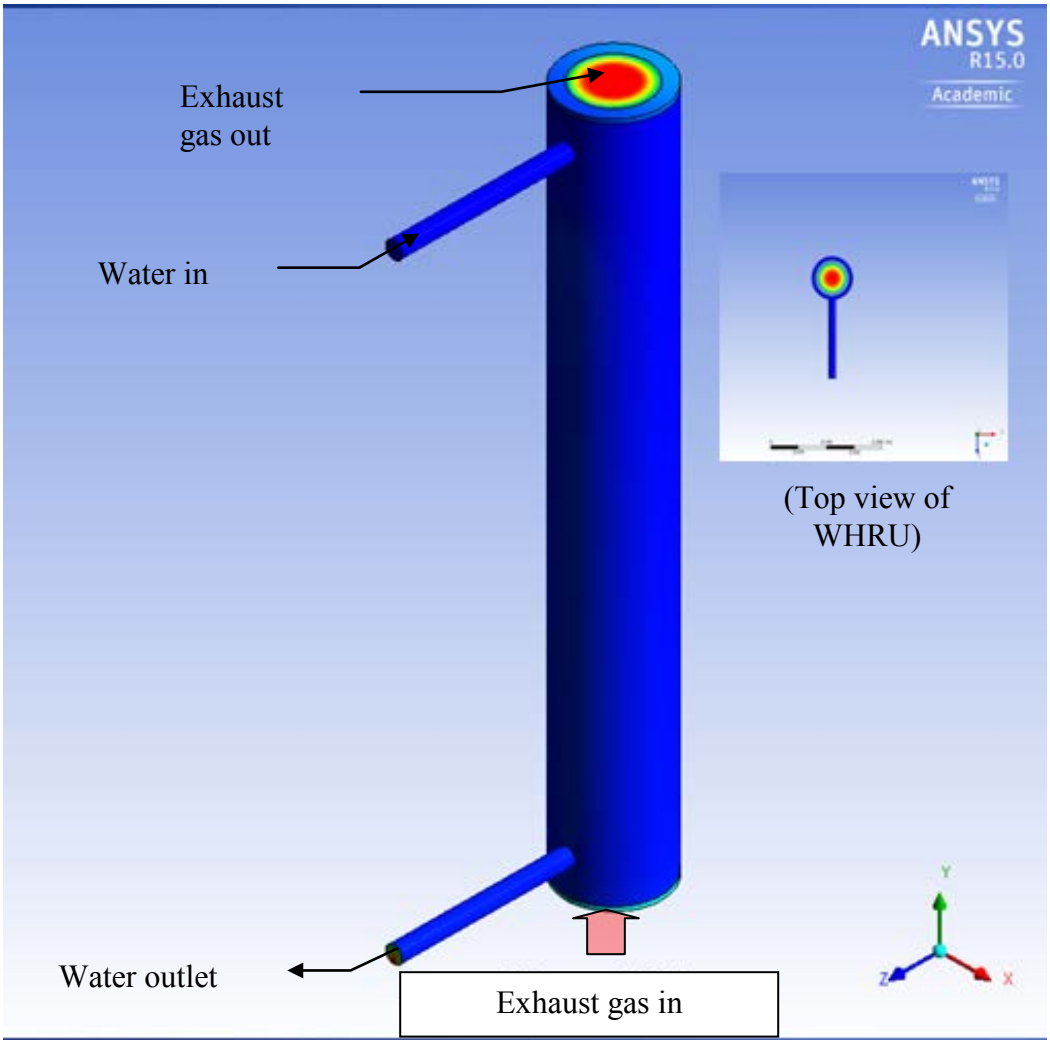

Figure 50. Isometric and top view of WHRU with water placement Type 1 (centerline water inlet and outlets on 6 o'clock side at y/L = 0.1 from the top and bottom edges of WHRU).

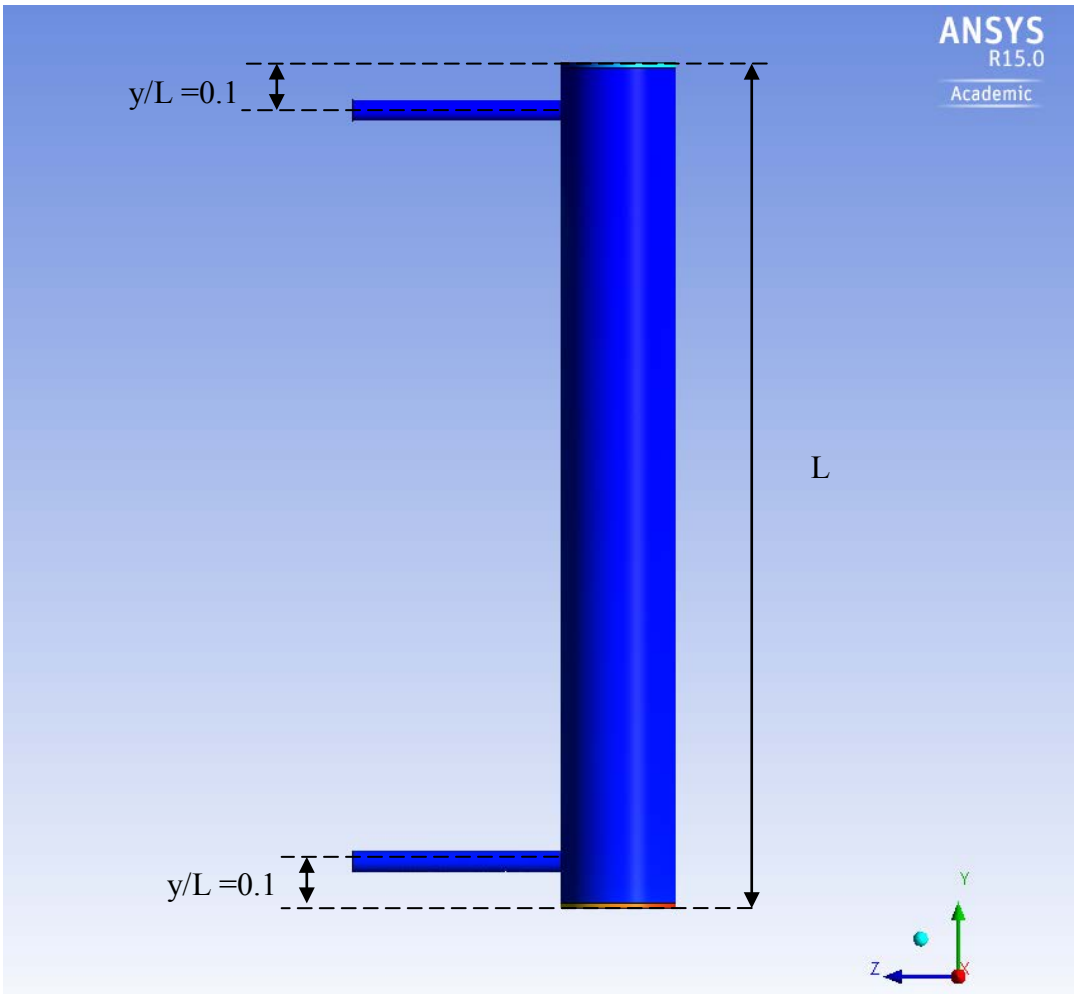

Figure 51. View from 3 o'clock of WHRU with water placement Type 1 (centerline water inlet and outlets on 6 o'clock side at y/L = 0.1 from the top and bottom edges of WHRU).

2. Placement Type 2: Centerline Inlet and Outlet on Opposite Sides of WHRU

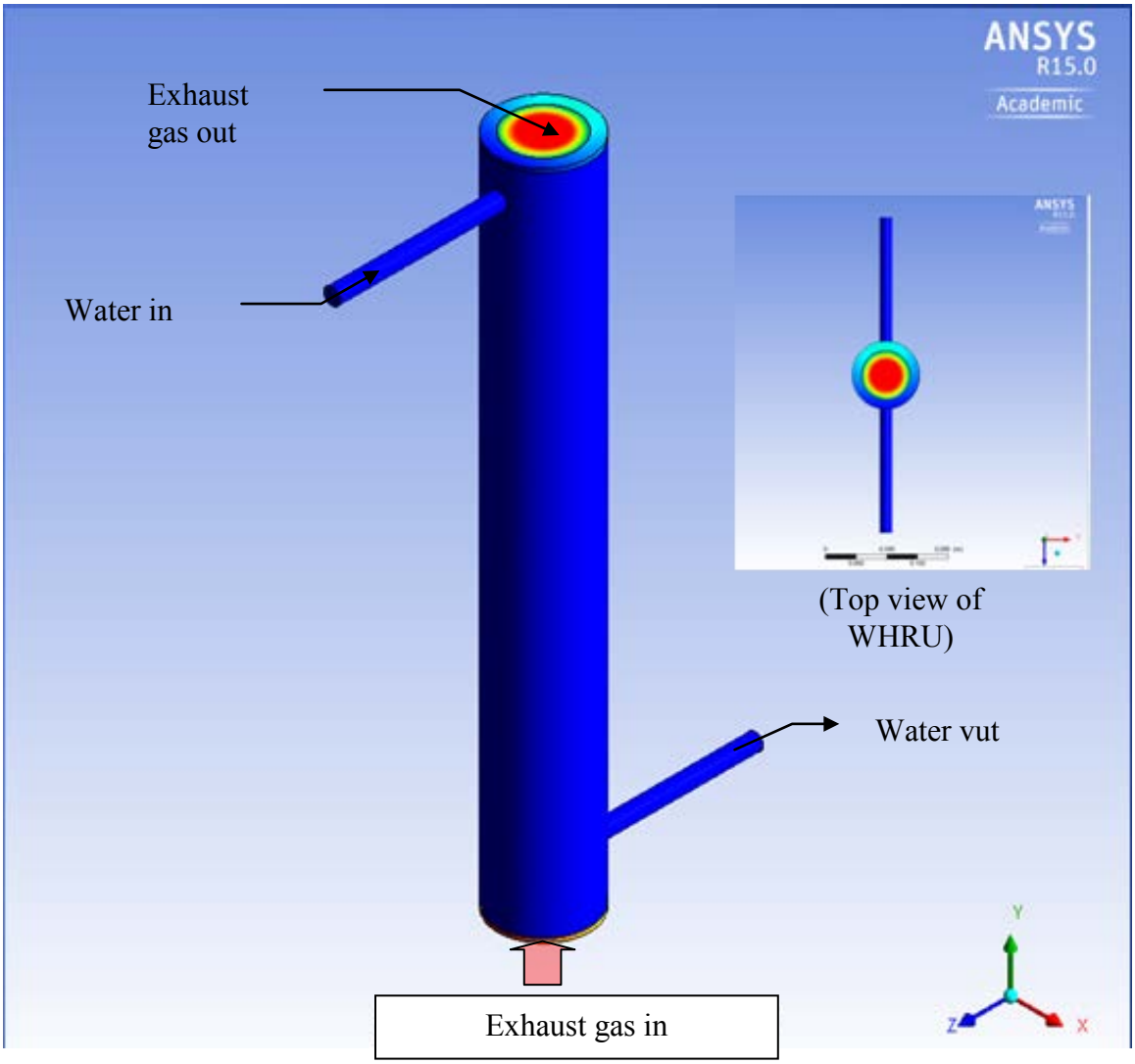

Figure 52. Isometric view and top view of water placement Type 2 (centerline water inlet on 6 o'clock side and water outlet on 12 o'clock side at y/L = 0.1 from the top and bottom edges of WHRU).

3. Placement Type 3: Inlet and Outlet on Same Side of WRU, Shifted by x*= ± 0.8

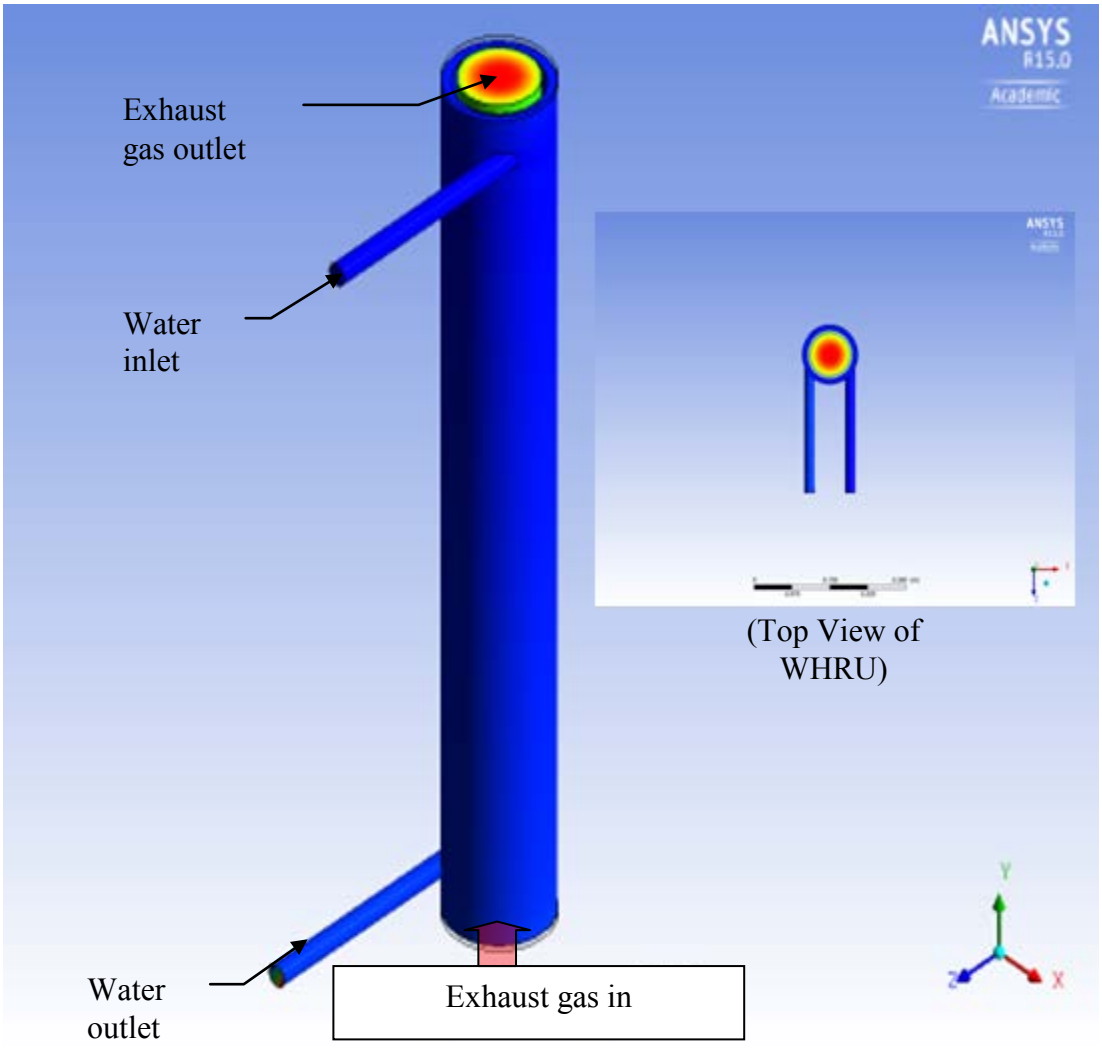

Figure 53. Isometric view (and top view) of CFD model with water placement Type 3 (water inlet and outlet located at x*= ±0.8 from centerline and y/L = 0.1 from the top and bottom edges of WHRU).

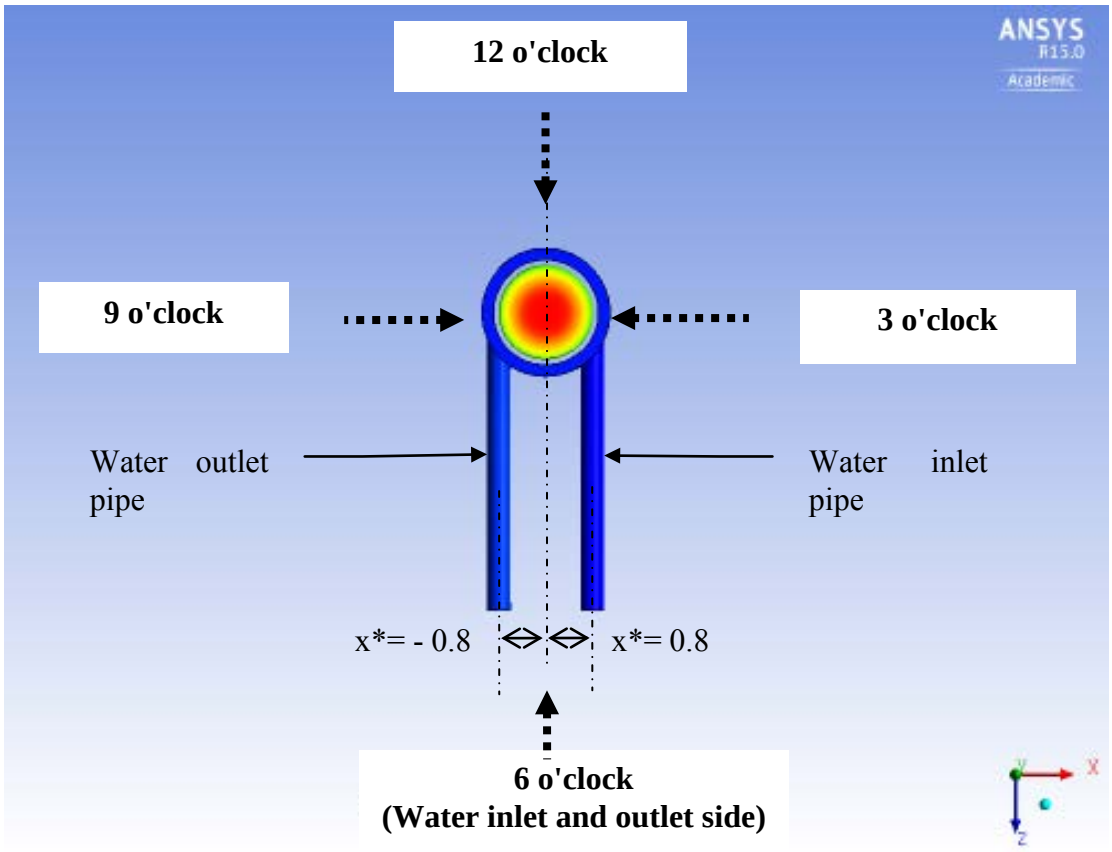

Figure 54. Top view of CFD model with water placement Type 3 (water inlet and outlet located shifted x*= ±0.8 from centerline).

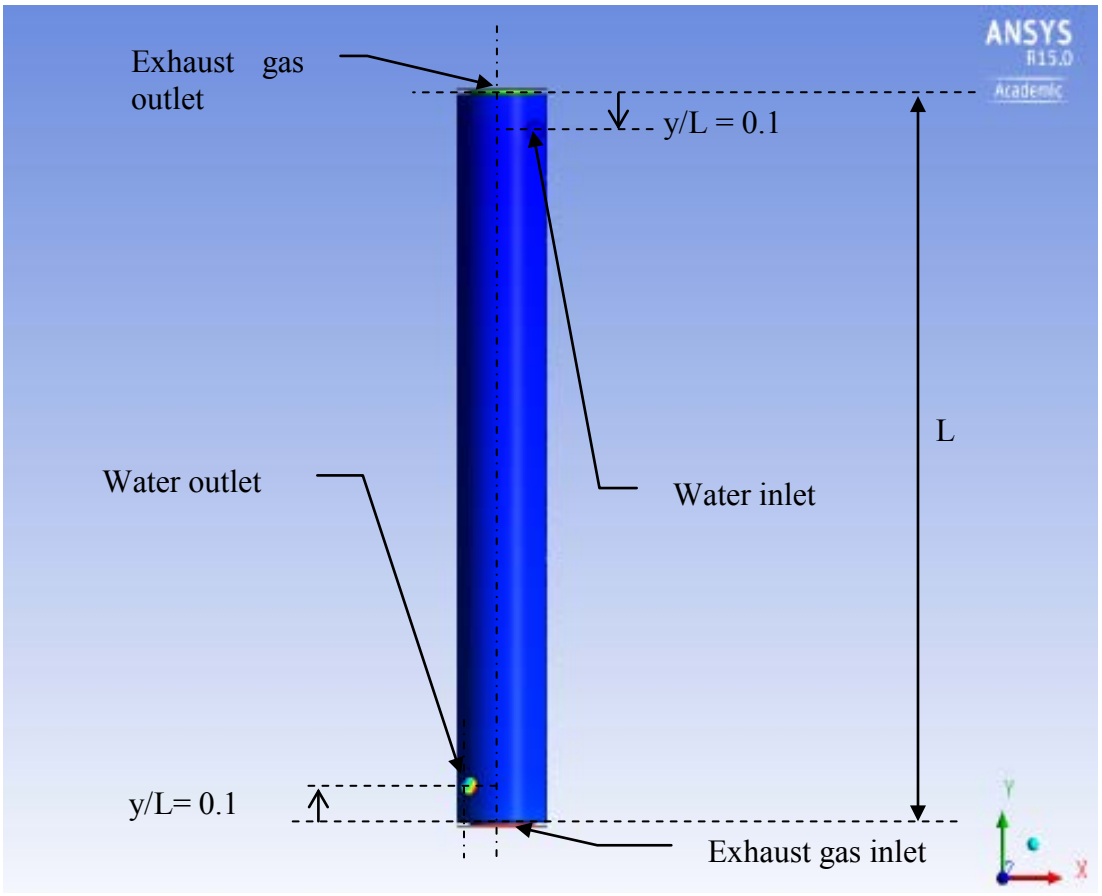

Figure 55. The 6 o'clock view of WHRU with water placement Type 3 showing (water inlet and outlet located y/L = 0.1 from top and bottom edges of the WHRU).

4. Effect of Water Inlet and Outlet Placements on Non-dimensional Heat Recovery (q*)

A comparison of heat recovery from the water placement types are plotted in Figure 56. When water inlet and outlets are placed on opposite sides (placement Type 2) compared to being on the same side (placement Type 1), the heat recovery performance was reduced marginally by 0.1% to 0.7%.

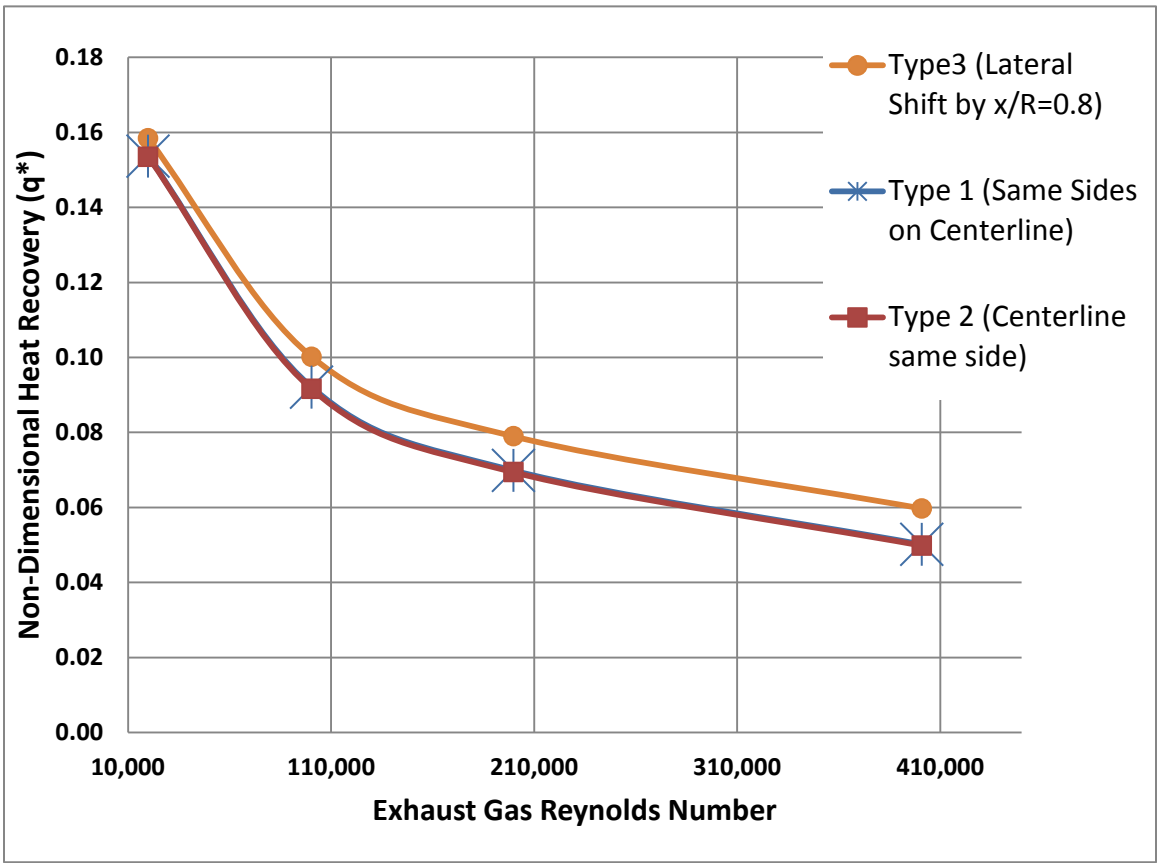

Figure 56. Comparison of non-dimensional heat recovery (q*) from three water inlet and outlet placement types based on water jacket WHRU of L/d=10, D/d=1.25 with steel tube of t* = 0.0625. Re_{exh} from 20,000 to 400,000 with no exhaust swirl with Re_{water} = 8,300.

However, when the water inlet and outlet were shifted laterally by x*=$\pm$0.1 from the centerline in placement Type 3, a 3% to 19% improvement in heat recovery was achieved. The shift in the water inlets and outlets caused water in the jacket to flow around the WHRU tube which in turn improved the heat recovery. Plots in Figure 56

showed a greater heat recovery improvement at higher exhaust Reynolds number, making this finding applicable toward the waste heat recovery for the USN 501K SSGTG.

5. Effect on Non-dimensional Exhaust Side Pressure Drop (ΔP*)

Based on the results from the CFD models in Figure 57, it can be concluded that water placement did not have any significant impact on the exhaust side pressure drop. A lateral shift of water inlet and outlet (placement Type 3) reduced the exhaust side pressure drop marginally by 1% to 3% compared to a WHRU with centerline water inlet and outlets on the same side (placement Type 1). With the water inlet and outlet placed on opposite sides (placement Type 2), exhaust side pressure drop was increased by 0.15%.

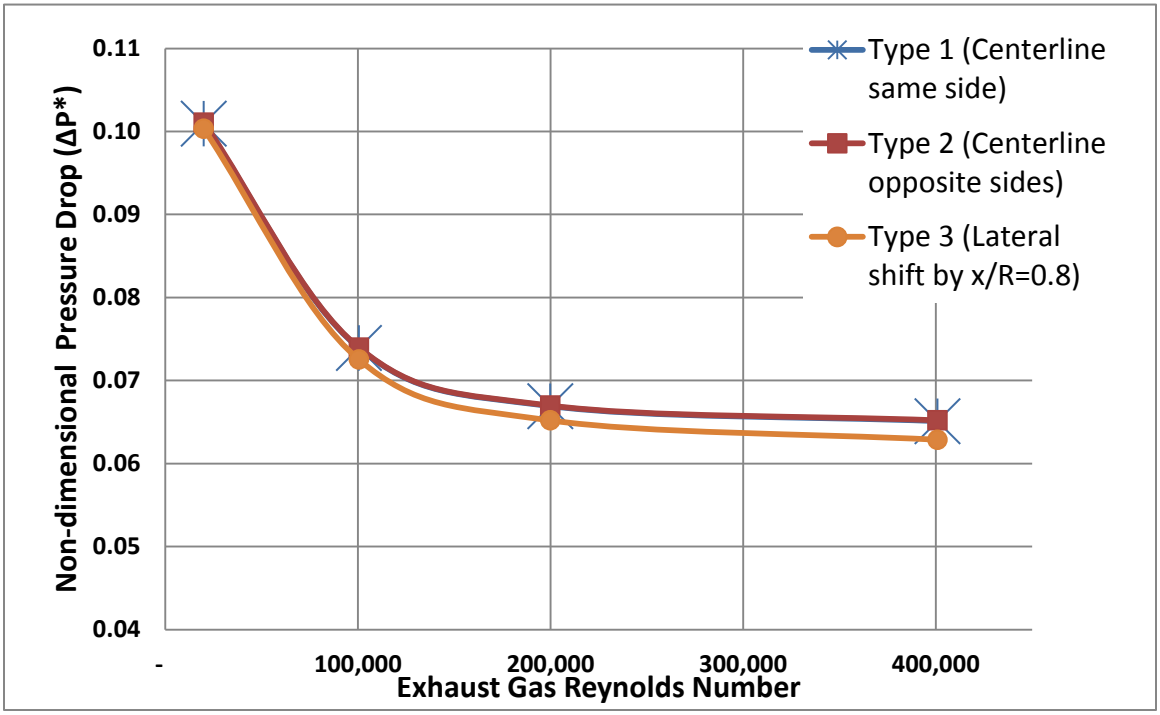

Figure 57. Comparison of non-dimensional pressure drop (ΔP*) of three water inlet and outlet placement types based on water jacket WHRU of L/d=10, D/d=1.25 with steel tube of t* = 0.0625; Re_{exh} from 20,000 to 400,000 with no exhaust swirl; Re_{water} = 8,300.

6. Effect on Non-dimensional Temperature Profiles

The effect of the three water placements types on tube temperature profile were compared at Re_{exh} = 400,000. Figure 58 compares the temperature profiles between placement Type 1 (centerline water inlet and outlet on the same side) and Type 2 (centerline water inlet and outlet on opposite sides). In both placement Type 1 and Type 2, adverse temperature profiles occurred between the 6 o'clock and 12 o'clock positions nearly throughout the length of the WHRU tube. Results from Figure 58 also show that placing the water inlet and outlet opposite each other in placement Type 2 caused the temperature profiles between the 6 o'clock and 12 o'clock positions to be worsened.

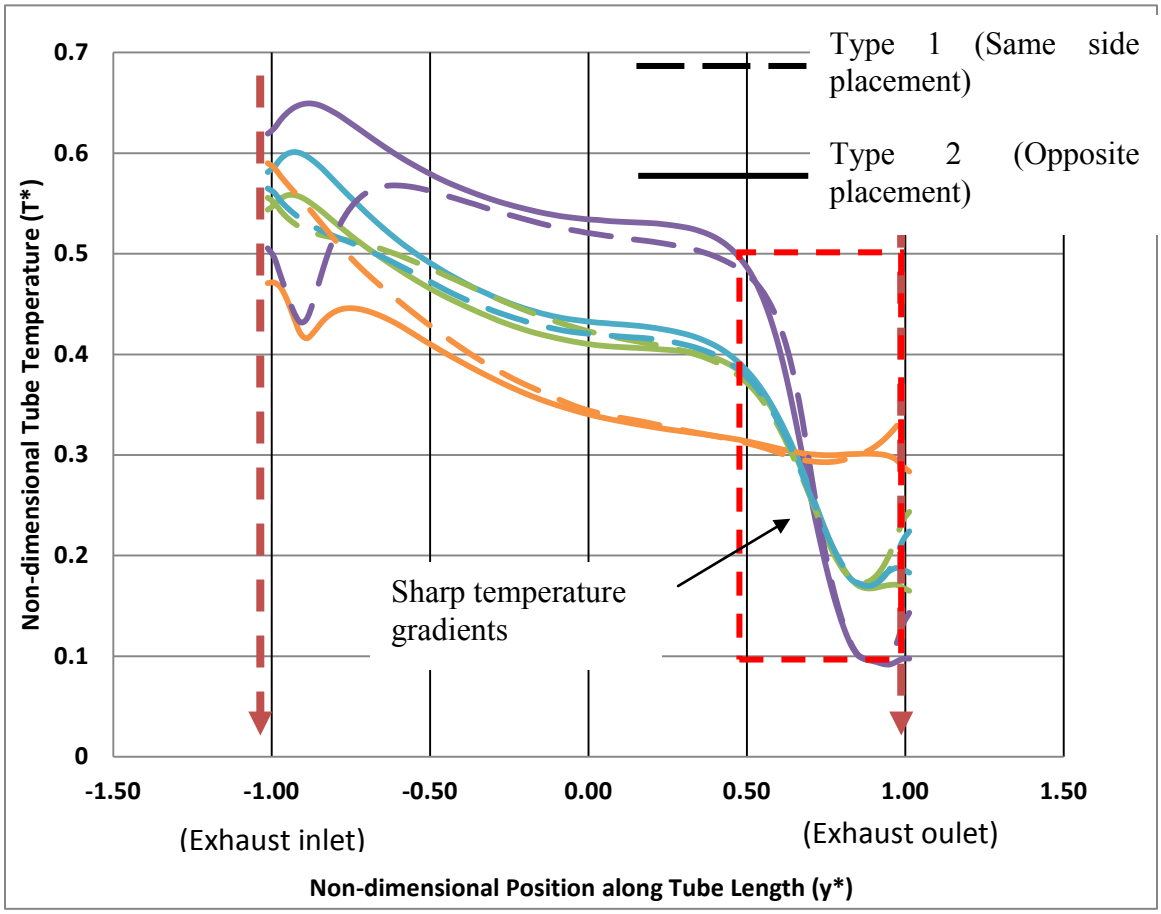

Figure 58. Comparison of WHRU tube temperature profiles between placement Type 1 (centerline water inlet and outlet on the same side) and Type 2 (centerline water inlet and outlet on opposite sides) for WHRU of L/d=10, D/d=1.25, t*=0.0625. Re_{Exh} of 20,000 to 400,000 with no exhaust swirl. Re_{water} = 8,300.

Sharp temperature gradients were also observed at the upper 25% of the WHRU between y* = 0.5 and y*=1. The adverse tube temperature profiles of placement Type 1 and placement Type 2 can be attributed to uneven water flow distribution in their water jacket depicted by streamlines and water velocity vector plots. Figure 59 and Figure 60 depict the streamlines and water velocity vector plots for water placement Type 1 while Figure 61 and Figure 62 depict the streamlines and water velocity vector plots for water placement Type 2.

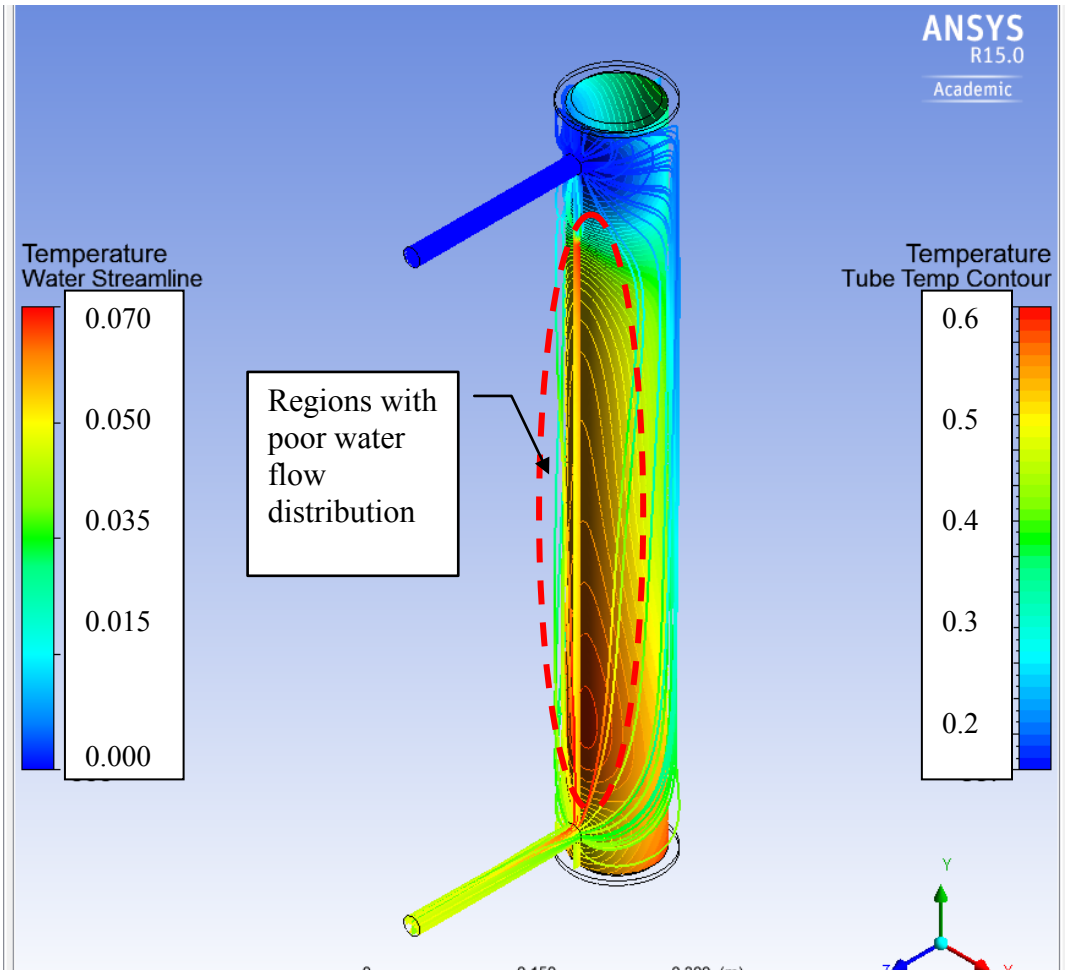

Figure 59. Water streamlines and tube temperature contours for WHRU with water placement Type 1 (centerline water inlet and outlet placement on same side), L/d = 10; D/d=1.25, t*=0.0625 at Re_{exh} = 400,000; Re_{water} = 8,300, and no exhaust swirl.

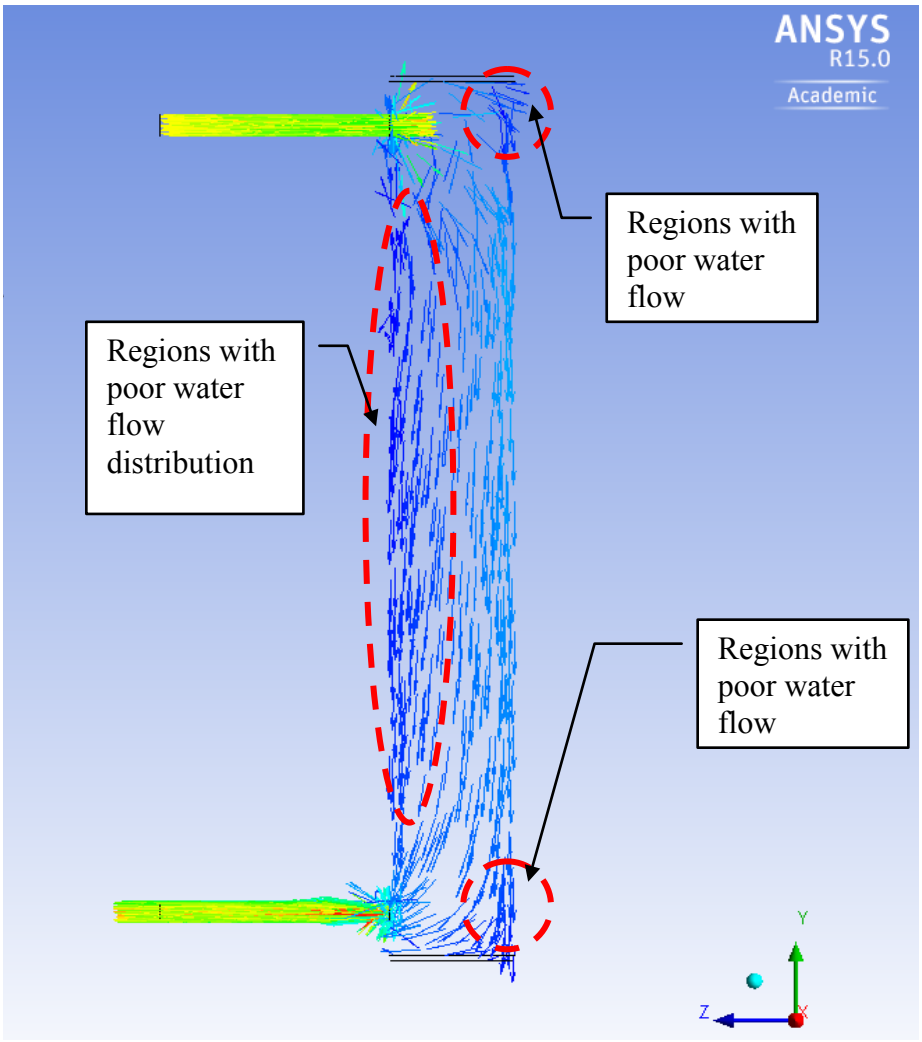

Figure 60. Water velocity vectors of WHRU with water placement Type 1 (centerline water inlet and outlet placement on same side), for L/d =10, D/d=1.25, t*=0.0625 at Re_{exh}=400,000, Re_{water} =8,300 with no exhaust swirl.

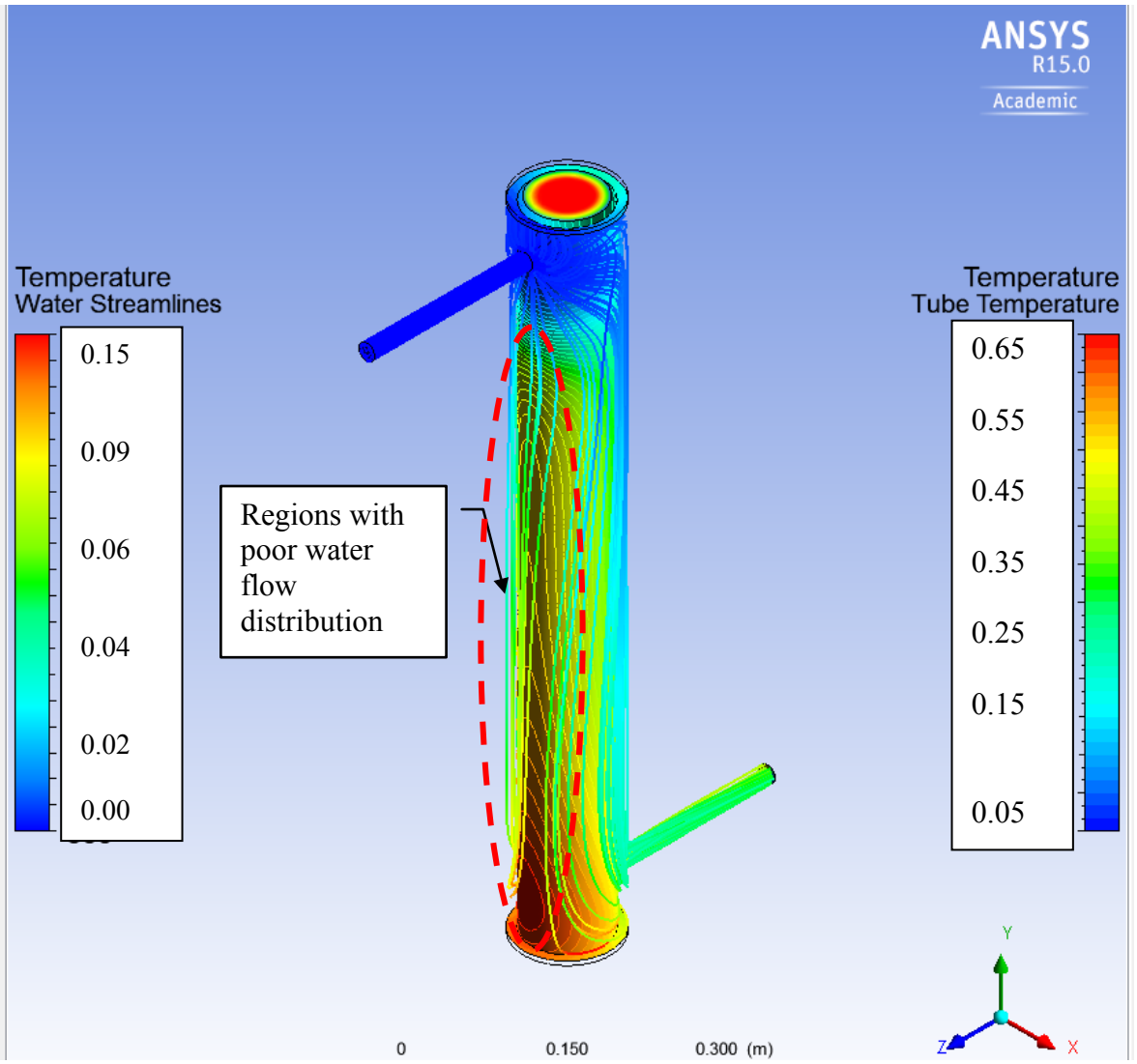

Figure 61. Water streamlines and tube temperatures for WHRU with water placement Type 2 (centerline water inlet and outlet placement on opposite sides), L/d = 10. D/d=1.25, t*=0.0625, No Exhaust Swirl, Re_{exh} = 400,000, Re_{water} = 8,300.

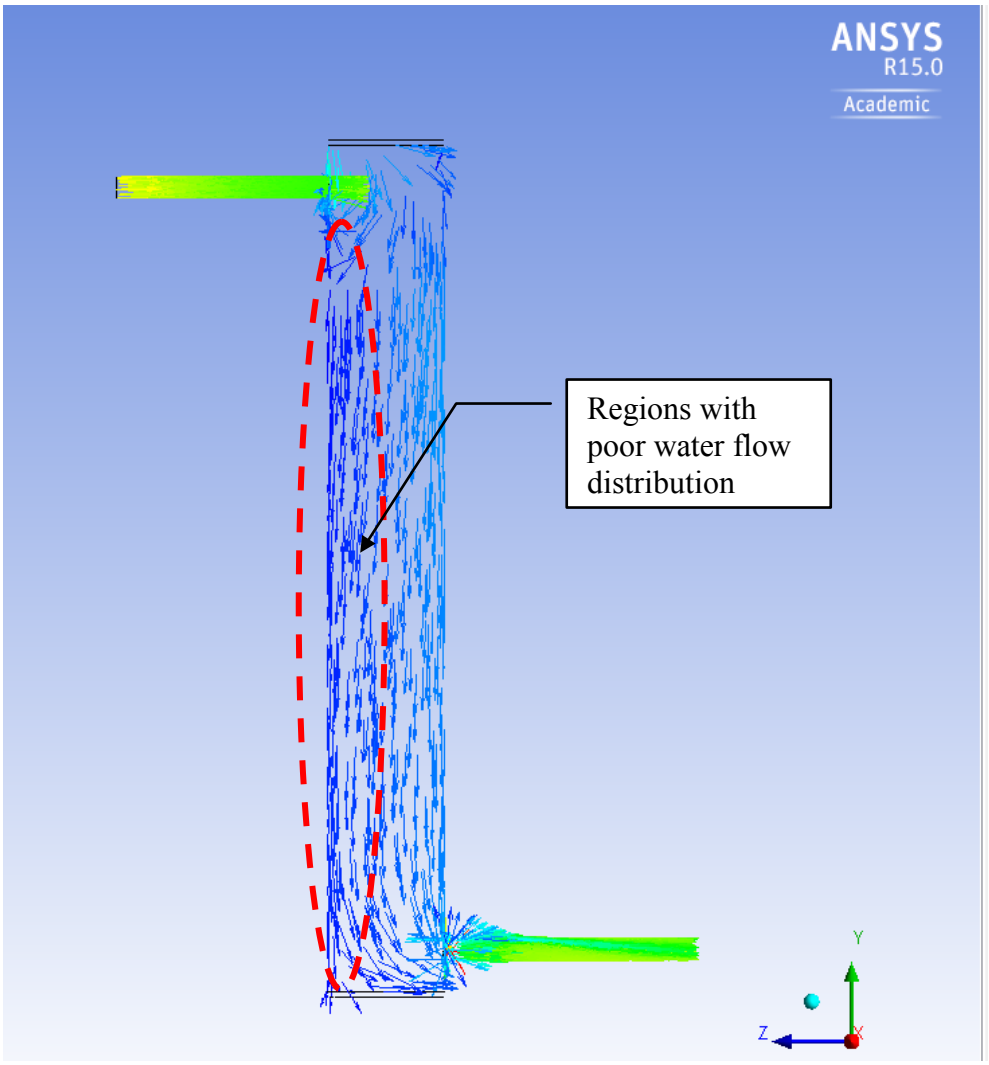

Figure 62. Water velocity vectors of WHRU with water placement Type 2 (centerline water inlet and outlet placement on opposite sides), L/d = 10. D/d=1.25, t*=0.0625, no exhaust swirl, Re_{exh} = 400,000, Re_{water} = 8,300.

Instead of improving the temperature profiles, the placement of the inlet and outlets on opposite sides of the WHRU resulted in temperature profiles which were more adverse, negatively impacting the WHRUs' reliability. This finding is interesting considering these two types of water placement are very prevalent in the heat exchanger industry. The adverse temperature profiles could have contributed toward premature failure of similar configurations.

The comparison of tube temperature profiles between water placement Type 3 and water placement Type 1 is shown in Figure 63. The results from the CFD models showed that temperature profiles from the WHRU with placement Type 3 to be gradual. The adverse 6 o'clock and 12 o'clock temperature difference that was characteristic of the centerline water placement types was not observed. The sharp temperature gradients between y* = 0.5 and y*=1 were also effectively mitigated by the lateral shifting of water inlet and outlet from centerline.

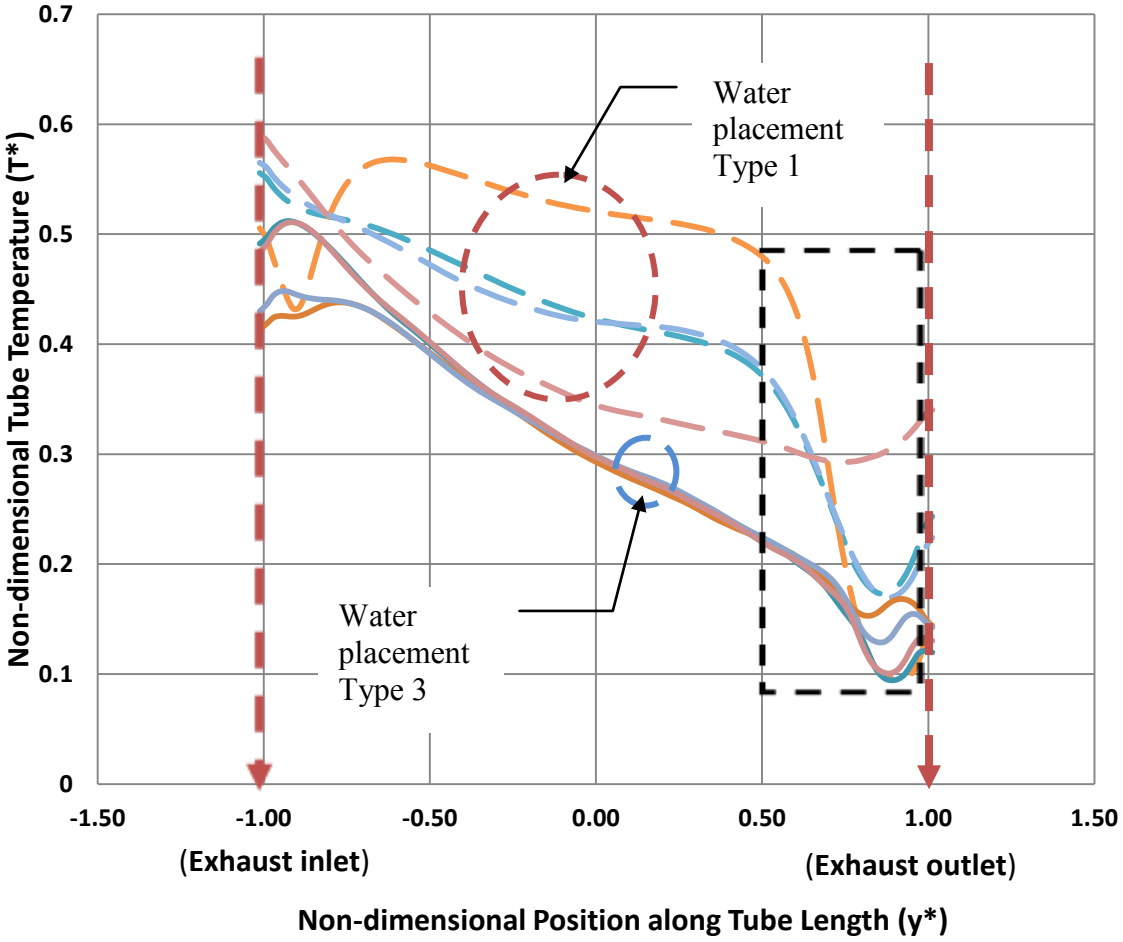

Figure 63. Comparison of tube temperature profile between WHRU with water inlet and outlet shifted laterally by x*=0.8 (placement Type 3) and WHRU with centerline water inlet and outlet on the same side (placement Type 1). L/d=10, D/d=1.25, t*=0.0625. Re_{exh} of 20,000 to 400,000 with no exhaust swirl; Re_{water} = 8,300.

The shift of the water inlet and outlet caused water to flow uniformly around WHRU tube as shown in Figure 64. The improved flow stream improved heat transfer throughout the tube, increasing heat recovery and mitigating the adverse temperature profile. The maximum local temperature fluctuation occurs around y* = ±0.95m where the water inlet and outlet are located.

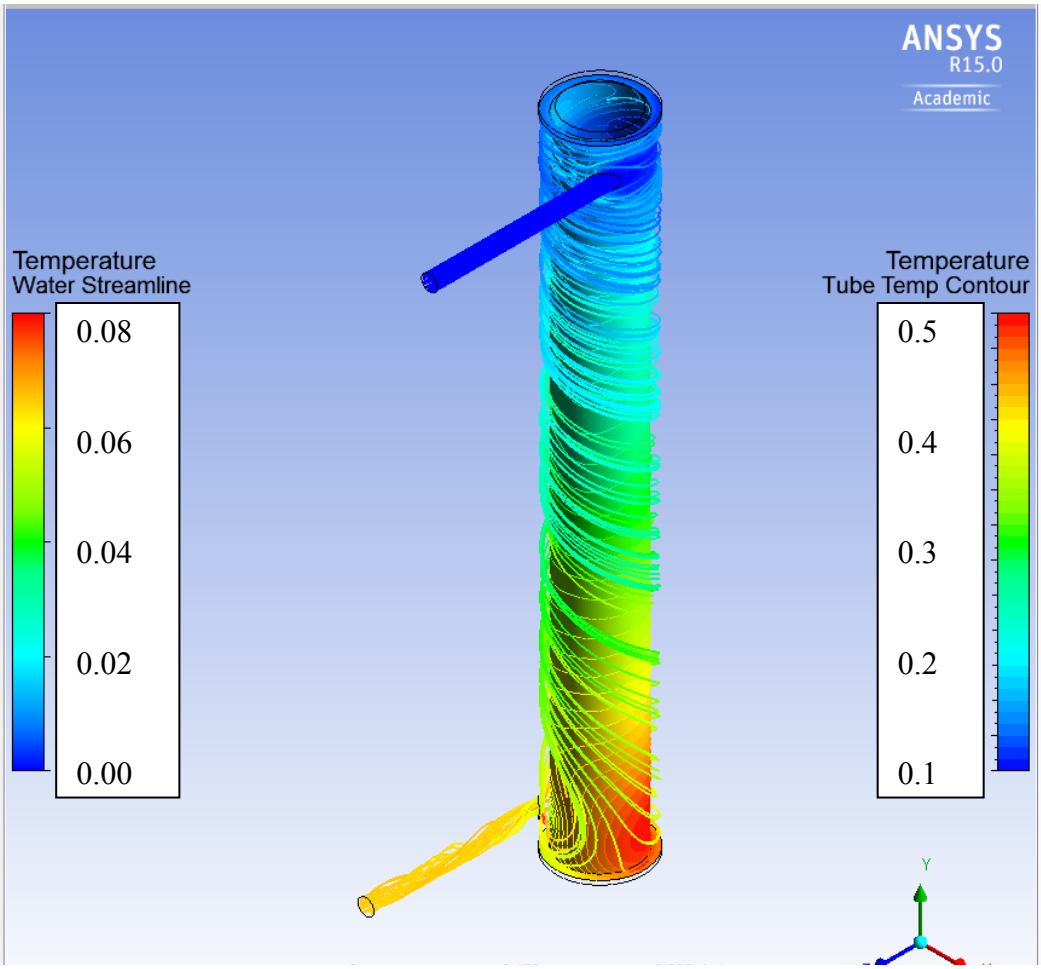

Figure 64. Water streamlines and temperature contour for WHRU with water inlet and outlet shifted laterally by x*=0.8 (placement Type 3) with L/d = 10; D/d=1.25, t*=0.0625, no exhaust swirl at Re_{exh} = 400,000, Re_{water} = 8,300.

In comparison, water streamlines in the water jacket shown in Figure 59 and Figure 61 depict that a WHRU with centerline water inlet and outlet placements has flow profiles which are highly uneven and non-uniform.

Water velocities were observed to be higher at the 12 o'clock position and lower at the 6 o'clock position. This resulted in uneven heat transfer, which translates to an adverse temperature profile. In contrast, the water streamlines for water placement Type 3 shown in Figure 64 are evenly distributed. The velocity vectors shown in Figure 65 also illustrate uniform flow distribution in the water jacket. This contributes toward even heat transfer throughout the WHRU. As such, gradual temperature profiles are achieved, reducing differential expansions and thermal stresses. This contributes toward improvement of WHRU reliability.

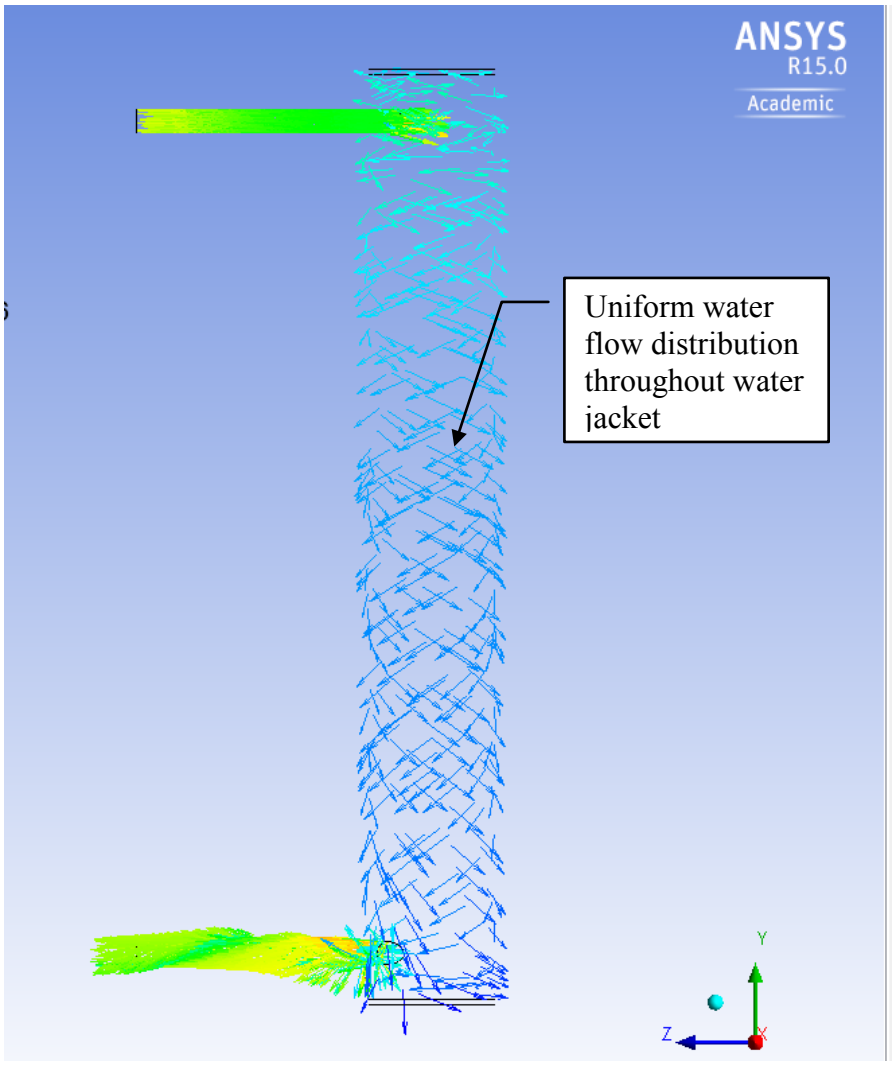

Figure 65. Velocity vectors depicting uniform flow in the water jacket of a WHRU with water inlet and outlet shifted laterally by x*=0.8 (placement Type 3) with L/d = 10, D/d=1.25, t*=0.0625, no exhaust swirl at Re_{exh} = 400,000, Re_{water} = 8,300.

VII. CONCLUSION

The thesis achieved the intended objectives of gaining insight on how reliability and performance of an exhaust gas water jacket WHRU are affected by features associated with design, construction, and operating conditions. These contribute toward the build-up of subject matter expertise in the USN-NPS WHR Capability Roadmap so as to formulate solutions to overcome the reliability and performance challenges that have limited the success of the USN's WHR program.

The features that were varied include exhaust tube diameter ratio (D/d), length-to-tube diameter ratio (L/d), exhaust flow conditions, tube materials, heat spreader feature, and placement of water inlet and outlet. The impact of these features was parametrically studied using analytical and CFD models based on USMC's MEP803A DG and USN's 501K SSGTG. Non-dimensional variables and parameters were used in the models in order for the results to be applied over a wider range of values. Due to its simplicity and the relative ease with which it can be retrofitted onto existing exhaust tubes with minimum impact on the associated power plants, a water jacket configuration was chosen as the baseline design for this study.

The analytical models were able to quickly provide estimates of heat recovery and pressure drop over a wide range of L/d and D/d ratios but faced limitations when studies involving more complex features such as swirling exhaust gas flows or water inlet and outlet placements were involved. CFD models were used to overcome these limitations, and to produce information on temperature profiles and flow fields within the WHRU. This information is crucial in the study to mitigate adverse temperature gradients and reduce thermal stresses in order to improve the reliability of the WHRU.

While large temperature gradients may be favorable to heat recovery, they also cause differential expansions and thermal stresses, which are detrimental to the WHRU reliability. Both analytical and CFD models verified that optimal non-dimensional heat recovery performance is achieved with the highest at L/d ratios, small D/d ratio, and low exhaust gas Reynolds number. It was also ascertained that an increase in the L/d ratio is

more effective in increasing heat recovery compared to reduction of D/d ratios. This is due to the increase in heat transfer area when length is increased. However, once the maximum possible heat recovery is achieved, further increase in L/d only increases the exhaust side pressure drop, which in turn increases the exhaust gas back pressure of the power plant upstream. Excessive back pressure is detrimental to the performance and reliability of the power plant. During design, attention must be given to this detail in order to optimize heat recovery with minimum pressure drop.

With the exhaust tube diameter (d) being fixed, varying the water jacket diameter (D) to get small D/d ratios was also found to complement heat recovery without any increase in the exhaust side pressure losses. At higher exhaust Reynolds numbers, heat recovery performance was found to be sensitive to changes in D/d; an inflection point was observed at a D/d ratio of 2. As such, a small D/d ratio of 1.25 was chosen for subsequent CFD models. As the exhaust tube diameter was held constant, reduction of D/d ratio did not increase the exhaust gas pressure drop.

Swirling exhaust gas flows were found to increase heat recovery by up to 52%. However, severe exhaust side pressure drops as high as 740% were induced as a consequence. This increase was induced even when non-intrusive swirl generators were used. The pressure drop increase would result in an exhaust back pressure in the power plant upstream of the WHRU, negatively impacting its performance and fuel consumption, defeating the purpose of WHR in the first place. It was also ascertained that swirling of the exhaust gas flow in the exhaust tube has minimal effects on the shape of the temperature profiles. Addition of swirl in the exhaust flow stream increased the average temperatures and did not mitigate the adverse temperature profiles within the WHRU. As such, swirling of exhaust gases does not contribute toward the improvement of WHRU performance or reliability.

Different tube materials were found to have some impact on heat recovery performance. A WHRU with exhaust tube constructed of "Pyroceram," a ceramic material with thermal conductivity 20 times lower than steel, reduced heat recovery by 8% to 35%. Copper, whose thermal conductivity is seven times higher than steel, improved heat recovery by up to 5%.

Results from this also showed that copper was able to contribute toward the mitigation of adverse temperature profiles and gradients in the WHRU. A WHRU constructed with copper tube mitigated the temperature profile difference by 41% and temperature gradient by 25% when compared to a WHRU with steel tube. Material with very low thermal conductivity, such as "Pyroceram," was also able to reduce temperature gradients in the WHRU. It can be concluded that materials with either very high or very low thermal conductivity could be beneficial toward the mitigation of adverse temperature profiles and improvement of WHRU reliability.

One of the most important findings in this study is the importance of proper water inlet and outlet placement toward the control of the temperature profile in the WHRU. WHRUs with water inlets and outlets located in the centerline of the WHRU (placement Type 1 and Type 2) experienced poor and uneven distribution of flow in the water jacket. Such placements are prevalent in available heat exchanger technologies.

The finding related to centerline water inlet and outlet placement was consistently found in WHRUs with different geometric ratios, tube materials, heat spreader features, or presence of swirl in exhaust gas flows. The poor distribution of water flow resulted in adverse temperature profiles between the 6 o'clock and 12 o'clock positions and sharp temperature gradients at the upper section of the WHRU where the exhaust outlet and water inlet are located (y/L=0.5 to y/L =1.0). This adverse temperature profile produces differential expansions and thermal stress, initiating failure mechanisms such as fatigue and stress corrosion cracking that increase probability of premature failure in WHRUs. The poor distribution of water flow also reduced the heat recovery potential of the affected WHRU. This finding is crucial as centerline water inlet and outlet placements are very prevalent in cylindrical-shaped WHRUs or heat exchangers.

The problem was subsequently resolved by shifting the water inlet and outlet from the centerline by a lateral distance of $x^* = \pm 0.8$. This change in the water placement improved the flow in the water jacket and eradicated the adverse temperature profiles. Heat recovery performance of the WHRU also increased as much as 19% with no increase in exhaust side pressure loss.

Results from this study provide insights into the complex relationships involved in the design of a WHRU that is both reliable and high performing. Designers or program managers of waste heat recovery projects need to consider performance and reliability from a total system point of view. The increase in heat recovery is often linked to an increased exhaust side pressure drop, which in turn impacts the power plant upstream in a detrimental manner. In order to optimize reliability and performance further, follow-on study of the water inlet and outlet of water jacket WHRUs could be conducted looking at the effects of shapes, vertical or horizontal locations, and sizes of the water inlet and outlet.

APPENDIX A

A sample of the CFX solver report and results are included in this appendix. The data were generated from Run 4 which models a WHRU with L/d=10, D/d=1.25, Steel tube of t* = 0.0625, Re_{exh}=400,000, Re_{water} = 8,300 with centerline water placement without any exhaust swirl in the flow.

REPORT FOR CFX MODEL (FOR RUN 4)

1. File Report

Table 1. File Information for CFX.

Case	CFX
File Path	C:\SCRATCH\Erik_K\Baseline_4_files\dp0\CFX\CFX\Fluid Flow CFX_005.res
File Date	22 August 2014
File Time	08:21:10 PM
File Type	CFX5
File Version	15.0

2. Physics Report

Table 2. Domain Physics for CFX.

Domain - Exhaust	
Type	Fluid
Location	B10
Materials	
Air Ideal Gas	
Fluid Definition	Material Library
Morphology	Continuous Fluid
Settings	
Buoyancy Model	Non Buoyant

Domain Motion	Stationary
Reference Pressure	1.0000e+00 [atm]
Heat Transfer Model	Thermal Energy
Turbulence Model	k epsilon
Turbulent Wall Functions	Scalable
Domain - Tube	
Type	Solid
Location	B22
Settings	
Domain Motion	Stationary
Domain - Water	
Type	Fluid
Location	B39
Materials	
Water	
Fluid Definition	Material Library
Morphology	Continuous Fluid
Settings	
Buoyancy Model	Non Buoyant
Domain Motion	Stationary
Reference Pressure	1.0000e+00 [atm]
Heat Transfer Model	Thermal Energy
Turbulence Model	k epsilon
Turbulent Wall Functions	Scalable
Domain Interface - Exhaust to Tube	
Boundary List1	Default Fluid Solid Interface Side 1 1
Boundary List2	Default Fluid Solid Interface Side 1
Interface Type	Fluid Solid
Settings	

Interface Models	General Connection
Heat Transfer	Conservative Interface Flux
Material	Steel
Heat Transfer Interface Model	Thin Material
Thickness	5.0000e+00 [mm]
Mesh Connection	GGI
Domain Interface - Water to Tube	
Boundary List1	Water to Tube Side 1
Boundary List2	Water to Tube Side 2
Interface Type	Fluid Solid
Settings	
Interface Models	General Connection
Heat Transfer	Conservative Interface Flux
Material	Steel
Heat Transfer Interface Model	Thin Material
Thickness	5.0000e+00 [mm]
Mesh Connection	GGI

Table 3. Boundary Physics for CFX.

Domain	Boundaries	
Exhaust	Boundary - Exhaust_in	
	Type	INLET
	Location	Exh_in
	Settings	
	Flow Direction	Normal to Boundary Condition
	Flow Regime	Subsonic
	Heat Transfer	Static Temperature
	Static Temperature	7.7300e+02 [K]
	Mass And Momentum	Mass Flow Rate

	Mass Flow Rate	4.6120e-01 [kg s^-1]
	Turbulence	Medium Intensity and Eddy Viscosity Ratio
	Boundary - Default Fluid Solid Interface Side 1 1	
	Type	INTERFACE
	Location	F11.10
	Settings	
	Heat Transfer	Conservative Interface Flux
	Mass And Momentum	No Slip Wall
	Wall Roughness	Smooth Wall
	Boundary - Exhaust_out	
	Type	OUTLET
	Location	Exh_out
	Settings	
	Flow Regime	Subsonic
	Mass And Momentum	Average Static Pressure
	Pressure Profile Blend	5.0000e-02
	Relative Pressure	0.0000e+00 [Pa]
	Pressure Averaging	Average Over Whole Outlet
Tube	Boundary - Default Fluid Solid Interface Side 1	
	Type	INTERFACE
	Location	F23.22
	Settings	
	Heat Transfer	Conservative Interface Flux
	Boundary - Water to Tube Side 2	
	Type	INTERFACE
	Location	F29.22
	Settings	
	Heat Transfer	Conservative Interface Flux

	Boundary - Tube Default	
	Type	WALL
	Location	F24.22, F25.22, F26.22, F27.22, F28.22, F30.22
	Settings	
	Heat Transfer	Adiabatic
Water	Boundary - water_in	
	Type	INLET
	Location	Water_in
	Settings	
	Flow Direction	Normal to Boundary Condition
	Flow Regime	Subsonic
	Heat Transfer	Static Temperature
	Static Temperature	3.0000e+02 [K]
	Mass And Momentum	Mass Flow Rate
	Mass Flow Rate	1.1560e-01 [kg s^-1]
	Turbulence	Medium Intensity and Eddy Viscosity Ratio
	Boundary - Water to Tube Side 1	
	Type	INTERFACE
	Location	F46.39
	Settings	
	Heat Transfer	Conservative Interface Flux
	Mass And Momentum	No Slip Wall
	Wall Roughness	Smooth Wall
	Boundary - Water_out	
	Type	OUTLET
	Location	Water_out
	Settings	
	Flow Regime	Subsonic

	Mass And Momentum	Average Static Pressure
	Pressure Profile Blend	5.0000e-02
	Relative Pressure	0.0000e+00 [Pa]
	Pressure Averaging	Average Over Whole Outlet
	Boundary - Water Default	
	Type	WALL
	Location	F40.39, F41.39, F42.39, F43.39, F44.39
	Settings	
	Heat Transfer	Adiabatic
	Mass And Momentum	No Slip Wall
	Wall Roughness	Smooth Wall

CFX SOLVER RESULTS (FOR RUN 4)

==

Termination and Interrupt Condition Summary

==

CFD Solver: All target criteria reached
(Equation residuals)

==

Boundary Flow and Total Source Term Summary

==

+--+

```
|                    U-Mom-Exhaust                    |
+-----------------------------------------------------+
Boundary      : Default Fluid Solid Interface Side 1 1  2.1472E-03
Boundary      : Exhaust_in                             -2.8443E-07
Boundary      : Exhaust_out                            -2.1500E-03
                                                      -----------
Domain Imbalance:                                      -3.0103E-06

+-----------------------------------------------------+
|                    V-Mom-Exhaust                    |
+-----------------------------------------------------+
Boundary      : Default Fluid Solid Interface Side 1 1 -6.8980E+00
Boundary      : Exhaust_in                             9.7651E+01
Boundary      : Exhaust_out                            -9.0756E+01
                                                  -----------
Domain Imbalance:                                      -2.6734E-03

+-----------------------------------------------------+
|                    W-Mom-Exhaust                    |
+-----------------------------------------------------+
Boundary      : Default Fluid Solid Interface Side 1 1  2.2887E-02
Boundary      : Exhaust_in                             -1.3690E-07
Boundary      : Exhaust_out                            -2.2886E-02
                                                  -----------
Domain Imbalance:                                       4.6084E-07

+-----------------------------------------------------+
|                    P-Mass-Exhaust                   |
+-----------------------------------------------------+
Boundary      : Exhaust_in                             4.6120E-01
Boundary      : Exhaust_out                            -4.6120E-01
                                                  -----------
Domain Imbalance:                                      -7.6188E-07

+-----------------------------------------------------+
|                     U-Mom-Water                     |
+-----------------------------------------------------+
Boundary      : Water Default                          -1.3544E-03
Boundary      : Water to Tube Side 1                    1.3440E-03
Boundary      : Water_out                              1.0420E-05
Boundary      : water_in                               -1.2582E-09
                                                  -----------
Domain Imbalance:                                       6.5064E-09

+-----------------------------------------------------+
```

```
|                    V-Mom-Water                    |
+---------------------------------------------------+
Boundary       : Water Default                -2.2156E-03
Boundary       : Water to Tube Side 1          2.2756E-03
Boundary       : Water_out                    -6.0035E-05
Boundary       : water_in                     -3.7131E-10
                                              ----------
Domain Imbalance:                             -7.8595E-10

+---------------------------------------------------+
|                    W-Mom-Water                    |
+---------------------------------------------------+
Boundary       : Water Default                 2.1828E-01
Boundary       : Water to Tube Side 1         -8.5256E-02
Boundary       : Water_out                    -4.3420E-02
Boundary       : water_in                     -8.9606E-02
                                                    ----------
Domain Imbalance:                             -2.4253E-09

+---------------------------------------------------+
|                    P-Mass-Water                   |
+---------------------------------------------------+
Boundary       : Water_out                    -1.1560E-01
Boundary       : water_in                      1.1560E-01
                                              ----------
Domain Imbalance:                              3.1625E-11

+---------------------------------------------------+
|                  H-Energy-Exhaust                 |
+---------------------------------------------------+
Boundary       : Exhaust_in                    2.1996E+05
Boundary       : Exhaust_out                  -2.0887E+05
Domain Interface: Exhaust to Tube (Side 1)    -1.1099E+04
                                              ----------
Domain Imbalance:                             -3.7569E-01

+---------------------------------------------------+
|                   T-Energy-Tube                   |
+---------------------------------------------------+
Domain Interface: Exhaust to Tube (Side 2)     1.1099E+04
Domain Interface: Water to Tube (Side 2)      -1.1099E+04
                                              ----------
Domain Imbalance:                             -2.2368E-02

+---------------------------------------------------+
```

H-Energy-Water
Boundary : Water_out -1.1993E+04
Boundary : water_in 8.9430E+02
Domain Interface: Water to Tube (Side 1) 1.1099E+04

Domain Imbalance: -1.6096E-02

Normalised Imbalance Summary		
Equation	Maximum Flow	Imbalance (%)
U-Mom-Exhaust	9.7651E+01	0.0000
V-Mom-Exhaust	9.7651E+01	-0.0027
W-Mom-Exhaust	9.7651E+01	0.0000
P-Mass-Exhaust	4.6120E-01	-0.0002
U-Mom-Water	2.1828E-01	0.0000
V-Mom-Water	2.1828E-01	0.0000
W-Mom-Water	2.1828E-01	0.0000
P-Mass-Water	1.1560E-01	0.0000
H-Energy-Exhaust	2.1996E+05	-0.0002
T-Energy-Tube	2.1996E+05	0.0000
H-Energy-Water	2.1996E+05	0.0000

==========

Wall Force and Moment Summary

==========

Notes:
1. Pressure integrals exclude the reference pressure. To include
it, set the expert parameter 'include pref in forces = t'.

Pressure Force On Walls

X-Comp. Y-Comp. Z-Comp.

Domain Group: Exhaust

Default Fluid Solid Interface Si-2.2406E-03 1.4194E-15 -2.2824E-02

Domain Group Totals: -2.2406E-03 1.4194E-15 -2.2824E-02

+----------+
| Viscous Force On Walls |
+----------+

X-Comp. Y-Comp. Z-Comp.

Domain Group: Exhaust

Default Fluid Solid Interface Si 9.3384E-05 6.8980E+00 -6.3044E-05

Domain Group Totals: 9.3384E-05 6.8980E+00 -6.3044E-05

+----------+
| Pressure Moment On Walls |
+----------+

X-Comp. Y-Comp. Z-Comp.

Domain Group: Exhaust

Default Fluid Solid Interface Si-1.2082E-02 -5.8540E-10 -3.4594E-04

Domain Group Totals: -1.2082E-02 -5.8540E-10 -3.4594E-04

+----------+
| Viscous Moment On Walls |
+----------+

X-Comp. Y-Comp. Z-Comp.

Domain Group: Exhaust

Default Fluid Solid Interface Si 1.4405E-03 7.4118E-08 -1.0289E-03

Domain Group Totals: 1.4405E-03 7.4118E-08 -1.0289E-03

+--+
| Pressure Force On Walls |
+--+

	X-Comp.	Y-Comp.	Z-Comp.
Domain Group: Water			
Water Default	1.3479E-03	5.0214E-03	-2.1922E-01
Water to Tube Side 1	-1.3396E-03	-5.0283E-06	8.7648E-02
Domain Group Totals:	8.3710E-06	5.0164E-03	-1.3158E-01

+--+
| Viscous Force On Walls |
+--+

	X-Comp.	Y-Comp.	Z-Comp.
Domain Group: Water			
Water Default	6.4302E-06	-2.8058E-03	9.4114E-04
Water to Tube Side 1	-4.3889E-06	-2.2706E-03	-2.3912E-03
Domain Group Totals:	2.0413E-06	-5.0764E-03	-1.4501E-03

+--+
| Pressure Moment On Walls |
+--+

	X-Comp.	Y-Comp.	Z-Comp.
Domain Group: Water			
Water Default	-2.3176E-02	7.7241E-06	-7.3817E-04
Water to Tube Side 1	1.2201E-02	-1.0676E-07	7.5017E-04
Domain Group Totals:	-1.0975E-02	7.6174E-06	1.2001E-05

+--+
| Viscous Moment On Walls |
+--+

	X-Comp.	Y-Comp.	Z-Comp.
Domain Group: Water			

Water Default -4.6298E-03 -4.1961E-06 -6.6378E-06
Water to Tube Side 1 -9.8439E-04 -1.2941E-08 -1.0003E-06
---------- ---------- ----------
Domain Group Totals: -5.6142E-03 -4.2090E-06 -7.6381E-06

Locations of Maximum Residuals		
Equation	Domain Name	Node Number
U-Mom-Exhaust	Exhaust	99162
V-Mom-Exhaust	Exhaust	99097
W-Mom-Exhaust	Exhaust	99174
P-Mass-Exhaust	Exhaust	2028
U-Mom-Water	Water	339770
V-Mom-Water	Water	331149
W-Mom-Water	Water	329475
P-Mass-Water	Water	348641
H-Energy-Exhaust	Exhaust	106668
T-Energy	Tube	24001
H-Energy-Water	Water	329462
K-TurbKE-Exhaust	Exhaust	40054
E-Diss.K-Exhaust	Exhaust	107997
K-TurbKE-Water	Water	329466
E-Diss.K-Water	Water	348702

==========

False Transient Information		
Equation	Type	Elapsed Pseudo-Time
U-Mom-Exhaust	Auto Timescale	1.96018E+01
V-Mom-Exhaust	Auto Timescale	1.96018E+01
W-Mom-Exhaust	Auto Timescale	1.96018E+01
P-Mass-Exhaust	Auto Timescale	1.96018E+01

U-Mom-Water	Auto Timescale	2.78180E+03
V-Mom-Water	Auto Timescale	2.78180E+03
W-Mom-Water	Auto Timescale	2.78180E+03
H-Energy-Exhaust	Auto Timescale	3.92036E+03
T-Energy-Tube	Auto Timescale	2.99902E+06
H-Energy-Water	Auto Timescale	5.56360E+05
K-TurbKE-Exhaust	Auto Timescale	1.96018E+01
E-Diss.K-Exhaust	Auto Timescale	1.96018E+01
K-TurbKE-Water	Auto Timescale	2.12037E+03
E-Diss.K-Water	Auto Timescale	2.12037E+03

Average Scale Information

Domain Name: Exhaust

Global Length	= 1.5958E-01
Minimum Extent	= 8.0000E-02
Maximum Extent	= 8.1000E-01
Density	= 4.6641E-01
Dynamic Viscosity	= 1.8310E-05
Velocity	= 1.9867E+02
Advection Time	= 8.0326E-04
Reynolds Number	= 8.0760E+05
Speed of Sound	= 5.5280E+02
Mach Number	= 3.5938E-01
Thermal Conductivity	= 2.6100E-02
Specific Heat Capacity at Constant Pressure	= 1.0044E+03
Specific Heat Capacity at Constant Volume	= 7.1730E+02
Specific Heat Ratio	= 1.4003E+00
Prandtl Number	= 7.0462E-01
Temperature Range	= 1.2196E+02

Domain Name: Water

Global Length	= 1.3814E-01
Minimum Extent	= 1.1000E-01
Maximum Extent	= 8.0000E-01
Density	= 9.9700E+02
Dynamic Viscosity	= 8.8990E-04
Velocity	= 3.1145E-01
Advection Time	= 4.4354E-01

Reynolds Number = 4.8202E+04
Thermal Conductivity = 6.0690E-01
Specific Heat Capacity at Constant Pressure = 4.1817E+03
Prandtl Number = 6.1316E+00
Temperature Range = 4.1571E+01

Domain Name: Tube
Global Length = 1.0360E-01
Minimum Extent = 1.0996E-01
Maximum Extent = 8.1000E-01
Density = 7.8540E+03
Thermal Conductivity = 6.0500E+01
Specific Heat Capacity at Constant Pressure = 4.3400E+02
Thermal Diffusivity = 1.7749E-05
Average Diffusion Timescale = 6.0476E+02
Minimum Diffusion Timescale = 6.8125E+02
Maximum Diffusion Timescale = 3.6965E+04
Temperature Range = 2.4236E+02

+----------+
| Variable Range Information |
+----------+

Domain Name: Exhaust

Variable Name	min	max
Density	4.57E-01	5.42E-01
Specific Heat Capacity at Constant Pressure	1.00E+03	1.00E+03
Dynamic Viscosity	1.83E-05	1.83E-05
Thermal Conductivity	2.61E-02	2.61E-02
Isothermal Compressibility	9.75E-06	9.87E-06
Static Entropy	7.84E+02	9.57E+02
Velocity u	-3.89E-01	4.24E-01
Velocity v	1.34E+02	2.11E+02
Velocity w	-4.07E-01	3.93E-01
Pressure	-8.53E+00	1.23E+03
Turbulence Kinetic Energy	4.85E-01	3.25E+02
Turbulence Eddy Dissipation	1.40E+02	3.21E+06
Eddy Viscosity	6.84E-05	6.43E-03
Temperature	6.51E+02	7.73E+02
Static Enthalpy	3.55E+05	4.77E+05

Domain Name: Water

Variable Name	min	max
Density	9.97E+02	9.97E+02
Specific Heat Capacity at Constant Pressure	4.18E+03	4.18E+03
Dynamic Viscosity	8.90E-04	8.90E-04
Thermal Conductivity	6.07E-01	6.07E-01
Static Entropy	2.57E+01	5.68E+02
Velocity u	-3.97E-01	4.01E-01
Velocity v	-3.98E-01	3.86E-01
Velocity w	-4.23E-01	5.00E-01
Pressure	-1.20E+02	2.23E+02
Turbulence Kinetic Energy	3.80E-06	1.48E-02
Turbulence Eddy Dissipation	3.15E-07	1.46E+00
Eddy Viscosity	1.85E-03	3.77E-02
Temperature	3.00E+02	3.42E+02
Static Enthalpy	7.70E+03	1.82E+05

Domain Name: Tube

Variable Name	min	max
Density	7.85E+03	7.85E+03
Specific Heat Capacity at Constant Pressure	4.34E+02	4.34E+02
Thermal Conductivity	6.05E+01	6.05E+01
Static Entropy	5.37E+01	2.89E+02
Temperature	3.37E+02	5.80E+02
Static Enthalpy	1.71E+04	1.22E+05

CPU Requirements of Numerical Solution - Total

Subsystem Name	Discretization (secs.)	Discretization %total	Linear Solution (secs.)	Linear Solution %total
Momentum and Mass - 1	2.82E+02	6.5 %	6.73E+01	1.5 %
Momentum and Mass - 2	1.18E+03	27.0 %	3.04E+02	7.0 %
Heat Transfer	6.91E+02	15.9 %	2.57E+02	5.9 %
TurbKE and Diss.K - 1	6.90E+01	1.6 %	2.88E+01	0.7 %
TurbKE and Diss.K - 2	3.49E+02	8.0 %	2.03E+02	4.7 %
Subsystem Summary	2.57E+03	59.0 %	8.60E+02	19.8 %

```
Variable Updates              2.45E+02    5.6 %
GGI Intersection              4.00E-01    0.0 %
File Reading                  1.34E+01    0.3 %
File Writing                  2.68E+01    0.6 %
Miscellaneous                 6.37E+02   14.7 %
                           --------
Total                         4.35E+03

+---------------------------------------------------------------------+
|                Job Information at End of Run                        |
+---------------------------------------------------------------------+

+--------------------------+------+----------+----------+-----------+
| Host                     | Mesh |     Job Finished    |    CPU    |
|                          | Part | DD/MM/YY | hh:mm:ss |  seconds  |
+--------------------------+------+----------+----------+-----------+
| ETL-WA138-026            |    1 | 22/08/14 | 20:13:33 | 1.087E+03 |
|                          |    2 | 22/08/14 | 20:13:33 | 1.087E+03 |
|                          |    3 | 22/08/14 | 20:13:33 | 1.087E+03 |
|                          |    4 | 22/08/14 | 20:13:33 | 1.088E+03 |
+--------------------------+------+----------+----------+-----------+

 Total wall clock time: 1.087E+03 seconds
          or: (          0:         0:        18:     7.422 )
              (       Days:     Hours:   Minutes:   Seconds )


 --> Final synchronization point reached by all partitions.
End of solution stage.

+---------------------------------------------------------------------+
| The results from this run of the ANSYS CFX Solver have been         |
| written to                                                          |
| C:/SCRATCH/Erik_K/Baseline_4_pending_tasks/dp0_CFX_Solution/Fluid  |
| Flow CFX_005.res                                                    |
+---------------------------------------------------------------------+


This run of the ANSYS CFX Solver has finished.
```

APPENDIX B

Table 8. Inlet and outlet temperatures and energy balance from ANSYS CFX model runs.

	Exhaust ($C_{p,exh}$ = 1004.4 W/Kg.K)				Water ($C_{p,exh}$ = 4181.7 W/Kg.K)						
Run	**m_{exh} [Kg/s]**	**Re_{exh}**	**$T_{exh,in}$ [K]**	**$T_{exh,out}$ [K]**	**m_{water} [Kg/s]**	**Re_{water}**	**$T_{water,in}$ [K]**	**$T_{water,out}$ [K]**	**Energy In [W]**	**Energy Out [W]**	**Energy Balance (%)**
1	0.023	19,992	772.776	700.14	0.1156	8,270	300	303.509	162873.409	162891.697	0.011%
2	0.1156	100,482	772.87	729.349	0.1156	8,270	300	310.539	234758.241	234799.677	0.018%
3	0.23	199,922	772.908	739.887	0.1156	8,270	300	315.921	323572.379	323640.415	0.021%
4	0.4612	400,886	772.94	749.221	0.1156	8,270	300	322.949	503069.796	503176.111	0.021%
5	0.023	19,992	772.756	730.868	0.1156	8,270	300	302.021	162872.947	162882.244	0.006%
6	0.1156	100,482	772.848	747.659	0.1156	8,270	300	306.131	234755.686	234794.779	0.017%
7	0.23	199,922	772.89	753.712	0.1156	8,270	300	309.302	323568.221	323634.501	0.020%
8	0.4612	400,886	772.925	758.576	0.1156	8,270	300	313.666	503062.847	503022.176	-0.008%
9	0.023	19,992	772.778	643.97	0.1156	8,270	300	306.167	162873.455	162878.991	0.003%
1	0.1156	100,482	772.875	694.289	0.1156	8,270	300	318.913	234758.821	234776.937	0.008%
1	0.23	199,922	772.914	713.271	0.1156	8,270	300	328.56	323573.765	323601.549	0.009%
1	0.4612	400,886	772.945	730.396	0.1156	8,270	300	340.857	503072.112	503112.628	0.008%
1	0.023	19,992	772.684	677.979	0.1156	8,270	300	304.563	162871.284	162889.259	0.011%

1	0.1156	100,482	772.838	718.498	0.1156	8,270	300	313.187	234754.525	234819.837	0.028%
1	0.23	199,922	772.889	732.729	0.1156	8,270	300	319.417	323567.990	323676.813	0.034%
1	0.4612	400,886	772.93	744.732	0.1156	8,270	300	327.348	503065.163	503223.171	0.031%
1	0.023	19,992	772.762	663.377	0.1156	8,270	300	305.258	162873.086	162887.902	0.009%
1	0.1156	100,482	772.885	709.093	0.1156	8,270	300	315.435	234759.982	234814.529	0.023%
1	0.23	199,922	772.922	726.433	0.1156	8,270	300	322.393	323575.613	323660.974	0.026%
2	0.4612	400,886	772.948	741.283	0.1156	8,270	300	330.603	503073.502	503198.975	0.025%
2	0.023	19,992	772.823	695.369	0.1156	8,270	300	303.714	162874.495	162880.579	0.004%
2	0.1156	100,482	772.931	727.371	0.1156	8,270	300	310.984	234765.323	234785.129	0.008%
2	0.23	199,922	772.964	738.716	0.1156	8,270	300	316.43	323585.316	323615.953	0.009%
2	0.4612	400,886	772.983	748.594	0.1156	8,270	300	323.469	503089.715	503137.036	0.009%
2	0.023	19,992	772.782	701.102	0.1156	8,270	300	303.447	162873.548	162883.949	0.006%
2	0.1156	100,482	772.881	731.062	0.1156	8,270	300	310.124	234759.518	234797.958	0.016%
2	0.23	199,922	772.919	741.754	0.1156	8,270	300	315.021	323574.920	323636.650	0.019%
2	0.4612	400,886	772.949	751.065	0.1156	8,270	300	321.166	503073.965	503168.395	0.019%
2	0.023	19,992	772.771	699.445	0.1156	8,270	300	303.528	162873.293	162884.826	0.007%
3	0.1156	100,482	772.863	728.327	0.1156	8,270	300	310.788	234757.428	234801.381	0.019%
3	0.23	199,922	772.901	738.468	0.1156	8,270	300	316.461	323570.762	323573.647	0.001%

3	0.4612	400,886	772.933	748.121	0.1156	8,270	300	324.013	503066.553	503180.901	0.023%
3	0.023	19,992	772.806	706.07	0.1156	8,270	300	303.209	162874.102	162883.665	0.006%
3	0.1156	100,482	772.912	738.26	0.1156	8,270	300	308.385	234763.117	234793.067	0.013%
3	0.23	199,922	772.946	749.005	0.1156	8,270	300	311.533	323581.157	323625.603	0.014%
3	0.4612	400,886	772.97	757.573	0.1156	8,270	300	314.882	503083.693	503145.377	0.012%
3	0.023	19,992	772.767	697.886	0.1156	8,270	300	303.604	162873.201	162885.550	0.008%
3	0.1156	100,482	772.857	725.499	0.1156	8,270	300	311.476	234756.731	234805.608	0.021%
3	0.23	199,922	772.817	735.494	0.1156	8,270	300	318.045	323551.357	323652.330	0.031%
4	0.4612	400,886	772.925	744.679	0.1156	8,270	300	327.351	503062.847	503200.070	0.027%
4	0.023	19,992	772.777	700.227	0.1156	8,270	300	303.489	162873.432	162884.038	0.007%
4	0.1156	100,482	772.872	729.58	0.1156	8,270	300	310.482	234758.473	234798.944	0.017%
4	0.23	199,922	772.909	740.098	0.1156	8,270	300	315.816	323572.610	323638.401	0.020%
4	0.4612	400,886	772.939	749.378	0.1156	8,270	300	322.749	503069.332	503152.157	0.016%

THIS PAGE INTENTIONALLY LEFT BLANK

LIST OF REFERENCES

Agrawal, A. K., & Sengupta, S. (1993). Laminar fluid flow and heat transfer in an annulus with an externally enhanced inner tube. *International Journal of Heat and Fluid Flow, 14*(1), 54–63.

Akpinar, E. K. (2006). Evaluation of heat transfer and exergy loss in a concentric double pipe exchanger equipped with helical wires. *Energy Conversion and Management, 47*, 3473–3486.

Albadr, J., Tayal, S., & Alasadi, M. (2013). Heat transfer through heat exchanger using Al2O3 nanofluid at different concentrations. *Case Studies in Thermal Engineering 1*, 38–44.

ANSYS. (2013, November). *ANSYS CFX-Solver theory guide*. Canonsburg, PA: ANSYS, Inc.

Bailey, M. M. (1985). *Comparative evaluation of three alternative power cycles for waste heat recovery from the exhaust of adiabatic diesel engines.* Washington, DC: U.S. Department of Energy.

BCS. (2008). *Waste heat recovery: Technology and opportunities in U.S. industry.* Washington, DC: U.S. Department of Energy.

Boyce, M. P. (2012). Effect of controllable losses to the output and heat rate. In *Gas turbine engineering handbook* (4th ed.). Houston, TX: Gulf Professional Publishing.

Breaux, D., & Davies, K. (1978, April). Design and service of a marine waste heat boiler. *Naval Engineers Journal*, 165–178.

Carapellucci, R., & Giordano, L. (2012, April). The Recovery of Exhaust Heat from Gas Turbines. In V. Konstantin (Ed.), *Efficiency, performance and robustness of gas turbines* (pp. 165–190). InTech. doi:10.5772/37920.

CHP Focus. (2014). *Gas turbine performance*. Retrieved August 10, 2014, from http://chp.decc.gov.uk/cms/gas-turbine-performance/

Daniels, D. G. (2014, Feb). *How to identify, prevent waterside failure mechansims in your HRSG.* Retrieved February 8, 2014, from http://www.ccj-online.com/3q-2005/grsg-waterside-failure/

Deputy Assistant Secretary of the Navy (DASN) Energy Office. (2010, October). *Department of the Navy's Energy Program for Security and Independence.* Retrieved August 9, 2014, from http://www.navy.mil/secnav/

Dooley, R., Paterson, S., & Pearson, M. (2005). *Diagnostic/troubleshooting monitoring to identify damaging cycle chemistry or thermal transients in heat recovery steam generator pressure parts.* Palo Alto, CA: Electrical Power Research Institute.

Durmus, A. (2002). Heat transfer and energy loss in a concentric heat exchanger with snail entrance. *International Communication Heat Mass Transfer, 29*(3), 303–312.

EPRI. (2005). *Heat exchanger thermal performance margin guideline.* Palo Alto, CA: Electrical Power Research Institute.

———. (2009). *HRSG startup and shutdown guidelines for avoiding heat recovery steam generator pressure part failure.* Palo Alto, CA: Electric Power Research Institute.

Greenship.org. (2014). *Green ship of the future.* Retrieved July 31, 2014, from Greenship website: http://www.greenship.org/fpublic/greenship/dokumenter /GSF%20brochure%20-%20maga/Green%20Shipping%20is% 20the%20future.pdf

Halkola, J. T., Campbell, A., & Jung, D. (1983, July). RACER conceptual design. *Journal of Engineering for Power, 105*, 621–626.

Hield, P. (2011). *The effect of back pressure on the operations of a diesel engine.* Victoria, Australia: Maritime Platforms Division, Defense Science and Technology Organization.

Incropera, F. P., Bergman, T. L., Lavine, A. S., & Dewitt, D. P. (2011). *Introduction to heat transfer* (6th ed.). Hoboken, NJ: John Wiley & Sons, Inc.

Kakac, S., & Liu, H. (2002). *Heat Exchangers Selection, Rating and Thermal design* (2nd ed.). Danvers, MA: CRC Press.

Khalil, A., Zohir, A., & Farid, A. (2010). Heat transfer characteristics and friction of turbulent swirling air flow through abrupt expansion. *American Journal of Scientific and Industrial Research, 1*(2), 364–374.

Kreith, F., & Margolis, D. (1959). Heat transfer and friction in turbulent vortex flow. *Applied Scientific Research Section A, 8*(1), 457–473.

Macdonald, J. A. (2014, May). *Energy-tech.* Retrieved August 4, 2014, from http://www.energy-tech.com/article.cfm?id=17567

Masliyah, J., & Nandakumar, K. (1976). Heat transfer in internally finned tubes. *Journal of Heat Transfer*, 257–261.

Mastronarde, T. P. (1982, April). Energy conservation utilizing waste heat boilers - The challenges, problems and solutions. *Naval Engineers Journal*, 277–285.

Munson, B. R., Young, D. F., Okiishi, T. H., & Huebsch, W. W. (2009). *Fundamentals of fluid mechanics* (6th ed.). Hoboken, NJ: John Wiley & Sons, Inc.

Paanu, T., Niemi, S., & Rantanen, P. (2012). *Waste heat recovery – Bottoming cycle alternatives.* Vaasa, Finland: University of Vaasa.

Paratherm. (n.d.). High temperature heat transfer fluids. Retrieved July 10, 2014, from http://www.paratherm.com/heat-transfer-fluids/high-temperature-heat-transfer-fluids/paratherm-hr/

Pardhi, C., & Baredar, P. (2012). Performance improvement of double pipe heat exchanger by using turbulator. *International Journal of Engineering Science & Advanced Technology, 2*(4), 881–885.

Patankar, S. V. (1980). *The turbulence-kinetic-energy equation.* New York: Hemisphere Publishing Corporation.

Patel, M., Parmar, K., & Soni, U. R. (2014). Enhance the performance of heat exchangers with twisted tape insert: A review. *International Journal on Recent and InnovationTrends in Computering and Communication, 2*(2), 202–207.

Rains, D. A., Beyer, K. M., Keene, W., Lindgren, J. J., Mogil, E., Page, T., . . . Youngworth, J. (1976, October). Design appraisal - DD-963. *Naval Engineers Journal*, 43–61.

Sane, N., Taji, S. G., & Pachegaonkar, S. S. (2014). Performance analysis of double pipe heat exchnager with annular twisted tape insert. *International Journal of Engineering and Advanced Technology, 3*(3), 402–406.

Sathe, S. B., & Millsaps, K. (2014). U.S. Navy WHR Capability Roadmap. Monterey, CA: Mechanical and Aerospace Engineering Department, Naval Postgraduguate School.

Shah, R. K., & Sekulic, D. P. (2002). *Fundamentals of heat exchanger design*. Hoboken, NJ: John Wiley & Sons.

Shu, H.-T., & Kuo, S. (1982). *Flow distribution control characteristics in marine gas turbine waste heat steam generators.* East Hartford, CT: United Technologies Research Center.

Special Metals Corporation. (2013, August 13). *Special metals.* Retrieved July 5, 2014, from www.specialmetals.com

Woodyard, D. (2004). *Pounder's marine diesel engines and gas turbine* (8th ed.). Oxford, UK: Elsevier Ltd.

Yarin, L. (2012). *The Pi-Theorem: Applications to fluid mechanics and heat and mass transfer*. New York: Springer.

Zamanzadeh, M., Larkin, E. S., Bayer, G. T., & Linhart, W. J. (2007). *Failure analysis and investigation methods for boiler tube failures*. Paper presented at the Waterside Boiler Tube Failure Symposium, Pittsburgh, PA.

INITIAL DISTRIBUTION LIST

1. Defense Technical Information Center
   Ft. Belvoir, Virginia

2. Dudley Knox Library
   Naval Postgraduate School
   Monterey, California